INHIBITION OF VARIOUS RECEPTOR TYROSINE KINASE (RTK) FAMILIES

JIN HYUNG PARK

A DISSERTATION

in

Biochemistry and Molecular Biophysics

Presented to the Faculties of the University of Pennsylvania

in

Partial Fulfillment of the Requirements for the

Degree of Doctor of Philosophy

2016

Supervisor of Dissertation

_____

Mark A. Lemmon

Professor and Chairman of Biochemistry and Biophysics

Graduate Group Chairperson

_____

Kim Sharp, Associate Professor of Biochemistry and Biophysics

Dissertation Committee

Ronen Marmorstein, Professor of Biochemistry and Biophysics

Morris J. Birnbaum, Professor of Cell and Molecular Biology

Ben E. Black, Associate Professor of Biochemistry and Biophysics

Ravi Radhakrishnan, Professor of Bioengineering

Jeremy E. Wilusz, Assistant Professor of Biochemistry and Biophysics

Todd Strochlic, Assistant Professor of Biochemistry and Molecular Biology, Drexel University

ACKNOWLEDGMENT

I would like to express the deepest appreciation to my mentor, Mark A. Lemmon for his dedication and support throughout my graduate school years. He is truly an invaluable source of great guidance as to how best to carry projects forward even in dark hours, and his outstanding passion about science truly motivates and energizes me.

I thank all of past and present Lemmon lab members for their cheerful support and for creating an exceptional environment to work personally and professionally. They include Diego Alvarado, Steve Artim, Nick Bessman, Scott Bresler, Pamela Burgess-Jones, SungHee Choi, Dan Freed, Jon Kenniston, Anatoly Kiyatkin, Jeannine Mendrola, Jason Moore, Katarina Moravcevic, Camilla Oxley, Fumin Shi, Kelsey Speer, and Neo Wu. Thank you all for keeping me company on long walks. I also thank Kate Ferguson for her guidance and members of her lab, Atrish Bagchi, Ryan Emptage, and Yu-San Huoh for their support.

I am grateful to these collaborators for insightful discussions during our research together: Yael Mossé, Ravi Radhakrishnan, Kevan Shokat and members of their laboratories.

I also thank my thesis committee chair Prof. Ronen Marmorstein and other committee members Prof. Ben Black, Prof. Ravi Radhakrishnan, and Dr. Morris Birnbaum for their invaluable support and suggestions over the years.

Lastly, I would like to give very special thanks to all of my friends and family. I thank my father, mother and sister for continuous love, support and encouragement, and for believing in me.

ABSTRACT

INHIBITION OF VARIOUS RECEOPTOR TYROSINE KINASE (RTK) FAMILIES

Jin H. Park

Mark A. Lemmon

Activation of cell surface growth factor receptor tyrosine kinases (RTKs) results in cellular proliferation, differentiation and survival. Humans have 58 RTKs, categorized into twenty subfamilies based on their structural properties and ligand specificity. One of the most well-studied RTKs, the epidermal growth factor receptor (EGFR), is mutated or overexpressed in many human cancers including non-small cell lung cancer and glioblastoma. Several EGFR inhibitors have been approved by the FDA, and numerous additional inhibitors are being pursued as potential cancer therapeutics. Structural studies of the EGFR tyrosine kinase domain suggest that different inhibitors bind selectively to either the active or the inactive conformation of the kinase. Contrary to this supposition, computational studies of inhibitor-stabilized EGFR conformations have suggested that erlotinib can bind equally well to either the active or inactive forms of the EGFR kinase domain. We tested this hypothesis using a mutated EGFR kinase domain that can adopt either the inactive or active kinase conformation in crystals, and determined a structure with erlotinib bound to the inactive conformation – suggesting that this inhibitor can bind either 'state'. We also determined the crystal structure of this EGFR kinase variant bound to a novel ErbB2 inhibitor (55A) found in screens designed to select inhibitors that bind the active state. When bound to this compound, the EGFR kinase domain adopted only the active conformation, suggesting that erlotinib and 55A select different kinase 'states'. Collaborative approaches combining biochemical, structural and cell signaling studies suggest new considerations in predicting modes of inhibitor binding in the development of therapeutic agents for cancer.

Several activating mutations in the anaplastic lymphoma kinase (ALK) gene have been implicated in neuroblastoma. The small molecule tyrosine kinase inhibitor crizotinib, which inhibits ALK and Met, was recently approved by the FDA for the treatment of non-small cell lung cancer (NSCLC), and is currently in early-phase clinical testing in patients with neuroblastoma (NB). Numerous additional ALK inhibitors are also being pursued as potential therapeutics. However, more and more mutations in the ALK tyrosine kinase domain (TKD) are being found in patients with neuroblastoma. Several of these are associated with primary resistance to currently available ALK inhibitors, and several mutations in oncogenic ALK fusions have been linked to acquired crizotinib resistance. Understanding how different ALK mutations activate its kinase domain, and how they change inhibitor sensitivity, is therefore crucial for further clinical development of ALK-targeted therapeutics. We have studied the biochemical consequences of a wide variety of ALK kinase domain mutations in parallel both with studies of their transforming abilities and computational studies of their structural effects. Our first goal was to use these data to predict the effects of new clinically emerging ALK mutations on ALK's transforming ability, signaling activity, and drug sensitivity. A second goal was to identify the most potent ALK inhibitor that has inhibitory effects on the widest possible range of ALK mutants using biochemical and cellular assays, with a view to identifying a clinical path forward. Our studies provide valuable mechanistic insight into how ALK is regulated, and also lay important groundwork for guiding more refined targeted therapy in neuroblastoma patients.

TABLE OF CONTENTS

ACKNOWLEDGMENT ii

ABSTRACT iii

LIST OF TABLES viii

LIST OF ILLUSTRATIONS ix

CHAPTER 1: INTRODUCTION 1

1.1 Catalytic mechanism of receptor tyrosine kinase (RTK) family 2

1.2 General features of tyrosine kinase domains 4

1.3 Diverse mechanism of RTK activation 6

1.4 Autoregulatory mechanism of intracellular kinase domain in RTKs 8

1.5 RTKs in disease 13

1.6 RTKs are important therapeutic targets 15

1.7 References 17

CHAPTER 2: STRUCTURAL STUDIES OF ERBB RECEPTOR TYROSINE KINASE DOMAINS WITH SMALL MOLECULE INHIBITORS 23

2.1 Selective inhibition of EGFR 24

2.1.1 Introduction 24

2.1.2 Current view of conformational selectivity of EGFR inhibitors 28

2.1.3 Computational analysis of erlotinib binding to EGFR-TKD 30

2.1.4 Computational studies of erlotinib binding to inactive EGFR-TKD 33

2.1.5 Crystal structure of erlotinib bound to inactive EGFR-TKD 35

2.1.6 Conclusions 41

2.2 Selective inhibition of HER2/HER3 oncogenic complex 43

2.2.1 Introduction 43

2.2.2 Possible importance of the intrinsic kinase activity of ErbB3 in ErbB signaling 45

2.2.3 Identification of a novel inhibitor of the ErbB2/ErbB3 heterodimer through high throughput cell-based screening 48

2.2.4 55A is differentiated from clinically available ErbB inhibitors 51

2.2.5 Structural characterization of a 55A-bound ErbB kinase domain by X-ray crystallography 53

2.2.6 Conclusions 58

2.3 Experimental Procedures 58

2.3.1 Plasmid Construction 58

2.3.2 Protein production and purification 59

2.3.3 Crystallization and structure determination 59

2.3.4 Analysis of autophosphorylation by western blotting 61

2.3.5 Molecular modeling: System preparation and molecular docking 61

2.3.6 MD simulations 62

2.3.7 MM/PBSA (molecular mechanics/Poisson-Boltzmann surface area) calculation 62

2.4 References 62

CHAPTER 3: ACTIVATION AND INHIBITION OF ANAPLASTIC LYMPHOMA KINASE (ALK) IN NEUROBLASTOMA 69

3.1 Introduction 70

3.2 Activity of mutated ALK-TKD in its non-phosphorylated form is an excellent predictor of transforming ability in NIH 3T3 cells 72

3.3 Computational methodology for predicting structural consequences of ALK-TKD mutations with low false positives 77

3.4 Ongoing collaborative efforts to improve a predictive model with iteration between biochemical/cellular studies and MD-based computational analysis of mutated ALK TKDs 80

3.5 ALK variants found in neuroblastoma are differentially sensitive to the inhibitor crizotinib 83

3.6 Identification of the next-generation ALK/ROS1 inhibitor PF-06463922 as capable of overcoming primary resistance to crizotinib in ALK-driven neuroblastoma 84

3.7 PF-06463922 induces complete tumor regression in patient-derived and cell line- derived xenografts with and without primary resistance to crizotinib 86

3.8 PF-06463922 efficiently inhibits ALK phosphorylation *in vivo* 93

3.9 PF-06463922 inhibits growth of ALK-mutated neuroblastoma cell lines at approximately 20- to 125-fold lower concentrations than crizotinib 94

3.10 Comparison of effects on ALK phosphorylation in cell lines 97

3.11 Inhibition of NIH 3T3 cell transformation by mutated ALK 99

3.12 Conclusions 100

3.13 Experimental Procedures 102

3.13.1 Plasmid Construction 102

3.13.2 Recombinant protein expression and purification 103

3.13.3 Peptide phosphorylation assays 103

3.13.4 *In vitro* analysis of ALK-TKD variants Inhibition 104

3.13.5 *In vivo* efficacy studies 105

3.13.6 Statistical analysis of *in vivo* efficacy studies 105

3.13.7 Cell line and reagents 106

3.13.8 *In vitro* pharmacologic growth inhibition 106

3.13.9 Focus formation assays 107

3.13.10 Western blot analysis 108

3.13.11 Western blot analysis of xenograft tumors 109

3.14 References 109

CHAPTER 4:CONCLUSIONS AND FUTURE DIRECTIONS 114

LIST OF TABLES

Table 2.1 Erlotinib-binding energies calculated by Glide, MM/PBSA and FEP for wild-type and L834R EGFR-TKD in the active conformation ……32

Table 2.2 Data collection and refinement statistics (molecular replacement) ……..39

Table 2.3 Data collection and refinement statistics (molecular replacement) ……..57

Table 3.1 Computational predictions of effects of ALK TKD mutations……..79

Table 3.2 Statistical analysis for in vivo efficacy studies in PDXs from COG-N-453x and Felix cells, and xenografts from SH-SY5Y and NB-1643 cells ……..89

Table 3.3 Statistical analysis for Felix-PDX and SH-SY5Y *in vivo* efficacy studies testing two doses of PF-06463922 (10 mg/kg/day and 3 mg/kg/day) ……..91

Table 3.4 PF-06463922 is potent against ALK-mutated NB cell lines *in vitro*. ……..95

LIST OF ILLUSTRATIONS

Figure 1.1 Receptor tyrosine kinases families 3

Figure 1.2 Active structure of the Insulin receptor TKD 5

Figure 1.3 Sequence alignments of the partial catalytic domains from the 12 RTKs 6

Figure 1.4 Regulatory mechanisms of receptor tyrosine kinases 10

Figure 1.5 Allosteric activation of the EGFR TKD by asymmetric dimerization 12

Figure 2.1 Cartoon representation of the active and inactive conformations of the EGFR kinase domain. 26

Figure 2.2 Differential sensitivity of endogenously expressed glioma- versus lung cancer–specific EGFR mutants to lapatinib versus erlotinib. 28

Figure 2.3. Erlotinib binding to active EGFR-TKD in the crystal structure (1M17) and model 31

Figure 2.4: RMSD of erlotinib and key distances between EGFR-TKD and erlotinib, as well as the distance of waters from EGFR-TKD or erlotinib monitored during 10ns MD simulation. 32

Figure 2.5 Comparison of erlotinib binding to active and inactive EGFR-TKD models 34

Figure 2.6 Comparison of RMSD values for critical hydrogen bonds in active and inactive wild-type simulations. 35

Figure 2.7 Crystal structures of TKI-bound EGFR-TKD 38

Figure 2.8 Erlotinib binding to inactive EGFR-TKD 40

Figure 2.9 Influences of intrinsic kinase activity of ErbB3 in induced autophosphorylation of ErbB2/ErbB3 heterodimer and signaling 47

Figure 2.10 Schematic of a high-throughput screen to identify a novel ErbB2/ErbB3 inhibitor 50

Figure 2.11. 55A is able to interact with ErbB2 and ErbB3 52

Figure 2.12 Inhibition of ErbB3 kinase autophosphorylation *in vitro* 52

Figure 2.13 Crystal structure of 55A-bound EGFR V924R kinase 55

Figure 2.14 Comparison of erlotinib-bound <u>inactive</u> conformation and 55A-bound <u>active</u> conformation of EGFR-TKD$^{672\text{-}998}$ V924R structure 56

Figure 3.1 Distribution of ALK mutations in tumor samples from neuroblastoma patients 71

Figure 3.2 Effects of neuroblastoma mutations on the activity of non-phosphorylated and fully autophosphorylated ALK-TKD variants …… 74

Figure 3.3 Transformation potential of ALK mutations from NIH 3T3 focus formation assays …….. 76

Figure 3.4 Ongoing cellular transformation studies of ALK-TKD variants using NIH3T3 focus formation assays …… 82

Figure 3.5 Inhibitor sensitivities of ALK-TKD WT, F1174L, and R1275Q …… 84

Figure 3.6 In vitro Inhibition profiles of non-phosphorylated ALK-TKD mutants against Crizotinib and PF-0643922. …… 86

Figure 3.7 *In vivo* efficacy studies comparing PF-06463922 to crizotinib. …… 88

Figure 3.8 *In vivo* effects of crizotinib and PF-06463922 on event-free survival (EFS) in neuroblastoma PDX and xenograft models. ……90

Figure 3.9 *In vivo* efficacy studies comparing PF-06463922 treatment at 10 mg/kg/day (5 mg/kg BID) and 3 mg/kg/day (1.5 mg/kg BID) with crizotinib treatment at 100 mg/kg QD in Felix-PDX xenografts and SH-SY5Y xenografts. ……..92

Figure 3.10 PF-06463922 abrogates ALK phosphorylation more effectively than crizotinib *in vivo*. ……..93

Figure 3.11 PF-06463922 inhibits viability of neuroblastoma cell lines at concentrations corresponding to clinically relevant doses (≤100 nM)…….....96

Figure 3.12 PF-06463922 displays on-target activity in neuroblastoma and NSCLC cells. ……..98

Figure 3.13 PF-06463922 is more effective than crizotinib in inhibiting NIH 3T3 cell transformation by mutated ALK variants……....100

CHAPTER 1:

Introduction

1.1 Catalytic mechanism of receptor tyrosine kinase (RTK) family

Kinases are enzymes that catalyze phosphotransfer or phosphorylation reactions, and in combination with phosphatases, this reversible modification represents a wide and significant mechanism utilized to modify protein function. Following the initial identification of protein phosphorylation at serines and threonines, tyrosine phosphorylation of proteins was discovered over 30 years ago, through studies of animal tumor virus transforming proteins such as the Rous sarcoma virus c-Src protein (Hunter and Sefton, 1980)

Bioinformatics and targeted cDNA cloning revealed large numbers of protein kinases, which form a large family. The catalog of human protein kinases (the kinome) compiled by Manning et al (2002) contains 58 known receptor tyrosine kinases (RTK) which are subdivided into 20 families depending on their structural properties and ligand specificity (Lemmon and Schlessinger, 2010) (Figure 1.1). They all share a similar molecular architecture, with an extracellular ligand-binding region connected to an intracellular tyrosine kinase domain (TKD) by a single transmembrane domain. Additional intracellular regulatory regions are found either in the juxtamembrane regions or the carboxy terminal tail. Ligand binding to the extracellular region of RTKs promotes homo- or heterodimerization of receptors, bringing their intracellular kinase domains into close proximity and promoting allosteric *trans*-activation and autophosphorylation at multiple tyrosine sites. Some of these phosphorylation events serve to activate the kinase itself, typically those that occur in the so-called activation loop of the kinase. Other autophosphorylation sites serve as docking sites to recruit downstream signaling molecules, which bind to phosphotyrosines via their Src homology-2 (SH2) or phosphotyrosine binding (PTB) domains. The docked adaptor proteins couple the activated receptor to various downstream signaling molecules (for example, Ras, phospholipase Cγ, and phosphatidylinositol-3-kinase), which in turn signal towards the control of key transcription factors. These signal transduction cascades are essential for various cellular processes such as proliferation, differentiation, adhesion, migration and apoptosis (Blume-Jensen and Hunter, 2001; Ullrich and Schlessinger, 1990)

A small subset of RTKs that are known to lack kinase activity cannot function in this way. These kinase-inactive RTKs, called pseudokinases, must utilize different signal transducing mechanisms. In one such example, an inactive pseudokinase RTK dimerizes with a kinase-active RTK upon ligand binding and is then phosphorylated by the active RTK to create the binding sites for downstream signaling molecules. This is true for heterodimers of ErbB3 (a pseudokinase) with ErbB2 (an active kinase), for example. Alternatively, a cytoplasmic tyrosine kinase activated by another pathway might phosphorylate the inactive RTK and produce phosphorylation sites that recruit signaling molecules to the pseudokinase.

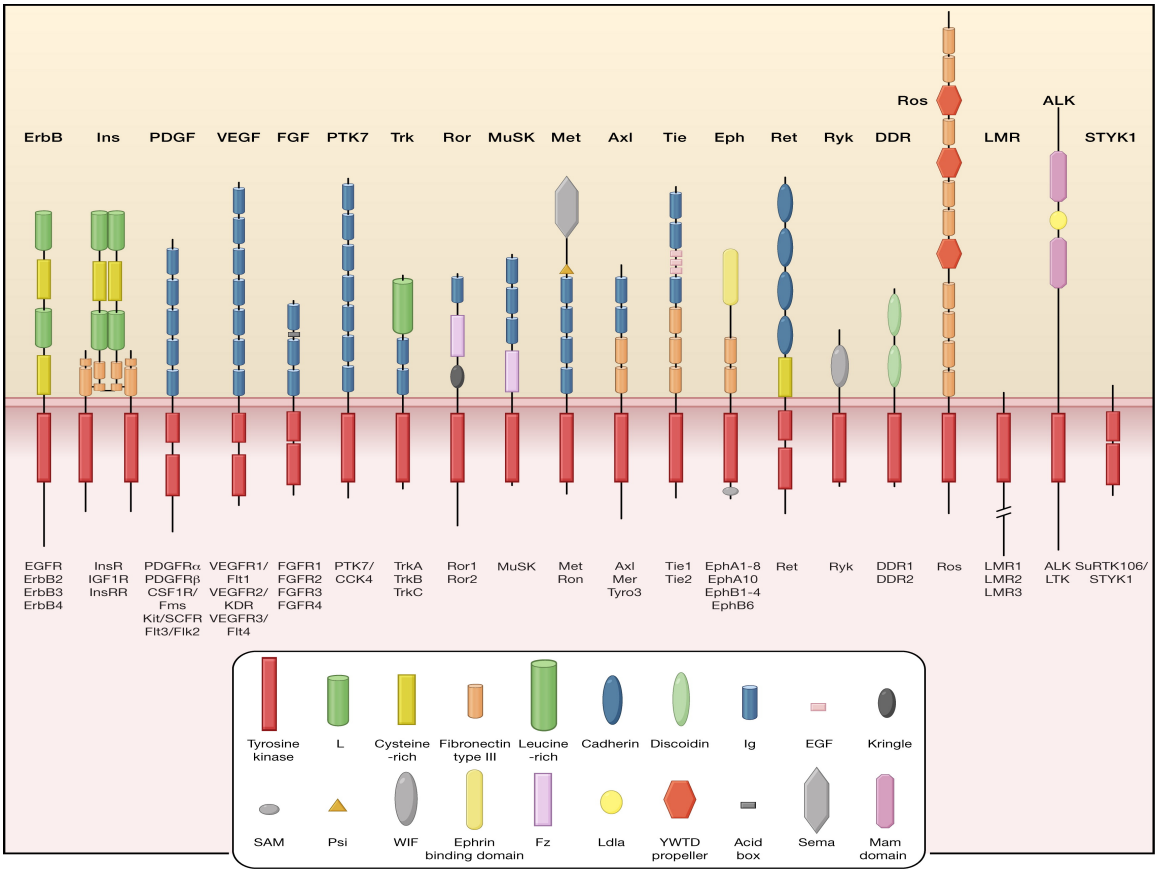

Figure 1.1 Receptor tyrosine kinases families

Schematic representation of 58 human RTKs, which fall into 20 subfamilies identified by structure determination and sequence analysis. Activation of cell surface growth factor RTKs results in cellular proliferation, differentiation and survival. (Lemmon and Schlessinger, 2010)

1.2 General features of tyrosine kinase domains

The overall structural fold is extremely well conserved among Ser/Thr and Tyr kinases, and is divided into two lobes (Huse and Kuriyan, 2002); the N-terminal lobe (N-lobe) which is involved in ATP binding and the C-terminal lobe (C-lobe) which binds the substrate while contributing to ATP binding and activation as well (Taylor et al., 2004). The ATP and peptide binding sites are formed by the interface between the two lobes. The smaller N-lobe is composed of a five-stranded β-sheet plus one α-helix (helix αC, which plays a key regulatory role), while the larger C-lobe is predominantly composed of α-helices. Protein kinase domains all adopt strikingly similar structures in the active state. Where they differ (if they differ) is in their inactive structure – each kinase family is inactivated by a unique set of autoinhibitory interactions (Lemmon and Schlessinger, 2010). Upon TKD activation through requisite receptor dimerization, these autoinhibitory interactions are broken, allowing the TKDs to adopt the canonical active structure that positions all of the critical elements involved in substrate binding and catalysis in both N- and C-lobes for phosphotransfer from the γ-phosphate of ATP to the hydroxyl group of tyrosine (Zhang et al., 2006). In most active RTKs, the activation loop – 20-30 residue-long loop providing peptide substrate binding sites when it is activated by phosphorylation – is phosphorylated and structured, leading to the stabilization of an open conformation. Helix αC in the N-lobe is also correctly positioned in the active structure by ionic interaction between a key glutamate side-chain in αC and a key lysine side-chain from β3 in the substrate binding pocket (Figure 1.2).

As shown in the sequence alignment below (Figure 1.3), there are several key well-conserved residues around the active site that are directly implicated in the catalytic mechanism. Three motifs are known to be essential. Those motifs are the Val-Ala-Ile-Lys (VAIK) motif, in which the lysine residue anchors and orients the ATP by interacting with α and β phosphates of ATP; the His-Arg-Asp (HRD) motif, in which the catalytic aspartate acts as a base acceptor to achieve proton transfer by enhancing nucleophilic attack of ATP; and the Asp-Phe-Gly (DFG) motifs where the aspartate residue chelates Mg^{2+} ions, bridging the β and γ phosphates of ATP in

the nucleotide binding cleft (Figure 1.2) (Boudeau et al., 2006). In fact, mutation of either K721 (VAIK motif) or D813 (HRD motif) in EGFR abolishes tyrosine autophosphorylation *in vivo* (Thiel and Carpenter, 2007; Zhang et al., 2006). Also, it is reported that reverting mutations of the 'DNA motif' in receptor-like tyrosine kinase (Ryk) to canonical 'DFG motif' restores catalytic activity (Katso et al., 1999). Kinase domains lacking one or more of these conserved motifs are assumed to be catalytically inactive and are termed pseudokinases.

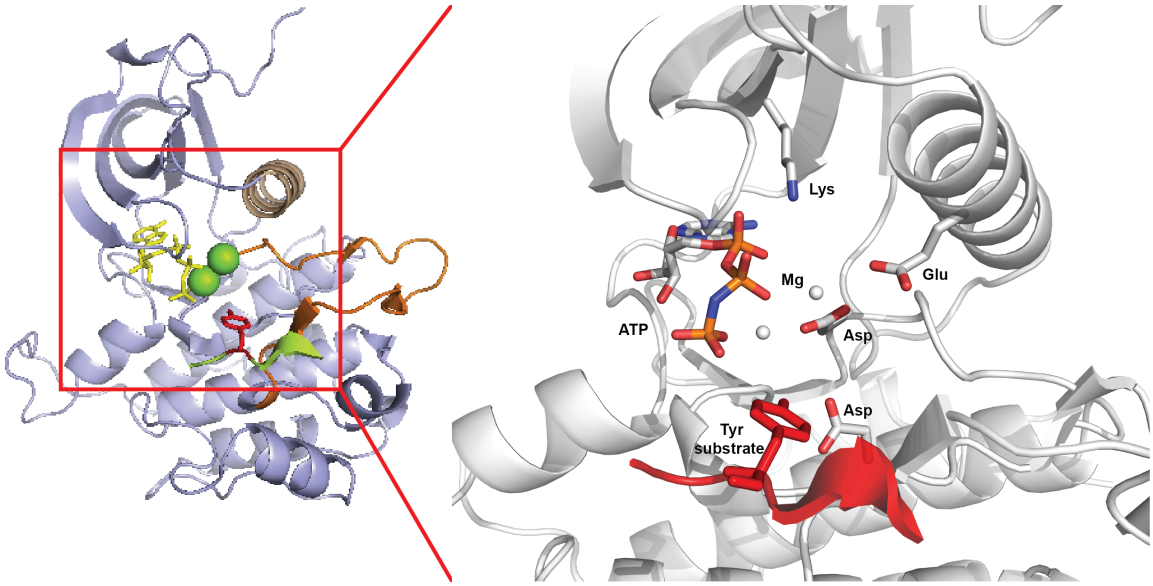

Figure 1.2 Active structure of the Insulin receptor TKD

Cartoon representation of the insulin receptor TKD in an active conformation (PDB: 1IR3), with zoomed view of the nucleotide and peptide binding cleft shown at right. Elements readily recognized in the active structure are an αC helix (colored brown) in the 'in' position, a fully ordered activation segment (colored orLysange), and a key salt bridge between the catalytic lysine residue and a glutamate residue in αC helix. Three essential motifs in catalytic domains are VAIK (subdomain II), HRD (subdomain VIb), DFG (subdomain VII).

```
VEGFR2      RIVAVKMLKEGATASEYKALMTELKILTHIGHHLNVVNLLGACTKQGG-----PLMVIVE 910  YCKYGNLSNYLKSKRDLFFLNKDAALHMEPKKEKMEPGLEQGKKPRLDSVTSSESFASSG 970
FGFR1       TKVAVKMLKSDATEKDLSDLISEMEMMKMIGKHKNIINLLGACTQDG------PLYVIVE 473  YASKGNLREYLQARR--------------------PPGLEYCYNPSHN------------ 501
PDGFR-B     MKVAVKMLKSTARSSEKQALMSELKIMSHLGPHLNVVNLLGACTKGG------PIYIITE 682  YCRYGDLVDYLHRNKHTFLQHHSDKRRPPSAELYSNALPVGLPLPSHVSLTGESDGGYMD 742
RET         TTVAVKMLKENASPSELRDLLSEFNVLKQVN-HPHVIKLYGACSQDG------PLLLIVE 805  YAKYGSLRGFLRESR------------------KVGPGYLGSGGSRNSSSLDHP------ 841
Ryk         KQAFVKVVKDQASEIQVTMMLTESCKLRGLH-HRNLLPITHVCIEEGE-----KPMVILP 415  YMNWGNLKLFLRQCK-----------------------LVEANNPQAISQQ--------- 443
TrkA        MLVAVKALKEASESAR-QDFQREALLTMLQ-HQHIVRFFGVCTEGR------PLLMVFE 590  YMRHGDLNRFLRSHG-------------------PDAKLLAGGEDVAPGPLGLG------ 625
INSR        TRVAVKIVNESASLRERIEFLNEASVMKGFT-CHHVVRLLGVVSKGQ------PTLVVME 1104 LMAHGDLKSYLRSLR-----------------------PEAENNPGRPPPTLQ------- 1134
CCK4        TLVLVKSLQSKD-EQQQLDFRRELEMFGKLN-HANVVRLLGLCREAE------PHYMVLE 876  YVDLGDLKQFLRISK-----------------------SKDEKLKSQPLSTK-------- 905
Axl         -VAVKMKIAICTRSELEDFLSEAVCMKEFD-HPNVMRLIGVCFQGSERESFPAPVVILP 612  FMKHGDLHSFLLYSR-------------------------LGDQPVYLPTQ--------- 638
Ror1        QLVALKTLKDYNNPQQWTEFQQEASLMAELH-HPNIVCLLGAVTQEQ------PVCMLFE 553  YINQGDLHEFLIMRSP-----------------HSDVGCSSDEDGTVKSSLDHG------ 590
Tie1        --AALKMLKEYASENDHRDFAGELEVLCKLGHHPNIINLLGACKNRG------YLYIAIE 918  YAPYGNLLDFLRKSR------------------VLETDPAFAREHGTASTLSSR------ 954
EGFR        IRVAIKELREATSPKANKEILDEAYVMASVD-NPHVCRLLGICLTST-------VQLITQ 791  LMPFGCLLDYVREHK--------------------------DNIGSQY------------ 813

VEGFR2      FQEDKSLSDVEEEEDSDGFYKEPITME--------------------------------D 998  LISYSFQVARGMEFLSSRKCIHRDLAARNILLSENNVVKICDFGLARDIYKNPDYVRKGD 1058
FGFR1       -------------------PEEQLSSK--------------------------------D 510  LVSCAYQVARGMEYLASKKCIHRDLAARNVLVTEDNVMKIADFGLARDIHHIDYYKKTTN 570
PDGFR-B     MSKDESVDYVPMLDMKGDVKYADIESSNYMAPYDNYVPSAPERTCRATLINESPVLSYMD 802  LVGFSYQVANGMEFLASKNCVHRDLAARNVLICEGKLVKICDFGLARDIMRDSNYISKGS 862
RET         -------------------DERALTMG--------------------------------D 850  LISFAWQISQGMQYLAEMKLVHRDLAARNILVAEGRKMKISDFGLSRDVYEEDSYVKRSQ 910
Ryk         ------------------------------------------------------------D 444  LVHMAIQIACGMSYLARREVHRDLAARNCVIDDTLQVKITDFGLSRDLFPMDYHCLGDN 504
TrkA        ------------------------------------------------------------Q 626  LLAVASQVAAGMVYLAGLHFVHRDLATRNCLVGQGLVVKICDFGMSRDIYSTDYYRVGGR 686
INSR        ------------------------------------------------------------E 1135 MIQMAAEIADGMAYLNAKKFVHRDLAARNCMVAHDFTVKIGDFGMTRDIYETDYYRKGGK 1195
CCK4        ------------------------------------------------------------Q 906  KVALCTQVALGMEHLSNNRFVHRDLAARNCLVSAQRQVKVSALLSKDVYNSEYYHFR-Q 965
Axl         ------------------------------------------------------------M 639  LVKFMADIASGMEYLSTKRFIHRDLAARNCMLNENMSVCVADFGLSKKIYNGDYYRQGRI 699
Ror1        ------------------------------------------------------------D 591  FLHIAIQIAAGMEYLSSHFFVHRDLAARNILIGEQLHVKISDLGLSREIYSADYYRVQSK 651
Tie1        ------------------------------------------------------------Q 955  LLRFASDAANGMQYLSEKQFIHRDLAARNVLVGENLASKIADFGLSR---GEEVYVKKTM 1012
EGFR        ------------------------------------------------------------     LLNWCVQIAKGMNYLEDRRLVHRDLAARNVLVKTPQHVKITDFGLAKLLGAEEKEYHAEG 873
```

Figure 1.3 Sequence alignments of the partial catalytic domains from the 12 RTKs

3 conserved motifs for catalysis are boxed, and highly conserved residues are indicated by black boxes with white lettering

1.3 Diverse mechanism of RTK activation

It is broadly accepted that ligand binding to RTKs induces receptor dimerization and thus leads to their activation (Ullrich and Schlessinger, 1990). For example, in the absence of bound growth factor EGF, the human epidermal growth factor receptor (EGFR) remains largely as monomers. Its extracellular region forms a ‘tethered’ conformation in which a key dimerization site is occluded by intramolecular interactions, and the intracellular kinase domain is inactive. However, when ligand binds to the extracellular regions of EGFR, it changes its conformation dramatically to an ‘extended’ conformation in which a key dimerization arm is exposed, and drives dimerization of the receptor (Burgess et al., 2003). This ligand-induced dimerization of the extracellular region brings the two kinase domains in an EGFR dimer into close proximity such that one activates the other allosterically in an activating intracellular dimer. Although the contribution of the single transmembrane (TM) helix that connects the extracellular and the intracellular regions to EGFR activation is not yet clear, it does appear that the TM helices do promote receptor dimerization in

some cases (Moore et al., 2008). A similar paradigm seemingly applies to many other RTKs such as stem cell factor receptor KIT, vascular endothelial growth factor receptor VEGFR, and nerve growth factor receptor TrkA, although details of both the dimerization mechanism and kinase activation mechanism have unique features.

Interestingly, there are also RTKs that form oligomers in the absence of activating ligand. For example, the insulin receptor (IR) and other members of the IR subfamily, including the insulin-like growth factor-1 receptor (IGF1R) are preformed, disulfide-linked heterotetramers with two extracellular alpha subunits and two membrane-spanning, tyrosine-kinase containing beta subunits on the cell surfaces. Ligand binding to the insulin and IGF1 receptors must promote activation by triggering conformational changes within the dimer to stimulate the tyrosine kinase domains (TKD) – activating the kinase by promoting *trans*-phosphorylation (Ward et al., 2007). In addition, the Eph and Tie2 angiopoietin cell surface receptors are suggested to require the formation of even larger oligomers for efficient signaling although the exact role of these larger oligomers is still not fully understood (Barton et al., 2006; Himanen and Nikolov, 2003). And of course, there are cases like anaplastic lymphoma kinase (ALK) receptor whose nature of ligand still remains elusive for binding and activation – although a ligand called augmentor has recently been proposed as an ALK activator (Murray et al., 2015).

In all cases, though, whether the RTK is monomeric or dimeric before ligand binding, the common paradigm is that ligand binding must stabilize a specific dimer in which a particular relationship between the receptor molecules is promoted and leads to activation. Once stimulated with ligand, one receptor of a dimer/oligomer phosphorylates one or more tyrosine in its neighbor, and the tyrosine-phosphorylated RTK functions as a docking site, enabling recruitment of intracellular signaling molecules containing pTyr-binding domain such as SH2 and PTB, and direct phosphorylation of substrate to propagate downstream signaling (Pawson et al., 2001; Schlessinger and Lemmon, 2003).

1.4 Autoregulatory mechanism of intracellular kinase domain in RTKs

It has been gradually uncovered how ligand-induced extracellular dimerization or oligomerization is coupled to activation of the intracellular tyrosine kinase domain (TKD) in many RTKs. Surprisingly, the activation mechanisms of different RTKs are quite different, although a common element of their activation in RTK signaling involves autophosphorylation of intracellular regions of the receptor. Each RTK is held in an inactive state by a characteristic set of autoinhibitory interactions. Release of this autoinhibition is responsible for receptor activation in response to extracellular stimuli, such as growth factors.

The first crystal structure of the insulin receptor TKD revealed the first RTK autoinhibition mechanism to be appreciated (Hubbard et al., 1994). In the absence of Mg^{2+}-ATP, the unphosphorylated activation loop in IRK makes autoinhibitory interactions, in which a key tyrosine Y1162 in the activation loop (in the sequence YxxxYY) projects into the active site of the kinase and makes a hydrogen bond with the catalytic base aspartate D1132. In this configuration (Figure 1.4, Inactive A), the N-terminal end of activation loop (DFG motif) also blocks access of ATP to the kinase. As a result, the insulin receptor kinase domain is *cis*-autoinhibited by its own activation loop (blocking ATP and protein substrate binding), and is activated following insulin binding by *trans*-autophosphorylation on Y1162 by its own partner to release these autoinhibitory interactions. A crystal structure of the fibroblast growth factor receptor 1 (FGFR1) tyrosine kinase domain revealed that FGFR1 also employs a conceptually similar autoinhibitory mechanism. Even though the unphosphorylated Y653 (equivalent to Y1162 in IRK) does not directly occupy the substrate-binding site, it is held in a location such that the C-terminal end of the activation loop interferes with substrate binding (Mohammadi et al., 1996). Upon FGF binding, receptor dimerization allows *trans*-phosphorylation of the activation loop tyrosines and thus breaks this *cis*-autoinhibitory interaction – allowing the kinase to adopt the characteristic active configuration (or destabilizing inactive configuration).

The intracellular regions of RTKs also contain other regulatory elements outside of the TKD, such as the intracellular juxtamembrane segment (iJM) and carboxy-terminal (C-terminal)

tail; these are also implicated in the mechanisms of intracellular kinase domain regulation. The JM region is known to play regulatory roles in *cis*-autoinhibition in the Eph receptors (Wybenga-Groot et al., 2001), the platelet-derived growth factor receptor (PDGFR) family Flt3 (Griffith et al., 2004) and KIT (Mol et al., 2004), and Musk (Till et al., 2002) from biochemical and structural studies. Again, the precise mechanisms differ in details among different RTKs, but all autoinhibitory interactions involve a key tyrosine in the JM region making extensive contacts with the TKD and stabilizing an autoinhibited inactive conformation of the receptor (Figure 1.4, Inactive B). Activation of these receptors requires disruption of *cis*-autoinhibitory interaction by *trans*-autophosphorylation promoted by ligand-induced receptor dimerization (Hubbard, 2004).
In KIT/PDGFR, the key residues that maintain autoinhibitory JM interactions turn out to be oncogenic hot spots; mutations that release the autoinhibitory restraints activate RTKs constitutively and are frequently found in human cancers (Dibb et al., 2004). Interestingly, the JM region of EGFR stands in contrast to these cases and functions as an activating (rather than inhibitory) domain, by stabilizing the dimerization interface between two interacting kinase domains (Jura et al., 2009; Red Brewer et al., 2009). A V665M mutation in this region that stabilizes JM-mediated interactions has been found to promote cellular transformation and tumorigenesis, highlighting the complexity of regulatory mechanisms in RTKs and the necessity of further understanding this JM region.

Additional autoregulatory interactions are seen that involve the C-terminal tail of the receptor, exemplified by the angiopoietin receptor Tie2. According to the general mechanism of RTK activation, the C-tail of each receptor serves as docking sites for SH2 and PTB domain containing proteins once phosphorylated; and its phosphorylation also works as a tool to tightly regulate catalytic activity of the kinase on multiple levels. In the Tie2 kinase domain, the activation loop adopts an active-like conformation independent of phosphorylation. In the inactive conformation of the receptor, however, the C-tail adopts an extended conformation and projects into the active site to block substrate access and inactivate the receptor (Figure 1.4, Inactive C) (Shewchuk et al., 2000). Mutated Tie2 with deleted C-terminal residues exhibits enhanced kinase

activity and signaling compared to wild-type Tie2 (Niu et al., 2002). In much the same way that *trans*-autophosphorylation of tyrosines in the activation loop or juxtamembrane segment release *cis*-autoinhibitory interaction in panels A and B of Figure 1.4 to activate RTKs, autophosphorylation of the C-tail of Tie2 is thought to be a key for disrupting its autoinhibitory interactions with TKD – leading to receptor activation.

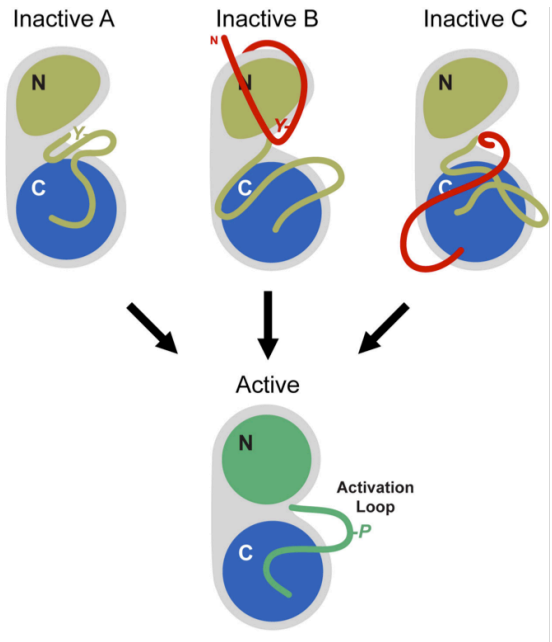

Figure 1.4 Regulatory mechanisms of receptor tyrosine kinases

Dimerization of RTKs allows autophosphorylation of tyrosine in the activation loop (Inactive A), the juxtamembrane segment (Inactive B), and/or the C-terminal tail (Inactive C) to release autoinhibitory interactions for activation of intracellular kinase domains of RTKs (Lemmon and Schlessinger, 2010).

We have so far seen that even though different RTKs are autoinhibited by mechanisms that differ in detail, *trans*-phosphorylation of a key 'inhibitory' tyrosine is a key step, whether that occurs in the activation loop, juxtamembrane segment, or C-tail. In each case, bringing two TKDs together into a specific dimer increases the probability of *trans*-phosphorylation at particular sites, which in turn leads to receptor activation. Interestingly, the one RTK family for which a phosphorylation event of this sort is not required is the EGFR/ErbB family (Burgess et al., 2003; Gotoh et al., 1992; Jura et al., 2011). Instead, crystal structures of the activated EGFR TKD, combined with mutational studies, have revealed that the EGFR TKD is activated by allosteric interaction between the kinase domains of adjacent molecules in a dimer. The mechanism is much like that observed in the activation of cyclin-dependent kinases (CDKs) by cyclins (Zhang et al., 2006). As depicted in Figure 1.5, the helical C-lobe of one EGFR TKD (the 'activator') abuts the N-lobe of another EGFR TKD (the 'receiver') in an asymmetric TKD dimer. This dimerization induces conformational changes in the asymmetric dimer interface that breaks *cis*-autoinhibitory interactions within the N-lobe of the receiver TKD seen in inactive EGFR TKD crystal structures, and causes the kinase to adopt the active conformation (αC helix in position, salt bridge between catalytic lysine residue and glutamate residue in αC helix, and fully structured activation loop). Helical cyclins achieve similar allosteric activation of CDKs by abutting their N-lobe. Mutational studies on the asymmetric EGFR TKD dimerization interface confirmed its importance for EGFR activation. Moreover, whereas the wild-type EGFR TKD always forms this asymmetric dimer in crystals – and is thus always seen in its active conformation, an EGFR TKD V924R mutant in which the interface is disrupted crystallizes in the inactive conformation (Zhang et al., 2006). The hydrophobic interaction at the asymmetric dimer interface promotes dimerization that induces conformational changes to the N-lobe of the acceptor kinase, leading to activation of EGFR TKD. ErbB4 and ErbB2 TKDs form similar dimers in crystals, arguing that they share this activation mechanism.

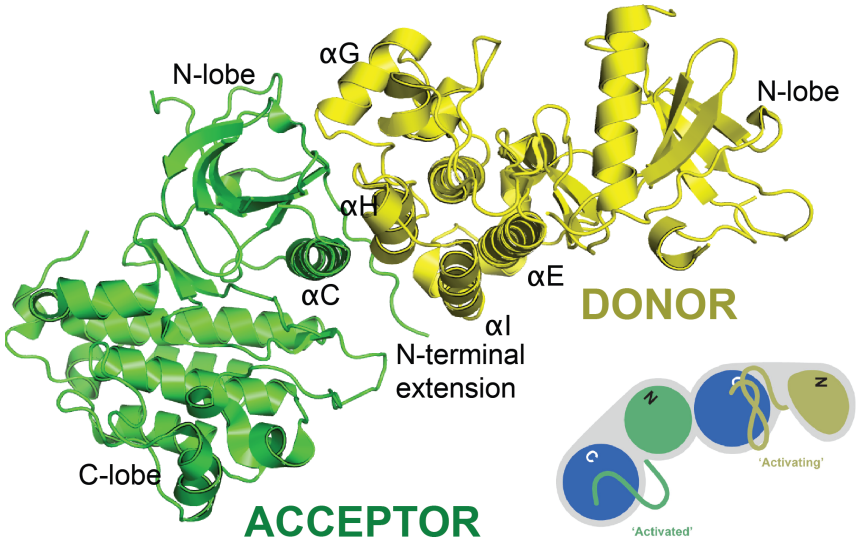

Figure 1.5 Allosteric activation of the EGFR TKD by asymmetric dimerization

The EGFR TKD does not require phosphorylation of the activation loop for TKD activation. Dimerization induces conformational changes in the EGFR TKD, which is allosterically activated by direct contacts between the C-lobe of the activator kinase (donor, colored yellow) and the N-lobe of receiver kinase (acceptor, colored green) (Red Brewer et al., 2009).

1.5 RTKs in disease

Activation of cell surface growth factor RTKs plays important roles in cellular proliferation, differentiation and survival. It is also well known that unregulated inappropriate activation of many RTKs is involved in development of various human cancers. From the initial observation of the effect of aberrant growth factor signaling in cell transformation in the 1960s (Temin, 1966), numerous studies of unregulated RTKs in human diseases have accumulated. RTK dysfunction in cancer can be categorized into four principal mechanisms: autocrine activation, gain-of-function mutations, overexpression, or chromosomal translocations (Lemmon and Schlessinger, 2010).

Gain-of-function mutations in KIT are located in a cluster within the TKD, intracellular JM region and extracellular ligand-binding region (Corless and Heinrich, 2008). Intracellular mutations disrupt *cis*-autoinhibitory restraints in the KIT TKD, and thus activate the receptor constitutively. Extracellular mutations stabilize homotypic interactions between the membrane-proximal D5 domains, thus promoting constitutive receptor dimerization (Lemmon and Schlessinger, 2010; Yuzawa et al., 2007). Overactivity of KIT due to these gain-of-function mutations has been observed in many diseases such as gastrointestinal-stromal tumors (GIST), acute myeloid leukemia (AML), mastocytosis, and melanoma (Lemmon and Schlessinger, 2010).

Chromosomal translocations result in the expression of dimeric fusion proteins with potent oncogenic function. Expression of activated fusion proteins containing the TKDs of FGFR1 or FGFR3 have been identified in variety of cancers. FGFR1 has 11 fusion partners, and most of them have been identified in patients with the myeloproliferative disorder stem cell leukemia/ lymphoma (SCLL). Translocation leading to FGFR3 overexpression under the control of a strong enhancer region has also been identified in multiple myelomas (MM) (Ahmad et al., 2012). Various types of skeletal dysplasias have been connected to gain-of-function mutations in FGFR1, FGFR2 and FGFR3 as well (Eswarakumar et al., 2005).

The EGFR/ErbB family RTKs are well known for their oncogenic potential, and EGFR is one of the most well-studied RTKs structurally and biochemically. Members of this family are overexpressed or mutated in several cancers. The orphan receptor ErbB2 adopts an extended conformation in its extracellular region in the absence of ligand (Burgess et al., 2003), and has been shown to exhibit strong transforming potential when overexpressed in NIH3T3 cells (Di Fiore et al., 1987). ErbB2 overexpression as a result of gene amplification is found in ~30% of breast cancer patient (Slamon et al., 1989). Amplification of the *EGFR* gene results in overexpression of EGFR in glioblastoma (Libermann et al., 1985). An oncogenic truncation, known as EGFR variant III (deletion of residues 6-273) and several point mutations in the extracellular region have been reported in glioblastoma patients (Lee et al., 2006). Surprisingly, EGFR variant III (vIII) shows constitutive TKD activity despite the absence of residues that correspond to the dimerization arm, which is known to be key for activation of the wild-type receptor (Burgess et al., 2003). The fact that EGFRvIII has constitutive kinase activity even though it cannot dimerize through the same mechanism as the wild-type receptor suggests the possibility of EGFRvIII aggregation in ER due to misfolding (Lemmon and Schlessinger, 2010). One example of an oncogenic mutated RTK that is known to be activated as a consequence of misfolding in the ER is Flt3-ITD (Choudhary et al., 2009). Point mutations in the EGFR extracellular region that are seen in glioblastoma may alternatively weaken the autoinhibitory tether and thus induce activation of EGFR.

Point mutations, insertions and deletions in the TKD of EGFR have been identified in non-small cell lung cancer (NSCLC) patients. In clinical trials of the EGFR-specific inhibitor gefitinib in NSCLC patients, it was found that about 10% of patients responded, and each of those that did respond carried somatic mutations in key elements of the EGFR TKD, leading to disruption of the *cis*-autoinhibitory interactions described above (Lynch et al., 2004; Sharma et al., 2007; Zhang et al., 2006). These mutations trigger constitutive activation and cause the EGFR to be an oncogenic driver. For example, the L834R mutation (also referred as L858R) lies in the activation loop and destabilizes a conserved hydrophobic interaction between the αC helix and a

short helix found in the activation loop in only the inactive conformation of the TKD. This mutation, which accounts for ~40% of EGFR mutations in cancer (Eck and Yun, 2010) mimicks the allosteric activation mechanism depicted in Figure 1.5. Another activating mutation, V665M, occurs in the JM region, and stabilizes key acceptor/donor interactions to constitutively activate EGFR in lung cancer (Red Brewer et al., 2009).

Oncogenic ALK alterations were initially discovered in anaplastic large cell lymphoma (ALCL), where a chromosomal translocation leads to fusion of the ALK intracellular region to nucleophosmin (NPM) making a dimeric (active) form of ALK-TKD that is expressed in the cytosol (Morris et al., 1994). Additional potent oncogenic fusion proteins are also found in non-small cell lung cancers (NSCLC), inflammatory myofibroblastic tumors (IMTs) and other cancers (Palmer et al., 2009; Soda et al., 2007). More recently, activating mutations in the full-length ALK RTK were discovered in approximately 8% of neuroblastoma (Chen et al., 2008; George et al., 2008; Janoueix-Lerosey et al., 2008; Mosse et al., 2008).

Advances in sequencing technology have dramatically accelerated the pace of discovery of RTK mutations in cancer, as listed in the COSMIC (Catalogue Of Somatic Mutation In Cancer) database (Shepherd et al., 2011). It has been quite clear from the beginning, however, that not all of these mutations are activating, and many of them are already known to be so-called 'passenger' mutations (or variants of unknown significance) rather than *bona fide* 'driver' mutations (Dancey et al., 2012). Biochemical and cellular analyses, aided by structural studies are essential in order to utilize these genetic studies to understand the consequence of each mutation and to identify the best strategies for inhibiting aberrant RTK activities pharmacologically.

1.6 RTKs are important therapeutic targets

Given that many RTKs are involved in development of human diseases, RTKs are highly promising therapeutic targets. Numerous drugs have been developed for treating diseases

driven by RTKs, and several FDA-approved drugs are now being applied in the clinic (Lemmon and Schlessinger, 2010). Pharmacological inhibitors of aberrant signaling by oncogenic RTKs generally fall into two categories: monoclonal antibodies and small molecule inhibitors. Monoclonal antibodies targeting the extracellular region of RTK can function either by competing with ligand binding or by binding to different region of the extracellular region to inactivate the receptor allosterically. In addition, antibodies can induce cell-mediated immunological responses against the target cancer cell. Cetuximab and trastuzmab are examples of chimeric or humanized monoclonal antibodies that bind to the extracellular regions of EGFR and ErbB2 respectively, and are used in treatment of mammary carcinoma (trastuzumab) and colorectal and head and neck cancers (cetuximab) (Reichert and Valge-Archer, 2007). Small molecule inhibitors target the ATP binding site of the intracellular kinase domain, competing with ATP for binding to the active site of kinase. Several are now in clinical use. Imatinib (Gleevec®) targets Abl kinase and KIT. Erlotinib (Tarceva®), gefitinib (Iressa®) and lapatinib (Tykerb®) all target EGFR (lapatinib also inhibits ErbB2). Crizotinib (Xalkori®), which is a subject of my research, as described later in this thesis, targets ALK and Met (Christensen et al., 2007; Shawver et al., 2002). These small molecule inhibitors have mostly been identified through chemical library screening. Although several have been successful in initial applications, subsequent development of acquired resistance (or discovery of primary resistance) has underlined the need for application of these drugs in patients to be accompanied by guidance from biochemical and genetic studies of the target RTKs. For example, the EGFR-specific inhibitor gefitinib did not seem very promising in initial trials, since there was no patient stratification based on EGFR – and an assumption that EGFR was generally important. The drug was not effective in the general population of lung adenocarcinoma patients (Fukuoka et al., 2003; Kris et al., 2003), but even showed high efficacy in lung cancer in a subset of patients (never-smoker Asian female) whose oncogenic driver mutations were later found in EGFR TKD (Thatcher et al., 2005). The lesson from this is that identifying the driver is key to the success of targeted therapies. Small molecule tyrosine kinase inhibitors have shown to successfully inhibit kinase activity in treatment of several different cancers, however there are still

significant hurdles to overcome such as the possibility of off-target effect especially, since these drugs all target the ATP binding site which look very similar among different kinases, as well as drug resistance through development of drug-resistant variants of the target or other compensatory signaling networks. Therefore, a full understanding the mechanism of activation as well as drug resistance guided by biochemical, genetic and structural studies is invaluable for guiding patent treatment and designing novel therapeutic approaches.

1.7 References

Ahmad, I., Iwata, T., & Leung, H. Y. (2012). Mechanisms of FGFR-mediated carcinogenesis. *Biochim Biophys Acta, 1823*(4), 850-860. doi: 10.1016/j.bbamcr.2012.01.004

Barton, W. A., Tzvetkova-Robev, D., Miranda, E. P., Kolev, M. V., Rajashankar, K. R., Himanen, J. P., & Nikolov, D. B. (2006). Crystal structures of the Tie2 receptor ectodomain and the angiopoietin-2-Tie2 complex. *Nat Struct Mol Biol, 13*(6), 524-532. doi: 10.1038/nsmb1101

Blume-Jensen, P., & Hunter, T. (2001). Oncogenic kinase signalling. *Nature, 411*(6835), 355-365. doi: 10.1038/35077225

Boudeau, J., Miranda-Saavedra, D., Barton, G. J., & Alessi, D. R. (2006). Emerging roles of pseudokinases. *Trends Cell Biol, 16*(9), 443-452. doi: 10.1016/j.tcb.2006.07.003

Burgess, A. W., Cho, H. S., Eigenbrot, C., Ferguson, K. M., Garrett, T. P., Leahy, D. J., . . . Yokoyama, S. (2003). An open-and-shut case? Recent insights into the activation of EGF/ErbB receptors. *Mol Cell, 12*(3), 541-552.

Chen, Y., Takita, J., Choi, Y. L., Kato, M., Ohira, M., Sanada, M., . . . Ogawa, S. (2008). Oncogenic mutations of ALK kinase in neuroblastoma. *Nature, 455*(7215), 971-974. doi: 10.1038/nature07399

Choudhary, C., Olsen, J. V., Brandts, C., Cox, J., Reddy, P. N., Bohmer, F. D., . . . Serve, H. (2009). Mislocalized activation of oncogenic RTKs switches downstream signaling outcomes. *Mol Cell, 36*(2), 326-339. doi: 10.1016/j.molcel.2009.09.019

Christensen, J. G., Zou, H. Y., Arango, M. E., Li, Q., Lee, J. H., McDonnell, S. R., . . . Los, G. (2007). Cytoreductive antitumor activity of PF-2341066, a novel inhibitor of anaplastic lymphoma kinase and c-Met, in experimental models of anaplastic large-cell lymphoma. *Mol Cancer Ther, 6*(12 Pt 1), 3314-3322. doi: 10.1158/1535-7163.MCT-07-0365

Corless, C. L., & Heinrich, M. C. (2008). Molecular pathobiology of gastrointestinal stromal sarcomas. *Annu Rev Pathol, 3*, 557-586. doi: 10.1146/annurev.pathmechdis.3.121806.151538

Dancey, J. E., Bedard, P. L., Onetto, N., & Hudson, T. J. (2012). The genetic basis for cancer treatment decisions. *Cell, 148*(3), 409-420. doi: 10.1016/j.cell.2012.01.014

Di Fiore, P. P., Pierce, J. H., Kraus, M. H., Segatto, O., King, C. R., & Aaronson, S. A. (1987). erbB-2 is a potent oncogene when overexpressed in NIH/3T3 cells. *Science, 237*(4811), 178-182.

Dibb, N. J., Dilworth, S. M., & Mol, C. D. (2004). Switching on kinases: oncogenic activation of BRAF and the PDGFR family. *Nat Rev Cancer, 4*(9), 718-727. doi: 10.1038/nrc1434

Eck, M. J., & Yun, C. H. (2010). Structural and mechanistic underpinnings of the differential drug sensitivity of EGFR mutations in non-small cell lung cancer. *Biochim Biophys Acta, 1804*(3), 559-566. doi: 10.1016/j.bbapap.2009.12.010

Eswarakumar, V. P., Lax, I., & Schlessinger, J. (2005). Cellular signaling by fibroblast growth factor receptors. *Cytokine Growth Factor Rev, 16*(2), 139-149. doi: 10.1016/j.cytogfr.2005.01.001

Fukuoka, M., Yano, S., Giaccone, G., Tamura, T., Nakagawa, K., Douillard, J. Y., . . . Baselga, J. (2003). Multi-institutional randomized phase II trial of gefitinib for previously treated patients with advanced non-small-cell lung cancer (The IDEAL 1 Trial) [corrected]. *J Clin Oncol, 21*(12), 2237-2246. doi: 10.1200/JCO.2003.10.038

George, R. E., Sanda, T., Hanna, M., Frohling, S., Luther, W., 2nd, Zhang, J., . . . Look, A. T. (2008). Activating mutations in ALK provide a therapeutic target in neuroblastoma. *Nature, 455*(7215), 975-978. doi: 10.1038/nature07397

Gotoh, N., Tojo, A., Hino, M., Yazaki, Y., & Shibuya, M. (1992). A highly conserved tyrosine residue at codon 845 within the kinase domain is not required for the transforming activity of human epidermal growth factor receptor. *Biochem Biophys Res Commun, 186*(2), 768-774.

Griffith, J., Black, J., Faerman, C., Swenson, L., Wynn, M., Lu, F., . . . Saxena, K. (2004). The structural basis for autoinhibition of FLT3 by the juxtamembrane domain. *Mol Cell, 13*(2), 169-178.

Himanen, J. P., & Nikolov, D. B. (2003). Eph signaling: a structural view. *Trends Neurosci, 26*(1), 46-51.

Hubbard, S. R. (2004). Juxtamembrane autoinhibition in receptor tyrosine kinases. *Nat Rev Mol Cell Biol, 5*(6), 464-471. doi: 10.1038/nrm1399

Hubbard, S. R., Wei, L., Ellis, L., & Hendrickson, W. A. (1994). Crystal structure of the tyrosine kinase domain of the human insulin receptor. *Nature, 372*(6508), 746-754. doi: 10.1038/372746a0

Hunter, T., & Sefton, B. M. (1980). Transforming gene product of Rous sarcoma virus phosphorylates tyrosine. *Proc Natl Acad Sci U S A, 77*(3), 1311-1315.

Huse, M., & Kuriyan, J. (2002). The conformational plasticity of protein kinases. *Cell, 109*(3), 275-282.

Janoueix-Lerosey, I., Lequin, D., Brugieres, L., Ribeiro, A., de Pontual, L., Combaret, V., . . . Delattre, O. (2008). Somatic and germline activating mutations of the ALK kinase receptor in neuroblastoma. *Nature, 455*(7215), 967-970. doi: 10.1038/nature07398

Jura, N., Endres, N. F., Engel, K., Deindl, S., Das, R., Lamers, M. H., . . . Kuriyan, J. (2009). Mechanism for activation of the EGF receptor catalytic domain by the juxtamembrane segment. *Cell, 137*(7), 1293-1307. doi: 10.1016/j.cell.2009.04.025

Jura, N., Zhang, X., Endres, N. F., Seeliger, M. A., Schindler, T., & Kuriyan, J. (2011). Catalytic control in the EGF receptor and its connection to general kinase regulatory mechanisms. *Mol Cell, 42*(1), 9-22. doi: 10.1016/j.molcel.2011.03.004

Katso, R. M., Russell, R. B., & Ganesan, T. S. (1999). Functional analysis of H-Ryk, an atypical member of the receptor tyrosine kinase family. *Mol Cell Biol, 19*(9), 6427-6440.

Kris, M. G., Natale, R. B., Herbst, R. S., Lynch, T. J., Jr., Prager, D., Belani, C. P., . . . Kay, A. C. (2003). Efficacy of gefitinib, an inhibitor of the epidermal growth factor receptor tyrosine kinase, in symptomatic patients with non-small cell lung cancer: a randomized trial. *JAMA, 290*(16), 2149-2158. doi: 10.1001/jama.290.16.2149

Lee, J. C., Vivanco, I., Beroukhim, R., Huang, J. H., Feng, W. L., DeBiasi, R. M., . . . Mellinghoff, I. K. (2006). Epidermal growth factor receptor activation in glioblastoma through novel missense mutations in the extracellular domain. *PLoS Med, 3*(12), e485. doi: 10.1371/journal.pmed.0030485

Lemmon, M. A., & Schlessinger, J. (2010). Cell signaling by receptor tyrosine kinases. *Cell, 141*(7), 1117-1134. doi: 10.1016/j.cell.2010.06.011

Libermann, T. A., Nusbaum, H. R., Razon, N., Kris, R., Lax, I., Soreq, H., . . . Schlessinger, J. (1985). Amplification, enhanced expression and possible rearrangement of EGF receptor gene in primary human brain tumours of glial origin. *Nature, 313*(5998), 144-147.

Lynch, T. J., Bell, D. W., Sordella, R., Gurubhagavatula, S., Okimoto, R. A., Brannigan, B. W., . . . Haber, D. A. (2004). Activating mutations in the epidermal growth factor receptor underlying responsiveness of non-small-cell lung cancer to gefitinib. *N Engl J Med, 350*(21), 2129-2139. doi: 10.1056/NEJMoa040938

Manning, G., Whyte, D. B., Martinez, R., Hunter, T., & Sudarsanam, S. (2002). The protein kinase complement of the human genome. *Science, 298*(5600), 1912-1934. doi: 10.1126/science.1075762

Mohammadi, M., Schlessinger, J., & Hubbard, S. R. (1996). Structure of the FGF receptor tyrosine kinase domain reveals a novel autoinhibitory mechanism. *Cell, 86*(4), 577-587.

Mol, C. D., Dougan, D. R., Schneider, T. R., Skene, R. J., Kraus, M. L., Scheibe, D. N., . . . Wilson, K. P. (2004). Structural basis for the autoinhibition and STI-571 inhibition of c-Kit tyrosine kinase. *J Biol Chem, 279*(30), 31655-31663. doi: 10.1074/jbc.M403319200

Moore, D. T., Berger, B. W., & DeGrado, W. F. (2008). Protein-protein interactions in the membrane: sequence, structural, and biological motifs. *Structure, 16*(7), 991-1001. doi: 10.1016/j.str.2008.05.007

Morris, S. W., Kirstein, M. N., Valentine, M. B., Dittmer, K. G., Shapiro, D. N., Saltman, D. L., & Look, A. T. (1994). Fusion of a kinase gene, ALK, to a nucleolar protein gene, NPM, in non-Hodgkin's lymphoma. *Science, 263*(5151), 1281-1284.

Mosse, Y. P., Laudenslager, M., Longo, L., Cole, K. A., Wood, A., Attiyeh, E. F., . . . Maris, J. M. (2008). Identification of ALK as a major familial neuroblastoma predisposition gene. *Nature, 455*(7215), 930-935. doi: 10.1038/nature07261

Murray, P. B., Lax, I., Reshetnyak, A., Ligon, G. F., Lillquist, J. S., Natoli, E. J., Jr., . . . Schlessinger, J. (2015). Heparin is an activating ligand of the orphan receptor tyrosine kinase ALK. *Sci Signal, 8*(360), ra6. doi: 10.1126/scisignal.2005916

Niu, X. L., Peters, K. G., & Kontos, C. D. (2002). Deletion of the carboxyl terminus of Tie2 enhances kinase activity, signaling, and function. Evidence for an autoinhibitory mechanism. *J Biol Chem, 277*(35), 31768-31773. doi: 10.1074/jbc.M203995200

Palmer, R. H., Vernersson, E., Grabbe, C., & Hallberg, B. (2009). Anaplastic lymphoma kinase: signalling in development and disease. *Biochem J, 420*(3), 345-361. doi: 10.1042/BJ20090387

Pawson, T., Gish, G. D., & Nash, P. (2001). SH2 domains, interaction modules and cellular wiring. *Trends Cell Biol, 11*(12), 504-511.

Red Brewer, M., Choi, S. H., Alvarado, D., Moravcevic, K., Pozzi, A., Lemmon, M. A., & Carpenter, G. (2009). The juxtamembrane region of the EGF receptor functions as an activation domain. *Mol Cell, 34*(6), 641-651. doi: 10.1016/j.molcel.2009.04.034

Reichert, J. M., & Valge-Archer, V. E. (2007). Development trends for monoclonal antibody cancer therapeutics. *Nat Rev Drug Discov, 6*(5), 349-356. doi: 10.1038/nrd2241

Schlessinger, J., & Lemmon, M. A. (2003). SH2 and PTB domains in tyrosine kinase signaling. *Sci STKE, 2003*(191), RE12. doi: 10.1126/stke.2003.191.re12

Sharma, S. V., Bell, D. W., Settleman, J., & Haber, D. A. (2007). Epidermal growth factor receptor mutations in lung cancer. *Nat Rev Cancer, 7*(3), 169-181. doi: 10.1038/nrc2088

Shawver, L. K., Slamon, D., & Ullrich, A. (2002). Smart drugs: tyrosine kinase inhibitors in cancer therapy. *Cancer Cell, 1*(2), 117-123.

Shepherd, R., Forbes, S. A., Beare, D., Bamford, S., Cole, C. G., Ward, S., . . . Futreal, P. A. (2011). Data mining using the Catalogue of Somatic Mutations in Cancer BioMart. *Database (Oxford), 2011*, bar018. doi: 10.1093/database/bar018

Shewchuk, L. M., Hassell, A. M., Ellis, B., Holmes, W. D., Davis, R., Horne, E. L., . . . Moore, J. T. (2000). Structure of the Tie2 RTK domain: self-inhibition by the nucleotide binding loop, activation loop, and C-terminal tail. *Structure, 8*(11), 1105-1113.

Slamon, D. J., Godolphin, W., Jones, L. A., Holt, J. A., Wong, S. G., Keith, D. E., . . . et al. (1989). Studies of the HER-2/neu proto-oncogene in human breast and ovarian cancer. *Science, 244*(4905), 707-712.

Soda, M., Choi, Y. L., Enomoto, M., Takada, S., Yamashita, Y., Ishikawa, S., . . . Mano, H. (2007). Identification of the transforming EML4-ALK fusion gene in non-small-cell lung cancer. *Nature, 448*(7153), 561-566. doi: 10.1038/nature05945

Taylor, S. S., Yang, J., Wu, J., Haste, N. M., Radzio-Andzelm, E., & Anand, G. (2004). PKA: a portrait of protein kinase dynamics. *Biochim Biophys Acta, 1697*(1-2), 259-269. doi: 10.1016/j.bbapap.2003.11.029

Temin, H. M. (1966). Studies on carcinogenesis by avian sarcoma viruses. 3. The differential effect of serum and polyanions on multiplication of uninfected and converted cells. *J Natl Cancer Inst, 37*(2), 167-175.

Thatcher, N., Chang, A., Parikh, P., Rodrigues Pereira, J., Ciuleanu, T., von Pawel, J., . . . Carroll, K. (2005). Gefitinib plus best supportive care in previously treated patients with refractory advanced non-small-cell lung cancer: results from a randomised, placebo-controlled, multicentre study (Iressa Survival Evaluation in Lung Cancer). *Lancet, 366*(9496), 1527-1537. doi: 10.1016/S0140-6736(05)67625-8

Thiel, K. W., & Carpenter, G. (2007). Epidermal growth factor receptor juxtamembrane region regulates allosteric tyrosine kinase activation. *Proc Natl Acad Sci U S A, 104*(49), 19238-19243. doi: 10.1073/pnas.0703854104

Till, J. H., Becerra, M., Watty, A., Lu, Y., Ma, Y., Neubert, T. A., . . . Hubbard, S. R. (2002). Crystal structure of the MuSK tyrosine kinase: insights into receptor autoregulation. *Structure, 10*(9), 1187-1196.

Ullrich, A., & Schlessinger, J. (1990). Signal transduction by receptors with tyrosine kinase activity. *Cell, 61*(2), 203-212.

Ward, C. W., Lawrence, M. C., Streltsov, V. A., Adams, T. E., & McKern, N. M. (2007). The insulin and EGF receptor structures: new insights into ligand-induced receptor activation. *Trends Biochem Sci, 32*(3), 129-137. doi: 10.1016/j.tibs.2007.01.001

Wybenga-Groot, L. E., Baskin, B., Ong, S. H., Tong, J., Pawson, T., & Sicheri, F. (2001). Structural basis for autoinhibition of the Ephb2 receptor tyrosine kinase by the unphosphorylated juxtamembrane region. *Cell, 106*(6), 745-757.

Yuzawa, S., Opatowsky, Y., Zhang, Z., Mandiyan, V., Lax, I., & Schlessinger, J. (2007). Structural basis for activation of the receptor tyrosine kinase KIT by stem cell factor. *Cell, 130*(2), 323-334. doi: 10.1016/j.cell.2007.05.055

Zhang, X., Gureasko, J., Shen, K., Cole, P. A., & Kuriyan, J. (2006). An allosteric mechanism for activation of the kinase domain of epidermal growth factor receptor. *Cell, 125*(6), 1137-1149. doi: 10.1016/j.cell.2006.05.013

CHAPTER 2:

Structural studies of ErbB receptor tyrosine kinase domains with small molecule inhibitors

2.1 Selective inhibition of EGFR

N.B. This is collaborative work with Yingting Liu from the laboratory of Ravi Radhakrishnan in the Department of Bioengineering at U. Penn, and can be found in Park *et al.* (2012) *Biochem. J.* 448, 417-423. Work contributed by Yingting Liu (Y.L.) is marked accordingly in tables and figures.

2.1.1 Introduction

Activating mutations in the epidermal growth factor receptor (EGFR) are now well accepted as oncogenic drivers in certain cancers, notably non-small cell lung cancer (NSCLC) (Sharma et al., 2007) and glioblastoma (Cancer Genome Atlas Research, 2008; Vivanco et al., 2012). Several drugs that inhibit EGFR signaling are now in clinical use, including antibody therapeutics and ATP-competitive small molecule tyrosine kinase inhibitors (TKIs) (Pao and Chmielecki, 2010). Approved EGFR-targeted TKIs include erlotinib and gefitinib (which are EGFR-specific), lapatinib (which inhibits both EGFR and HER2/ErbB2), and vandetanib (which inhibits EGFR, VEGFR, and Ret). Many more EGFR-targeted TKIs are currently being developed and/or tested.

Not all EGFR-driven cancers are sensitive to EGFR-targeted TKIs (Pao and Chmielecki, 2010). Effective clinical application of these agents presents several major challenges. The first is the identification of patients whose tumors are in fact dependent on EGFR. This has been illustrated best in non-small cell lung cancer (NSCLC). Broad initial clinical trials of EGFR-targeted TKIs in NSCLC gave disappointing results, but highlighted a subset of patients with activating EGFR mutations that responded very well to treatment (Lynch et al., 2004). The second major challenge is acquired resistance, a current area of intense activity. In EGFR-mutated NSCLC, for example, primary resistance is seen in about 25% of cases. Where responses are seen, acquired resistance to first generation TKIs invariably occurs (Janne et al., 2009) – often through secondary EGFR mutations (Yoshikawa et al., 2013; Yun et al., 2008). A third challenge is that not all EGFR-activating mutations are equal, and selectivity of response to different EGFR-targeted TKIs depends on how the receptor is activated.

Clinical trials in NSCLC with the EGFR-targeted TKIs erlotinib and gefitinib led to the discovery that the tumors of responding patients all harbored mutations in the EGFR intracellular tyrosine kinase domain (Sharma et al., 2007). Patients with these mutations frequently showed dramatic responses (Lynch et al., 2004). These studies appeared to identify a subgroup of NSCLC cases in which EGFR is clearly the oncogenic driver – raising the hope that all tumors with EGFR mutations might be responsive to these TKIs, and motivating efforts to identify EGFR mutations in many other cancers. Meanwhile, clinical experience with glioblastoma (GBM) has told a different, and rather puzzling, story. GBM was the first human tumor type in which amplification and mutation of EGFR was reported (Libermann et al., 1985), frequently expressing so-called 'variant III' EGFR (EGFRvIII) that has a 267aa deletion from its extracellular region (Sugawa et al., 1990) that activates the receptor. It seemed reasonable to expect that GBM patients might be primary beneficiaries of EGFR-targeted agents – but this has unfortunately not been the case. GBM patients expressing EGFRvIII have not responded well to gefitinib or erlotinib for reasons that remain unclear – although it is also true that the mechanism of EGFRvIII activation remains obscure (Lemmon and Schlessinger, 2010).

Mellinghoff and colleagues (Vivanco et al., 2012) made the remarkable discovery that efficacy depends on the type of the EGFR-targeted TKI that is used (Figure 2.1). Erlotinib and CI-1033 are so-called 'Type 1' TKIs that bind the active conformation of the kinase domain (Stamos et al., 2002), and are ineffective in GBM. By contrast, inhibitors that selectively bind the inactive conformation of the receptor's kinase domain were effective against EGFR variants found in GBM (including EGFRvIII) and efficiently induced cell death in EGFR-mutated GBM cells. Specifically, the inhibitors used were lapatinib and HKI-272, which are reversible and covalent/irreversible EGFR/ErbB2 dual-specific TKIs respectively that selectively bind the inactive conformation of EGFR's kinase domain (Wood et al., 2004; Yun et al., 2008). For ease of clarification of those inhibitors binding active or inactive conformation, they are classified here as 'Type 1' and 'Type 1.5' inhibitors (Liu and Gray, 2006), which both bind EGFR-TKD in the 'DFG (Asp-Phe-Gly) - in' conformation, but differ in the position of the αC helix in EGFR-TKD crystal structures. Type 1

inhibitors can bind with αC in the 'in' position seen in active kinases, whereas type 1.5 inhibitors require αC to be in the 'out' position seen in inactive kinases (Figure 2.1).

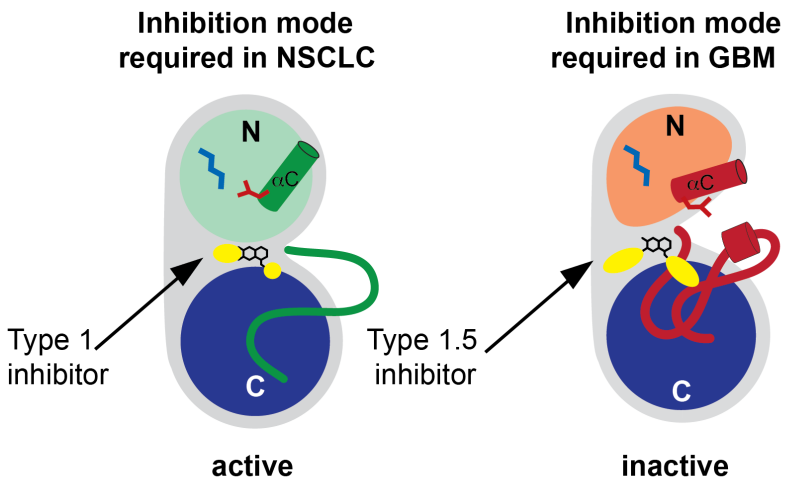

Figure 2.1 Cartoon representation of the active and inactive conformations of the EGFR kinase domain.

In the inactive state (right), the key αC helix is displaced, breaking an important salt bridge between a glutamate in αC (red sticks) and a lysine in the ATP-binding site (blue sticks). In the active conformation (left), αC is moved in towards the center of the N-lobe, so that this salt bridge forms to stabilize ATP binding. Type 1 inhibitors such as gefitinib and erlotinib bind to the active conformation (left), whereas type 1.5 inhibitors (such as lapatinib) bind only to the inactive (αC-out) conformation. Only type 1 inhibitors are effective in NSCLC, whereas only type 1.5 inhibitors effectively inhibit EGFR variants found in glioblastoma.

Just as type 1 inhibitors such as erlotinib are more effective in killing EGFR-addicted NSCLC cells than GBM cells, so is the reverse also true. Whereas the type 1.5 inhibitor lapatinib induced significant death in EGFR-addicted GBM cells, it was substantially less effective against NSCLC-derived EGFR variants, consistent with *in vitro* studies showing that EGFR harboring NSCLC-derived mutations is resistant to lapatinib (Wang et al., 2011) – or indeed cetuximab. EGFR mutations found in NSCLC are almost exclusively intracellular, within the tyrosine kinase domain of the receptor (Sharma et al., 2007). The GBM mutations (including that in EGFRvIII) are exclusively extracellular (Lee et al., 2006; Vivanco et al., 2012). The fact that the different classes of activating EGFR mutations yield receptor variants that are responsive to distinct types of EGFR-targeted TKIs implies that these mutations activate the receptor in different ways. Basal phosphorylation of EGFR promoted by all extracellular mutations tested is more potently inhibited by lapatinib than by erlotinib, whereas the opposite is true for NSCLC-derived intracellular kinase domain mutations (Figure 2.2) (Vivanco et al., 2012). By contrast, regardless of which mutations it harbors, the EGF-activated receptor is most effectively inhibited by erlotinib. This dichotomy in inhibitor sensitivity of oncogenic EGFR variants has important clinical implications, and other activating (and resistance) mutations may show an even wider range of specificities.

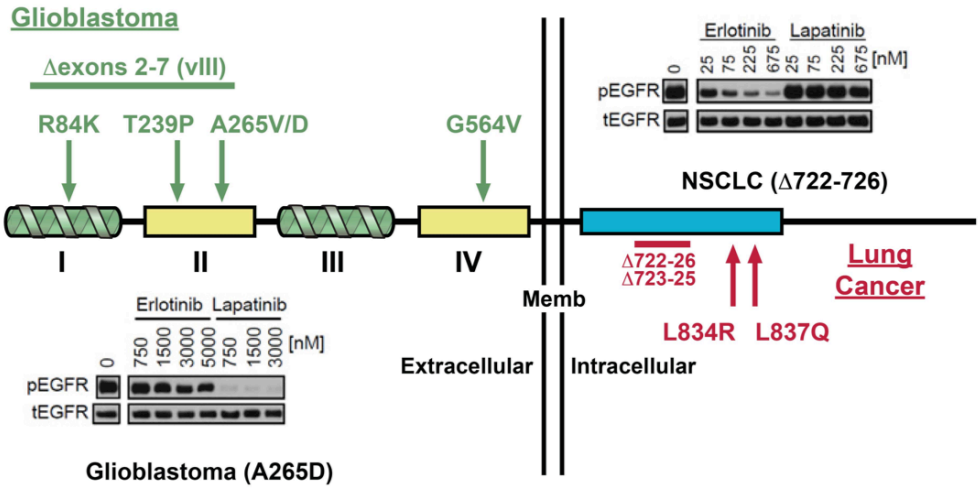

Figure 2.2 Differential sensitivity of endogenously expressed glioma- versus lung cancer–specific EGFR mutants to lapatinib versus erlotinib.

In this EGFR domain structure, mutations indicated in green have been documented in glioblastoma (GBM) but not in lung cancer, while those indicated in red are seen in non-small cell lung cancer (NSCLC) and not in GBM. The indicated GBM and lung cancer cell lines were treated with various doses of lapatinib or erlotinib (modified figure from Vivanco et al, 2012). Cells were harvested and analyzed by Western blotting with antibodies for phosphor EGFR (pEGFR) or total EGFR (tEGFR). Erlotinib (which can bind to the active conformation of the kinase) is effective in NSCLC, whereas only lapatinib (which binds only to the inactive conformation of the kinase) effectively inhibits EGFR variants found in GBM.

2.1.2 Current view of conformational selectivity of EGFR inhibitors

Previous structural studies of EGFR-TKD bound to different TKIs (Eck and Yun, 2010) suggest that individual drugs differ in their preference for the 'active' compared with 'inactive' conformation of the kinase. Crystal structures of erlotinib-bound (Stamos et al., 2002) or gefitinib-bound (Yun

et al., 2008) EGFR-TKD show the kinase in the same active conformation, allosterically stabilized by a characteristic asymmetric dimer that forms in the crystals (Zhang et al., 2006). By contrast, crystals of EGFR-TKD bound to lapatinib (Wood et al., 2004) or HKI-272 (neratinib) (Yun et al., 2008) show a distinct Src-like inactive conformation in which a short activation loop α-helix makes autoinhibitory interactions with the displaced αC helix in the 'out' position (Zhang et al., 2006). Based on these studies, erlotinib and gefitinib have been argued to bind only the active EGFR-TKD conformation, whereas lapatinib and neratinib are thought to bind only the inactive conformation.

Despite these structural views, biochemical and binding studies argue that EGFR-targeted TKIs may not in fact be so conformationally selective. Extensive direct binding studies suggested that erlotinib, gefitinib and lapatinib all bind similarly (within 3-fold) to both wild-type inactive and mutationally-activated forms of EGFR-TKD (Fabian et al., 2005). Erlotinib and gefitinib affinities were also reported (Lu et al., 2012) not to be affected by a C-lobe mutation (V924R) that prevents formation of the activated asymmetric dimer (Zhang et al., 2006), again suggesting that these inhibitors bind similarly to inactive and active EGFR-TKD. Moreover, studies of near full-length EGFR (Wang et al., 2011) indicated that the apparent K_i value for inhibition by lapatinib is increased only 1.8-fold upon receptor activation. It should be noted, however, that some other published data do suggest affinity differences between active and inactive EGFR-TKD for some of these inhibitors. For example, the apparent K_i for lapatinib inhibition of near full-length EGFR was increased >25-fold when activated by the oncogenic L834R mutation (Wang et al., 2011). Blocking EGFR activation with cetuximab also increased the apparent K_i for erlotinib (Wang et al., 2011), suggesting that inactive EGFR has a reduced affinity for erlotinib. Moreover, one set of direct gefitinib-binding studies suggested that this TKI binds more tightly to the activated (L834R) EGFR-TKD than to the inactive conformation (Yun et al., 2007). On balance, it therefore remains unclear whether EGFR inhibitors are truly conformationally selective. It is clear, however, that a

full understanding of which TKIs bind more tightly to which mutated EGFR variants found in patients could have significant potential impact on inhibitor choice in the clinic.

To investigate the conformational selectivity of EGFR inhibitors further, we undertook computational and crystallographic studies of erlotinib binding to EGFR-TKD in both its active and inactive states. Our computational studies predicted that erlotinib binds similarly to both inactive and active TKD conformations. We used X-ray crystallography to test this prediction, and describe here a structure of inactive EGFR-TKD with bound erlotinib. The findings of the present study cast further doubt on the conformational selectivity of EGFR inhibitors, and also suggest that other characteristics, such as differences in inhibitor dissociation (Wood et al., 2004) or cycling rates (Barkovich et al., 2012), may underlie the distinct effects of erlotinib and lapatinib on NSCLC and glioblastoma cell lines (Vivanco et al., 2012) summarized in Figure 2.2, and will need to be understood in order to counter TKI resistance in the clinic.

2.1.3 Computational analysis of erlotinib binding to EGFR-TKD

To investigate the possible basis for preferential binding of erlotinib to the active conformation of EGFR-TKD, we used computational approaches in collaboration with Yingting Liu from the Radhakrishnan lab. Docking erlotinib on to wild-type EGFR-TKD in its active conformation, as described in the Experimental section, closely reproduced the binding mode observed crystallographically in PDB entry 1M17 (Stamos et al., 2002), as shown in Figure 2.3, with N1 of the erlotinib quinazoline moiety accepting a predicted hydrogen bond from the amide nitrogen of Met^{769}. The docked structures were subjected to MD simulations, which showed that erlotinib was stable in this bound conformation (cyan in Figure 2.3) throughout the entire course of a 10 ns run (Figure 2.4). Notably, two water molecules (W1 and W2 in Figure 2.3) were also found to remain in the binding pocket, contributing to a stable network of hydrogen bonds involving residues Thr^{766}, Gln^{767} and Thr^{830} of EGFR-TKD. Docking erlotinib into L834R-mutated EGFR-TKD gave very similar results (J. H. Park et al., 2012). Moreover, estimates of binding energy using Glide (Friesner et al., 2006), MM/PBSA calculations (see the Experimental section) or FEP (Free

Energy Perturbation) calculations indicated no increase in erlotinib binding affinity to the L834R mutant (Table 2.1).

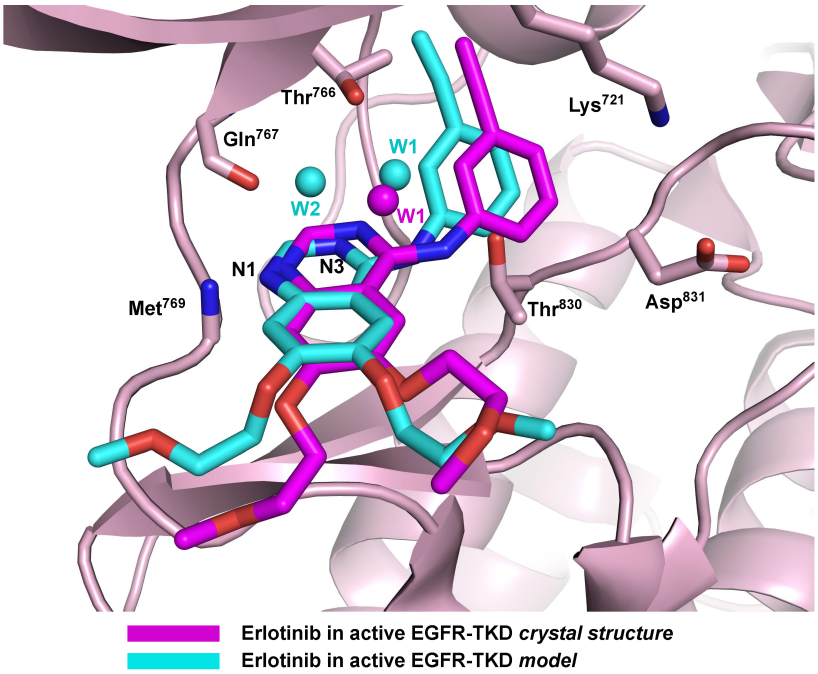

Figure 2.3. Erlotinib binding to active EGFR-TKD in the crystal structure (1M17) and model

Erlotinib is shown bound to active EGFR-TKD in our computational model (cyan) and in the erlotinib/EGFR-TKD (active conformation) crystal structure reported in PDB entry 1M17 (magenta). Functional groups in several EGFR-TKD residues that interact directly or indirectly with the bound erlotinib are shown, and the cartoon from only 1M17 is shown. The backbone amide of Met^{769} donates a predicted hydrogen-bond to N1 of the erlotinib quinazoline moiety. The backbone carbonyl of Gln^{767} and side-chains of Thr^{766} and Thr^{830} participate in a predicted hydrogen-bonding network to which water molecules (W1 and W2 in our model; W1 in 1M17) also contribute. The Lys^{721} and Asp^{831} side-chains are shown for reference. Polypeptide in the foreground has been removed for clarity. (Computational model was done by Y.L)

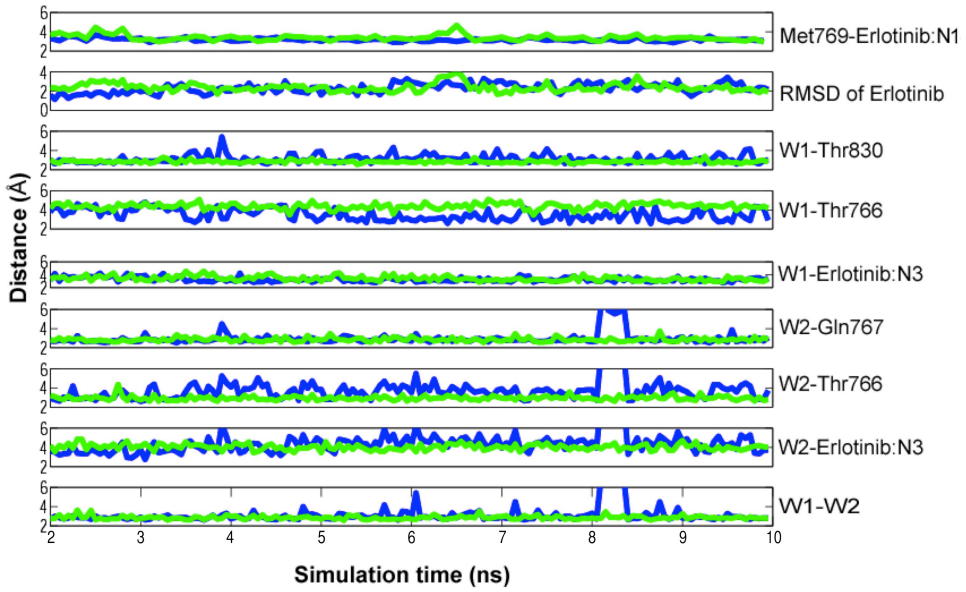

Figure 2.4: RMSD of erlotinib and key distances between EGFR-TKD and erlotinib, as well as the distance of waters from EGFR-TKD or erlotinib monitored during 10ns MD simulation. Data for the wild-type active-conformation simulation are blue, and data for the L834R (active conformation) simulation are green. Data from the first 2 ns (pre-equilibration) are not shown. (Experiments were done by Y.L)

Molecule	Glide score (kcal/mol)	MM/PBSA (kcal/mol)	FEP (kcal/mol)
Wild-type	−9.34	−28.2	
L834R	−9.35	−30.7	
$\Delta\Delta G$	−0.01	−2.5	0.83±1.16

Table 2.1 Erlotinib-binding energies calculated by Glide, MM/PBSA and FEP for wild-type and L834R EGFR-TKD in the active conformation (experiments were performed by Y.L)

2.1.4 Computational studies of erlotinib binding to inactive EGFR-TKD

To challenge the assumption that erlotinib, gefitinib and other related inhibitors only bind to (and stabilize) the active EGFR-TKD conformation, we used the same computational approaches to ask whether erlotinib can bind to the inactive conformation of the kinase. Surprisingly, docking erlotinib into a crystal structure of the inactive EGFR-TKD (PDB entry 1XKK), after removing lapatinib from the model, yielded a very similar Glide score (−9.72 kcal/mol) to that seen for active EGFR-TKD (−9.34 kcal/mol). Moreover, when the two models were overlaid (Figure 2.5), the orientation of erlotinib and the conformation of its binding site were very similar in active (cyan) and inactive (yellow) EGFR-TKD models. N1 of the erlotinib quinazoline moiety receives a hydrogen bond from the amide nitrogen of Met^{769} in both cases. The two water molecules (W1 and W2) mentioned above form essentially the same hydrogen-bonding network in each model, which also involves the Gln^{767} backbone carbonyl, the Thr^{766} side chain, nitrogen N3 of the erlotinib quinazoline moiety and the Thr^{830} side chain (Figure 2.5). An additional third strongly bound water molecule (W3 in Figure 2.5) was seen in the model of erlotinib-bound inactive EGFR-TKD. Distances between erlotinib and protein (and between bound waters and erlotinib) were stable throughout a 10 ns MD simulation, as plotted in Figure 2.6. Thus, our computational studies failed to provide any explanation for why erlotinib might bind preferentially to the active conformation of EGFR-TKD. Yun et al. (2007) suggested that favorable van der Waal's interactions between gefitinib and the back of the ATP-binding cleft in active EGFR-TKD may be lost in the inactive state, but this was not seen in our modeling.

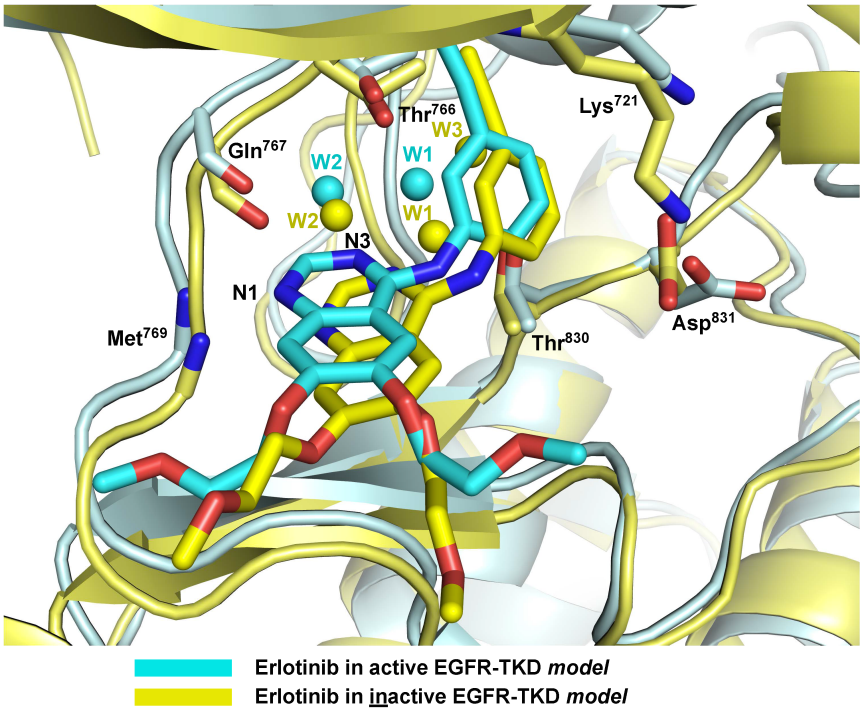

Figure 2.5 Comparison of erlotinib binding to active and inactive EGFR-TKD models

On the basis of the computational models described here, erlotinib is shown bound to both active EGFR-TKD (cyan) and inactive EGFR-TKD (yellow). The protein structure in the background is similarly colored (light cyan for active, yellow for inactive). Functional groups in several EGFR-TKD residues that interact directly or indirectly with the bound erlotinib are shown. The backbone amide of Met^{769} donates a hydrogen bond to N1 of the erlotinib quinazoline moiety. The backbone carbonyl of Gln^{767} and side chains of Thr^{766} and Thr^{830} participate in a hydrogen-bonding network to which water molecules (W1 and W2) also contribute. The Lys^{721} and Asp^{831} side chains are shown for reference. Polypeptide in the foreground has been removed for clarity.

(Computational model was done by Y.L)

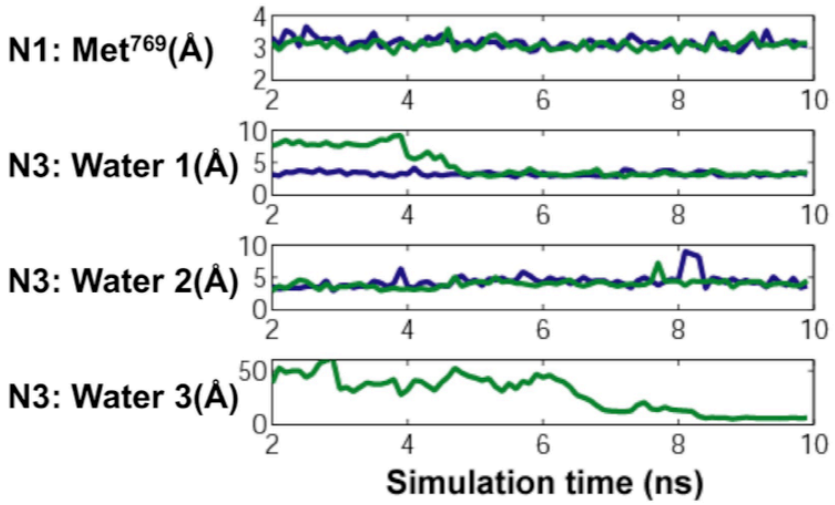

Figure 2.6 Comparison of RMSD values for critical hydrogen bonds in active and inactive wild-type simulations.

Values for the distance between N1 of the erlotinib quinazoline moiety and Met^{769}, as well as the distance from erlotinib N3 of the three waters shown in the model in Figure 2.8 (A) were monitored during the 10ns simulation (omitting the first 2ns), and are plotted in green. For comparison, data for the wild-type active EGFR-TKD conformation (as in Figure 2.4) are shown in blue. (Experiments were done by Y.L.)

2.1.5 Crystal structure of erlotinib bound to inactive EGFR-TKD

Following the unexpected suggestion from our collaborative computational studies that erlotinib binds similarly to active and inactive EGFR-TKD, I sought to crystallize the kinase domain in its inactive conformation with erlotinib bound. Previous crystal structures of active EGFR-TKD with erlotinib (Stamos et al., 2002) or gefitinib (Yun et al., 2007) bound were obtained by soaking the drug into pre-formed crystals. However, it is now clear that wild-type EGFR-TKD (or variants harboring NSCLC mutations) always adopt the active conformation in crystals (Stamos et al., 2002; Wood et al., 2004; Zhang et al., 2006), because of EGFR-TKD's intrinsic tendency to form

asymmetric dimers in which the C-lobe of one molecule associates with the N-lobe of its neighbor to allosterically stabilize the active conformation. Although EGFR-TKD co-crystallized with lapatinib (Wood et al., 2004), HKI-272 (Yun et al., 2008), or related inhibitors adopt the inactive conformation, wild-type EGFR-TKD only crystallizes in the inactive conformation when the asymmetric dimer is disrupted by a mutation in its interface (such as V924R in the C-lobe) (Jura et al., 2009; Zhang et al., 2006) or by a Mig6-derived peptide that binds to the C-lobe dimerization site (Zhang et al., 2007).

By soaking erlotinib into crystals formed by a V924R-mutated EGFR-TKD variant, I was able to determine the structure of erlotinib bound to inactive EGFR-TKD at a resolution of 2.75 Å (Table 2.2). As shown in Figure 2.7, my structure of inactive EGFR-TKD closely resembles that seen in PDB entry 1XKK (in complex with lapatinib). The RMSD (root mean square deviation) between α carbon positions in these two structures was 1.30 Å, and the α carbon RMSD for overlay of my inactive structure with PDB entry 3GT8 was 1.42 Å. As illustrated in Figure 2.8, the crystal structure shows erlotinib (green in Figure 2.8A) to be slightly shifted in the binding site compared with its predicted position in the computational model (yellow in Figure 2.8A); to the left in the aspect of Figure 2.8A by approximately 1 Å. The distance between the amide nitrogen of Met^{769} in EGFR-TKD and N1 of the erlotinib quinazoline moiety is maintained at 2.9 Å in the crystal structure and 3.2 Å in the model. The slight shift of erlotinib is associated with a similar shift in the polypeptide backbone in the region of residues 767–770. Other key side chains (Thr^{766}, Thr^{830}, Asp^{831} and Lys^{721}) shown in Figure 2.8A are located very similarly in the model and crystal structure. Importantly, the pattern of water molecules predicted by our model was also observed crystallographically (compare yellow and green waters in Figure 2.8A). W1 and W2 are in very similar positions in the crystal structure and model, providing crystallographic evidence that the predicted water-mediated hydrogen-bonding network involving the quinazoline moiety of erlotinib, and Thr^{766}/Gln^{767}/Thr^{830} of EGFR-TKD is maintained in the inactive conformation. Interestingly, equivalent waters are also seen in the published crystal structure of lapatinib-bound inactive EGFR-TKD (Figure 2.8B) (Wood et al., 2004). Moreover, a crystallographic water was

seen in our erlotinib/inactive EGFR-TKD structure close to the position of W3 in the computational model, and near the side chains of Thr^{766} and Thr^{830}. Additional waters labeled W4 and W5 in Figure 2.8A are seen in our erlotinib/EGFR-TKD crystal structure and not the model. Interestingly, as shown in Figure 2.8B, waters W3–W5 in our structure lie in the same pocket within inactive EGFR-TKD that is occupied by the (3-fluorobenzyl)oxy group of lapatinib in PDB entry 1XKK; these waters also interact with the EGFR-TKD backbone in parts of the αC helix (Met^{742}) and Phe^{832} of the DFG motif.

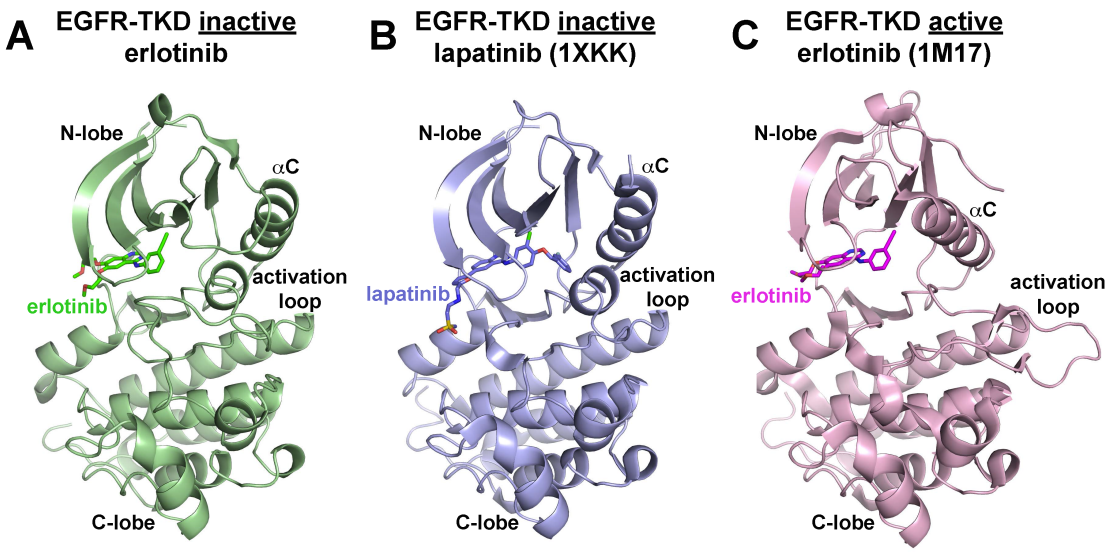

Figure 2.7 Crystal structures of TKI-bound EGFR-TKD

(A) The 2.75 Å resolution structure of V924R-mutated EGFR-TKD in its inactive form bound to erlotinib (green: PDB ID 4HJO) as described in the text and Table 2.2. (B) Crystal structure from PDB entry 1XKK showing lapatinib (blue) bound to inactive EGFR-TKD. (C) Crystal structure from PDB entry 1M17 showing erlotinib (magenta) bound to active EGFR-TKD. Note that the αC helix is in the 'in' or 'active' position in (C), but in the 'out' or 'inactive' position in (A) and (B), and that the characteristic short α-helix seen in the inactive EGFR-TKD activation loop is present in (A) and (B), but not (C). As described in the text, the crystal structure shown in (A) confirms our computational findings that erlotinib can bind to the inactive EGFR-TKD conformation.

Table 2.2 Data collection and refinement statistics (molecular replacement)

Each dataset was collected from a single crystal. Values for highest resolution shell are shown in parentheses.

	EGFR/erlotinib
Data collection	
Space group	$C222_1$
Cell dimensions	
a, *b*, *c* (Å)	78.0, 114.3, 84.9
a, b, g (°)	90, 90, 90
Resolution (Å)	64.4-2.75
R_{sym}	0.159 (0.494)
I/σ	12.8 (2.1)
Completeness (%)	96.1 (82.1)
Redundancy	4.8 (2.8)
Refinement	
Resolution (Å)	2.75
No. reflections	9712
R_{work} / R_{free}	0.25/0.28
No. atoms	
Protein	2201
Ligand	29
Water	26
B-factors	
Protein	44.6
Ligand	42.8
Water	35.1
R.m.s. deviations	
Bond lengths (Å)	0.008
Bond angles (°)	1.096

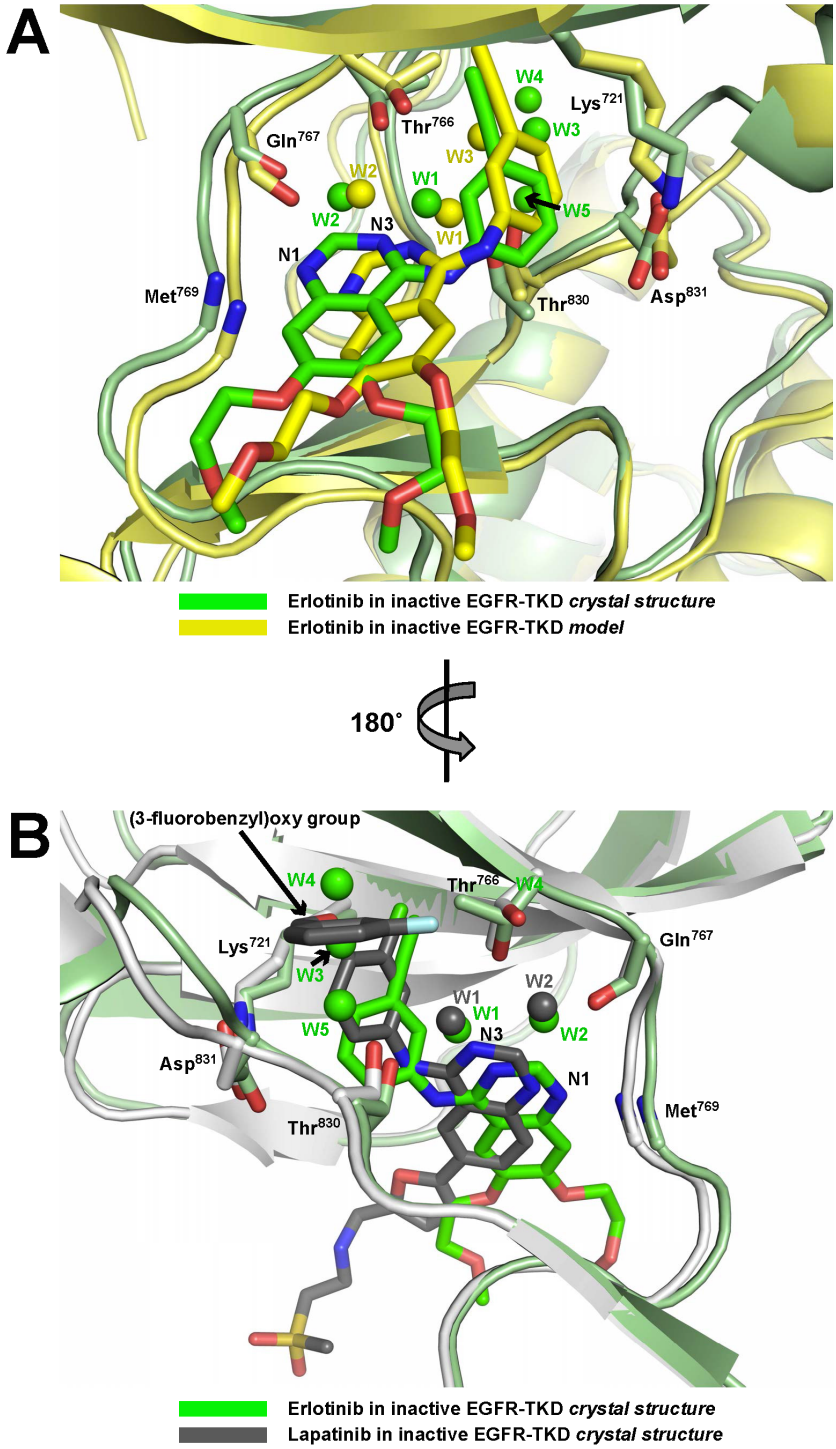
A
W4
Lys721
W3
Thr766
Gln767
W3
W2
W1
W5
W2
N3
W1
N1
Met769
Thr830
Asp831
Erlotinib in inactive EGFR-TKD crystal structure
Erlotinib in inactive EGFR-TKD model
180˚
B
(3-fluorobenzyl)oxy group
W4
Thr766
W4
Lys721
Gln767
W3
W2
W1
W1
W5
N3
W2
Asp831
N1
Met769
Thr830
Erlotinib in inactive EGFR-TKD crystal structure
Lapatinib in inactive EGFR-TKD crystal structure

Figure 2.8 Erlotinib binding to inactive EGFR-TKD

(A) The crystallographically observed mode of erlotinib binding to inactive EGFR-TKD (green: PDB ID 4HJO) is compared with the computational model (yellow). Protein structure in the background colored green for the crystal structure and yellow for the model. (B) The mode of erlotinib binding to inactive EGFR-TKD observed crystallographically (green) is compared with the mode of lapatinib binding to inactive EGFR-TKD in PDB entry 1XKK (grey), in a view rotated by 180° about a vertical axis compared with that seen in (A). Waters W1–W5 are labeled for the erlotinib/inactive EGFR-TKD structure. Waters W1 and W2 are also found in the lapatinib complex. W3–W5 in the erlotinib complex structure lie in a pocket occupied by the (3-fluorobenzyl)oxy group of lapatinib in PDB entry 1XKK. Functional groups, side chains and bound waters are shown as described in Figure 2.5. Polypeptide in the foreground has been removed for clarity.

2.1.6 Conclusions

It is generally assumed and stated that the EGFR inhibitors gefitinib and erlotinib bind selectively to the active conformation of EGFR-TKD, whereas lapatinib selectively binds the inactive configuration. A preference of lapatinib for inactive EGFR-TKD can easily be rationalized, since it has a bulky [(3-fluorobenzyl)oxy] substituent on its aniline ring that projects into the space opened up upon displacement of the αC helix in the inactive kinase (as shown in Figure 2.7B). For erlotinib, however, no significant difference in the binding affinity for inactive and active EGFR-TKD conformations could be detected – or rationalized – using a range of computational approaches. This led us to efforts to confirm crystallographically that erlotinib can indeed bind to EGFR-TKD in its inactive conformation (Figure 2.7A and Figure 2.8). These findings have several important implications.

First, our findings complicate suggestions in the literature that erlotinib and gefitinib drive EGFR dimerization by stabilizing the active configuration. Since asymmetric dimerization of EGFR-TKD promotes its acquisition of the active conformation, the converse should also be true: that stabilization of the active TKD conformation drives dimerization. Thus if erlotinib and gefitinib selectively bind and stabilize the active EGFR-TKD conformation, their binding should drive asymmetric dimer formation. Indeed, it has been reported that gefitinib stabilizes formation of EGFR-containing heterodimers in cells (Anido et al., 2003). Moreover, Springer and colleagues have reported in negative stain electron microscopy studies (Lu et al., 2012; Mi et al., 2011) that gefitinib promotes dimerization of near full-length EGFR by inducing structures that resemble asymmetric EGFR-TKD dimers – although it should be noted that this is only seen in the particles that they selected from images. The finding in the present study that erlotinib also binds to inactive (monomeric) EGFR-TKD is difficult to reconcile with the simple interpretation of these reports, as are other published data indicating that neither stabilizing the active conformation of EGFR-TKD with oncogenic mutations nor disrupting the asymmetric dimer interface with a V924R mutation (and thus stabilizing the inactive conformation) alters the affinity of EGFR-TKD for gefitinib or erlotinib (Fabian et al., 2005; Lu et al., 2012).

Secondly, the findings of this study argue that the relative abilities of erlotinib/gefitinib-type EGFR TKIs and lapatinib/neratinib TKIs to inhibit different mutationally activated EGFR variants is more complicated than previously thought. Given the results described here, the fact that NSCLC mutants and glioblastoma mutants are selectively (and exclusively) inhibited by erlotinib and lapatinib respectively (Vivanco et al., 2012) seems unlikely to reflect simply stabilization of different conformational states of EGFR-TKD in the two cancers (active for NSCLC, inactive for glioblastoma). Rather, the different sensitivities of the EGFR mutants are likely to reflect more complicated conformational, and dynamic, characteristics – as suggested by a previous study (Barkovich et al., 2012). It is clear, for example, that lapatinib dissociates from EGFR-TKD much more slowly than erlotinib or gefitinib (Wood et al., 2004) – although it is also true that covalent inhibitors dissociate even more slowly, yet still show differential effects. More extensive analysis

is required to identify the differences between these groups of inhibitors, which ultimately should aid in tailoring the type of inhibitor used clinically to the mode in which EGFR has been aberrantly activated in cancer.

2.2 Selective inhibition of HER2/HER3 oncogenic complex

N.B. This is collaborative work with Chris Novotny from the laboratory of Kevan Shokat at University of San Francisco. Work contributed by Chris Novotny (C.N.) is marked accordingly in tables and figures.

2.2.1 Introduction

Activation of members of the epidermal growth factor receptor/ErbB tyrosine kinase family involves an allosteric mechanism. Prior to activation, ErbB family kinases are auto-inhibited by hydrophobic interactions between helix αC and a short helix seen within the activation loop of the inactive (but not active) kinase. Asymmetric dimerization of the kinase domains within a receptor dimer disrupts these hydrophobic interactions, with the C-lobe of the 'activator' kinase abutting the N-lobe of the 'receiver' kinase and allosterically activating it (Jura et al., 2009; Zhang et al., 2006). Among four members of the ErbB/HER family of growth factor receptor tyrosine kinases (RTKs), ErbB3 (HER3) is known for it interestingly distinct features. When first cloned, it was noted as a likely 'kinase-dead' member of the family due to its unusual amino acid changes in highly conserved catalytic motifs, notably replacement of the catalytic base aspartate with an asparagine and loss of the key glutamate in helix αC (Hanks et al., 1988; Kraus et al., 1989). Early biochemical studies supported this idea (Citri et al., 2003), although it was since challenged (Shi et al., 2010), as described below. It is also important to note that the ErbB3 ligand, neuregulin (NRG), fails to induce ErbB3 homodimerization, making ErbB3 an obligate heterodimerization partner with other ErbBs (Berger et al., 2004; Citri et al., 2003; Ferguson et al., 2000).

ErbB3 plays an important role in cancer cell survival and proliferation by forming heterodimers with other ErbB receptors in which its TKD functions as the 'activator' kinase in the asymmetric dimer described above (Jura et al., 2009; Zhang et al., 2006). Heterodimerization causes allosteric activation of EGFR and ErbB2 in EGFR/ErbB3 and ErbB2/ErbB3 heterodimers respectively, and *trans*phosphorylation of C-tail tyrosines in ErbB3, which serve as binding sites for the p85 subunit of phosphoinositide 3-kinase (PI3K) at the plasma membrane (Baselga and Swain, 2009). Therefore, ErbB3 is crucial in activating the PI3K-Akt pathway. Overexpression of ErbB3 or its aberrant signaling has been observed in many forms of cancer, such as breast cancer (Holbro et al., 2003; Lee-Hoeflich et al., 2008; Vaught et al., 2012), NSCLC (H. Y. Chen et al., 2007), ovarian (Tanner et al., 2006), colon and gastric cancers (Sithanandam and Anderson, 2008).

Compared to other ligand-induced ErbB combinations, the ErbB2/ErbB3 heterodimer is generally considered to be the most potently mitogenic signaling complex. For example, mouse studies using transfected NIH3T3 cell transplantations showed most aggressive tumor growth with cells expressing this combination of receptors (Alaoui-Jamali et al., 2003; Citri et al., 2003; Holbro et al., 2003). Deletion of ErbB3 in the mammary epithelium of mice expressing ErbB2 dramatically reduces tumor formation (Vaught et al., 2012), and depletion of ErbB3 by RNAi in ErbB2-overexpressing breast cancer cell lines is just as toxic as – or more toxic than – knockdown of ErbB2 by RNAi (Lee-Hoeflich et al., 2008). Similarly, doxorubicin-mediated ablation of ErbB3 is as effective as lapatinib treatment in reducing ErbB2-dependent tumors in mice (Vaught et al., 2012). Overall, ErbB3 is required for both breast cancer development and tumor maintenance, and these findings implicate ErbB3 as a potentially very attractive therapeutic target. However, therapeutic antibodies or small molecule tyrosine kinase inhibitors (TKI) aimed at suppressing ErbB2/ErbB3 signaling have been focused largely on ErbB2 (J. W. Park et al., 2008). Examples of therapeutic agents targeting ErbB2 (HER2) are Herceptin and Tykerb (lapatinib), which have proven clinically effective in breast cancer (Bedard et al., 2009; Sergina and Moasser, 2007). ErbB3 has largely been ignored because it is generally considered a 'dead-

kinase', although several potentially useful ErbB3-targeted antibody therapeutics have now been described (Sala et al., 2012; Schaefer et al., 2011; Schoeberl et al., 2010).

Development of resistance – particularly to small molecule TKIs – has become a very significant problem (Bedard et al., 2009; F. L. Chen et al., 2008) in cancers treated with ErbB receptor inhibitors. It is in this regard that ErbB3 has recently become a focus of attention, as upregulation of ErbB3 phosphorylation appears to play an important role in resistance to EGFR- and ErbB2-targeted TKI drugs such as gefitinib and lapatinib (Engelman et al., 2007; Sergina et al., 2007). It has been shown that cancer cells increase the transcription, translation, and membrane localization of ErbB3 in response to multiple FDA-approved inhibitors of EGFR, ErbB2, PI3K, and other kinases within 96 hrs of treatment in cell culture experiments. This increase in ErbB3 levels is thought to allow the small amount of remaining kinase activity of either EGFR or ErbB2 to phosphorylate enough ErbB3 to keep Akt stimulated via PI3K activation . Inhibiting ErbB3 phosphorylation with inhibitors of the ErbB2 kinase releases feedback from the PI3K/Akt pathway to cause such an increase in total ErbB3 levels (Amin et al., 2010; Sergina et al., 2007). A similar increase in ErbB3 expression and phosphorylation is seen in cells treated with PI3K inhibitors (Chakrabarty et al., 2012). Upregulation of ErbB3 expression via FOXD3 has also been identified as being a critical short term adaptive response to BRAF mutant melanomas treated with PLX4720 (Abel et al., 2013). This raises the concern that traditional kinase inhibitors will be unable to alter ErbB3 signaling, since their activity will be mitigated by this feedback response.

2.2.2 Possible importance of the intrinsic kinase activity of ErbB3 in ErbB signaling

Despite possessing sequence alterations in catalytically important motifs, our lab previously demonstrated that the so-called 'dead-kinase' TKD in ErbB3 retains ATP binding ability (K_D = 1.1 μM) and sufficient kinase activity to carry out *trans*-autophosphorylation *in vitro* – although it's kinase activity was estimated to be 500-1000 fold less than that of the EGFR kinase domain

under similar conditions (Shi et al., 2010). Given the importance of ErbB3 in resistance to EGFR- and ErbB2-targeted therapies in breast and other cancers, our lab has focused on trying to determine whether the intrinsic kinase activity of ErbB3 is important for its signaling, using model Ba/F3 and CHO cell lines.

In order to investigate whether ErbB3's intrinsic kinase activity is required for *trans*phosphorylation of ErbB2 within a neuregulin-induced ErbB2/ErbB3 heterodimer, Ba/F3 cells (null background for endogenous ErbB receptors) were engineered to co-express wild type ErbB2 protein and ErbB3 (wild type or mutants). The ErbB3 variants tested here included K723M and V836A/R, which impair both ATP binding and (therefore) kinase activity (Shi et al., 2010), but do so through different mechanisms. Mutations at K723 (equivalent to K721 in EGFR) directly impact the ATP-binding and catalytic sites, whereas V836 (equivalent to L858 in EGFR) is more remote and is involved in interactions between αC and the activation loop helix that stabilize the inactive-like conformation of kinase. Neuregulin-induced tyrosine phosphorylation of ErbB2 and ErbB3 in Ba/F3 cells was determined by Western blotting (Figure 2.9A). Interestingly, ErbB3 mutations that block its kinase activity failed to impair neuregulin-induced ErbB2 and ErbB3 phosphorylation. These data suggest that the ErbB3 kinase activity detected *in vitro* is not required for ligand induced autophosphorylation of ErbB2/ErbB3 heterodimers.

Our next question was whether ErbB3 kinase domain mutations affect the ability of the receptor to activate PI3K/Akt signaling in response to neuregulin. Neuregulin-dependent Akt activation (detected with specific pAkt antibodies) can be detected in CHO cells overexpressing wild-type ErbB3, but not in parental cells. As shown in Figure 2.9B, neuregulin-dependent Akt activation was observed in CHO cells stably expressing any of the full-length ErbB3 variants, regardless of whether the mutations introduced impaired kinase activity. These results suggest that the kinase activity of ErbB3 is not required for signaling. We therefore concluded that ErbB3 plays an important role in ErbB2/ErbB3 heterodimer signaling even if its ability to signal via PI3K/Akt pathway is not a result of kinase activity.

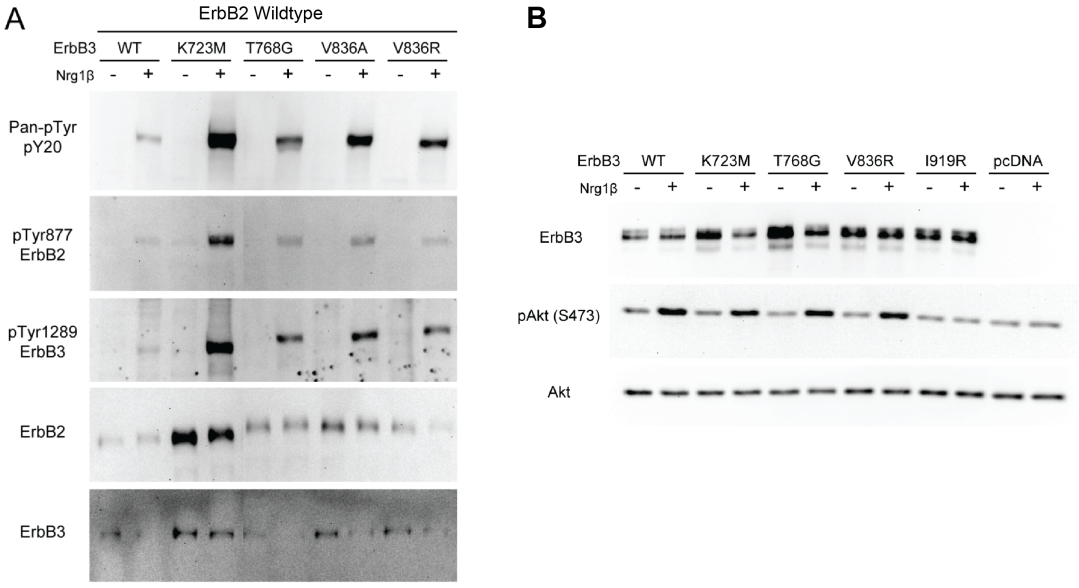

Figure 2.9 Influences of intrinsic kinase activity of ErbB3 in induced autophosphorylation of ErbB2/ErbB3 heterodimer and signaling

(A) Autophosphorylation of ligand induced ErbB2/ErbB3 heterodimers in BaF3 cells. BaF3 cells were stably transfected pIRES plasmids containing both wildtype ErbB2 and (wildtype or mutated) ErbB3 mutants allowing constitutive coexpression of both full length ErbB2 and ErbB3 in the cells. After sorted for high ErbB expression using FACS, BaF3 cells were serum starved for 6 hours, washed, and stimulated with neuregulin 1β (50ng/ml) for 10 min at 4°C. Lysed samples were analyzed by immunoblotting with indicated antibodies to detect ErbB2 and ErbB3 autophosphorylation.

(B) NRG-induced AKT activation in ErbB3 expressing CHO cells. CHO cells were transiently transfected with pcDNA3.1 plasmids containing full length ErbB3 (wildtype or mutant) or parental pcDNA3.1 plasmid. Cells were serum starved overnight, stimulated with neuregulin 1β (40ng/ml) for 30 min. Lysed samples were analyzed by immunoblotting with antibodies against ErbB3 (upper lane), pAkt (middle lane), and total Akt (lower lane) (Figure is from doctoral dissertation of Fumin Shi, Ph.D., University of Pennsylvania, 2012; AAT3551554)

2.2.3 Identification of a novel inhibitor of the ErbB2/ErbB3 heterodimer through high throughput cell-based screening

As mentioned above, the ErbB2/ErbB3 heterodimer can act as oncogenic driver, and its formation is responsible for resistance to existing ErbB2-targeted tyrosine kinase inhibitors. This motivated us to develop/identify novel small molecule inhibitors capable of inhibiting the active ErbB2/ErbB3 oncogenic complex in collaboration with the laboratory of Kevan Shokat at UCSF. The key issue is that the ErbB2 kinase domain is stabilized in its active form in neuregulin-induced ErbB2/ErbB3 heterodimers, with the C-lobe of the ErbB3 kinase domain inducing this conformational change via contacts with the ErbB2 TKD's N-lobe.

In order to identify inhibitors of mitogenic signaling by ErbB2/ErbB3 heterodimers, the Shokat laboratory screened almost a million compounds in a library from the California Institute for Biomedical Research (Calibr). They engineered Ba/F3 cells to be dependent on the formation of neuregulin-stimulated ErbB2/ErbB3 heterodimers. Survival and proliferation of Ba/F3 cells normally requires interleukin-3 (IL-3), but this requirement can be replaced by almost any RTK (including EGFR alone, or ErbB2/ErbB3 heterodimers), allowing EGF or neuregulin to promote IL-3 independent cell survival and proliferation in appropriately engineered Ba/F3 cells (Walker et al, 2004). Ba/F3 cells stably expressing ErbB3 and ErbB2 were generated sequentially selected. Since ErbB2 is capable of transforming cells independently of ErbB3, 9 tyrosines in the C-terminal tail of ErbB2 were mutated to phenylalanine (creating ErbB2YF) to prevent downstream signaling through ErbB2 homodimers, and to ensure that Ba/F3 cell survival and proliferation would be dependent on ErbB3. Neuregulin was then provided in the medium after withdrawal of IL-3 to select for neuregulin-dependent ErbB2YF/ErbB3wt heterodimers (2YF/3wt). The resulting 2YF/3wt cell line allowed screening for inhibitors of signaling by ErbB2/ErbB3 heterodimers.

Generally cytotoxic hits were efficiently removed with counter-screening of same 2YF/3wt cells in presence of IL-3. In addition, wild-type ErbB2 dependent cells and wild-type Axl (unrelated RTK that activates PI3K pathway) dependent cells were created in order to remove other hit

compounds that were not directly inhibiting the ErbB2/ErbB3 heterodimer. A diverse collection of 950,000 drug-like molecules (Z' ≥0.75) was screened as in the schematic representation shown in Figure 2.10. This led to the identification of 3 hit compounds that share the same scaffold and showed preferential inhibition of neuregulin-stimulated, ErbB2/ErbB3 heterodimer-dependent proliferation. SAR optimization was further pursued using an iterative scheme with 10-20 compounds per batch screened against the Ba/F3 panel, finally converging on compound 55A which yielded a large jump in specificity and potency in inhibition of NRG driven cells.

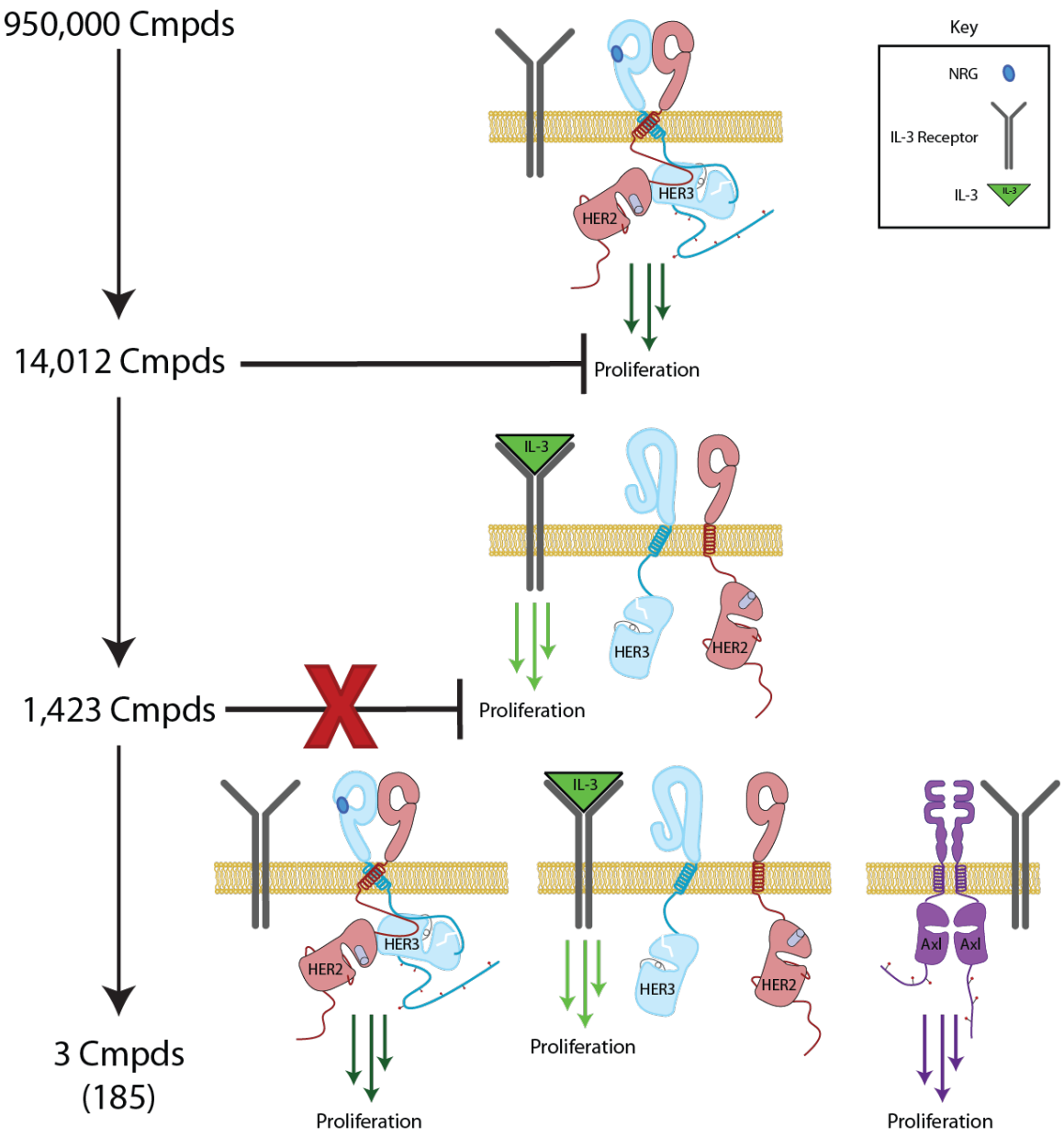

Figure 2.10 Schematic of a high-throughput screen to identify a novel ErbB2/ErbB3 inhibitor Compounds were first screened for the ability to inhibit the proliferation of the 2YF/3wt + neuregulin (NRG) cells (≥ 50% inhibition vs DMSO), counter-screened against the same cell line in the presence of IL-3 (≥ 2 fold change in IC_{50} for + NRG vs IL-3), and then screened in dose response against all 3 cell lines. (Designed and executed by C.N.)

2.2.4 55A is differentiated from clinically available ErbB inhibitors

Based on the *in vitro* biochemical and cell signaling studies outlined above, and described in the literature (Littlefield et al., 2014), we hypothesized that productive ErbB2/ErbB3 heterodimer signaling via the PI3K/Akt pathway might be inhibited selectively by small molecules capable of binding to the ErbB2 TKD in its 'active-like' conformation, or possibly to ErbB3 in its inactive-like conformation if disruption of allosteric ErbB2 activation could be achieved. The high potency and specificity of compound 55A observed in NRG stimulated ErbB2YF/ErbB3wt Ba/F3 cells might represent one of these possibilities.

In order to understand its mechanism of action further, we evaluated 55A's ability to interact with ErbB2 or ErbB3 using *in vitro* kinase assays and a thermofluor assay (Figure 2.11). In analyses of ErbB2 TKD inhibition *in vitro*, 55A turned out to have the same potency as the EGFR/ErbB2 inhibitor lapatinib, as seen in Figure 2.11A. 55A was also shown to be capable of binding the ErbB3 TKD – stabilizing it against thermal denaturation to the same extent as seen with ATP (Figure 2.11B). Current FDA-approved EGFR- and ErbB2-specific inhibitors (such as gefitinib, erlotinib and lapatinib) all target the ATP binding site of kinases, but none inhibit autophosphorylation of purified ErbB3 ICD *in vitro* (Shi et al., 2010). Intriguingly, 55A contrasts with these inhibitors in that it does block the autophosphorylation activity of ErbB3 (Figure 2.12), indicating that it binds to the active site of ErbB3 as well as ErbB2. Moreover, inhibitor profiling studies showed that 55A can inhibit the EGFR kinase domain.

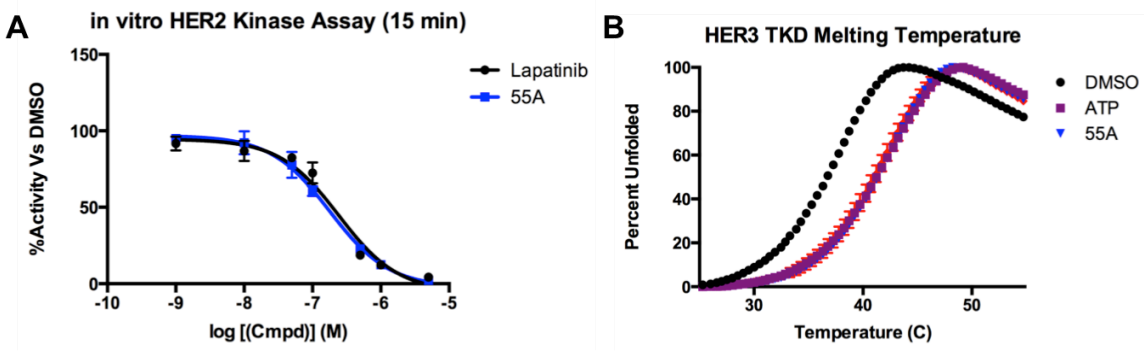

Figure 2.11. 55A is able to interact with ErbB2 and ErbB3

(A) 55A is as potent an ErbB2 inhibitor as lapatinib as assessed in *in vitro* kinase assays.

(B) 55A binds and stabilizes the ErbB3 kinase domain to the same extent as ATP – as determined by Thermofluor assay. (Experiments were done by C.N.).

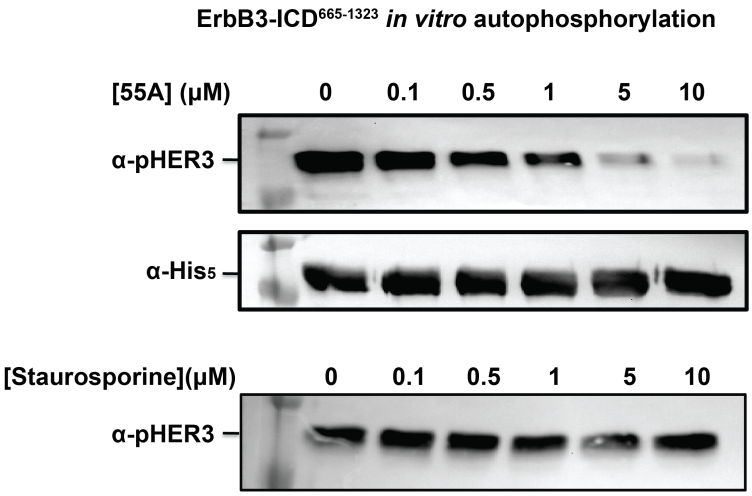

Figure 2.12 Inhibition of ErbB3 kinase autophosphorylation *in vitro*

Western blot to analyze the effect of inhibitors on ErbB3 activity. ErbB3 $ICD^{665-1323}$ (1 μM) protein was incubated with inhibitors and 10 μM lipid vesicles (10% NTA-Ni-DOGS in DOPC background) in 100 mM MOPS pH 7.4, containing 200 mM NaCl, 2mM $MnCl_2$, 5mM $MgCl_2$, 5 % glycerol, 0.1 mM DTT and 0.2 mM ATP for 1 hour at 25℃. The reaction mixture was separated by SDS-PAGE and immunoblotted using anti-phosphotyrosine(pY20) and anti-$(His)_5$.

2.2.5 Structural characterization of a 55A-bound ErbB kinase domain by X-ray crystallography

The EGFR- and ErbB2-targeted drug lapatinib can only bind to the inactive state of ErbB kinase (Wood et al., 2004) because its (3-fluorobenzyl)oxy group must occupy a hydrophobic pocket adjacent to the αC helix that is not available in the active state when αC occupies the 'in' position shown in Figure 2.1 (see also Figure 2.8). This preferential binding to the inactive state of ErbB2 poses a resistance problem clinically, because cancers dependent on the ErbB2/ErbB3 can rapidly escape the inhibitor when stimulated with growth factor, which induces formation of the active ErbB2/ErbB3 asymmetric dimer. We hypothesized that, in order to be useful, an ATP competitive inhibitor of the ErbB2/ErbB3 complex may need to be conformation-specific.

In order to understand how 55A interacts with ErbB kinases, I tried extensive co-crystallization of compound 55A with different ErbB kinase constructs. The ErbB3-TKD WT – which has been only ever been crystallized in an inactive-like conformation (Jura et al., 2009; Shi et al., 2010) failed to give single crystals. Given the results of kinase inhibitor profiling, which showed that 55A can also inhibit EGFR, I also attempted to co-crystallize 55A with the EGFR-TKD in active-like and inactive-like conformations. The WT EGFR-TKD almost always crystallizes in the 'active' conformation, whereas a V924R-mutated EGFR-TKD V924R variant has been shown to crystallize selectively in the inactive conformation, because this C-lobe mutation disrupts the activating N-lobe/C-lobe interactions (Jura et al., 2009; Stamos et al., 2002). EGFR WT/55A co-crystals did not diffract to better than ~8 Å resolution, whereas an EGFR V924R/55A co-crystal generated a useable 3.3 Å data set (Table 2.3).

Strikingly, as shown in Figure 2.13, the EGFR V924R variant did not adopt the expected inactive conformation when co-crystallized with 55A – whereas our previous work showed that it adopts the inactive state when bound to erlotinib (J. H. Park et al., 2012). Even though the V924R mutations breaks the asymmetric dimer normally responsible for adopting the active

conformation, this mutated TKD adopts the active conformation when bound to 55A – in the absence of the normal allosterically activating interactions. This crystallographic analysis suggests that 55A has a strong and unexpected conformational selectivity, and stabilizes the active conformation of ErbB kinase family members (Figure 2.14). Further analysis of Ba/F3 cell inhibition using a series of BaF3 cell lines dependent on NRG-induced HER2/HER3 heterodimers that possessed methionine gatekeeper mutations (TM) in either kinase (2YF/3TM and 2YFTM/HER3wt) or both (2YFTM/3TM) showed inhibition by 55A was only affected by the HER2 gatekeeper mutation, whereas the gatekeeper mutation in HER3 had little influence indicating cellular influences of 55A are mediated by its binding to ErbB2 rather than ErbB3. The effect of 55A thus appears to arise from inhibition of ErbB2 in its active conformation – although changing the conformation of ErbB3 (from 'inactive-like' to 'active-like') could potentially alter its ability to allosterically activate ErbB2, and may aid 55A effects.

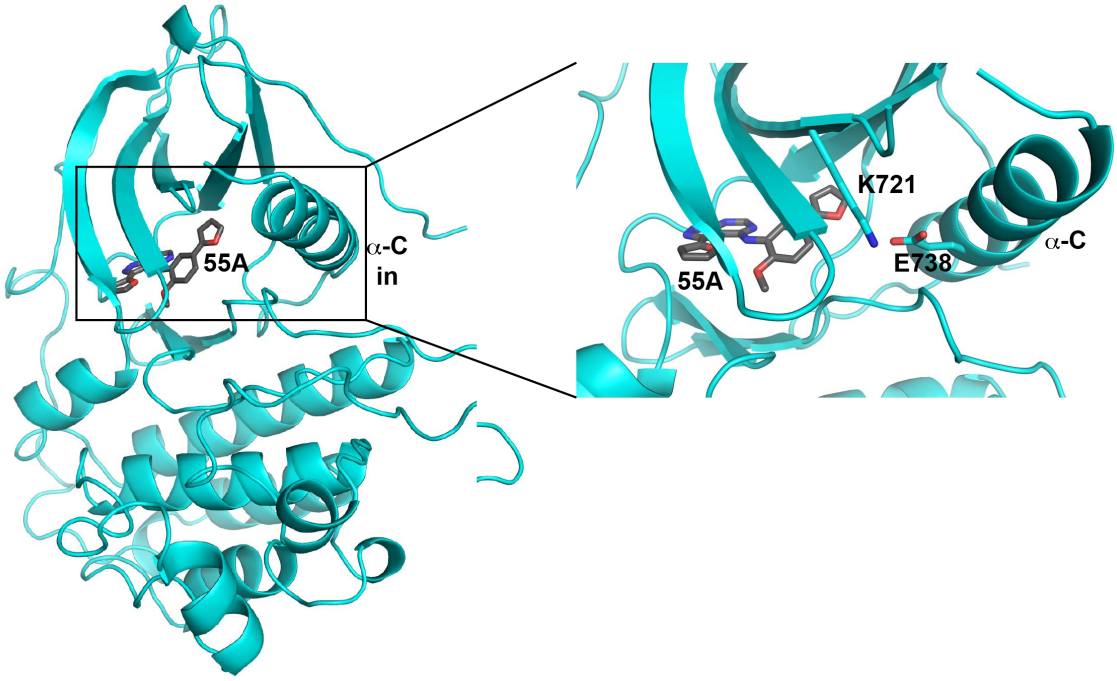

Figure 2.13 Crystal structure of 55A-bound EGFR V924R kinase

Cartoon representation is shown for EGFR-TKD$^{672\text{-}998}$ V924R/55A complex with a zoomed-in view of the active site at right. Key structural elements typically seen in kinases in their active conformation are clearly observed: conformation change in αC helix (in position), salt bridge between the catalytic lysine residue and a glutamate residue in the αC helix, and fully ordered activation segment.

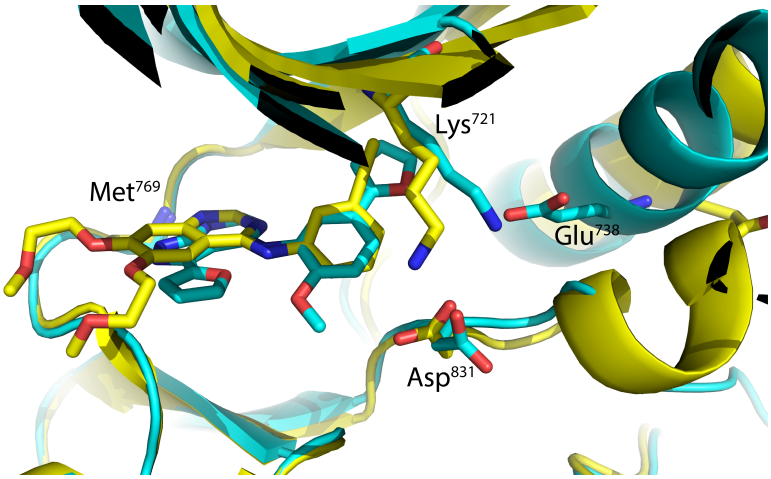

Figure 2.14 Comparison of erlotinib-bound <u>inactive</u> conformation and 55A-bound <u>active</u> conformation of EGFR-TKD$^{672\text{-}998}$ V924R structure

The crystallographically observed mode of erlotinib binding to inactive EGFR-TKD (yellow) is compared with that of 55A binding to active EGFR-TKD (cyan). The protein structure in the background is similarly colored. Sidechain shift of Asp^{831} (in DFG motif) due to 55A binding could be responsible for disruption of activation loop helical segment stabilizing 'inactive' hydrophobic interaction with αC helix.

Table 2.3 Data collection and refinement statistics (molecular replacement)

Each dataset was collected from a single crystal. Values for highest resolution shell are shown in parentheses.

	EGFR/55A
Data collection	
Space group	P 3_1 2 1
Cell dimensions	
a, *b*, *c* (Å)	69.4, 69.4, 192
a, b, g (°)	90, 90, 120
Resolution (Å)	50-3.30
R_{sym}	0.057 (0.982)
I/σ	21.4 (1.26)
Completeness (%)	99.7 (99.7)
Redundancy	3.4 (3.5)
Refinement	
Resolution (Å)	50-3.30
No. reflections	8562
R_{work} / R_{free}	0.24/0.27
No. atoms	
Protein	2333
Ligand/Ion	38
B-factors	
Protein	154.5
Ligand/Ion	128.5
R.m.s. deviations	
Bond lengths (Å)	0.003
Bond angles (°)	0.630

2.2.6 Conclusions

We have identified a novel inhibitor 55A that preferentially binds and inhibits the active state of ErbB2 through a high throughput screen of Ba/F3 cells dependent on neuregulin-stimulated HER2/HER3. The complete mechanism of action of this compound is still under investigation, and there is room for further optimization as well. However, I hope to gain some insights from the inhibitor-bound structure on how small molecule kinase inhibitors prefer 'inactive-like' or 'active-like' conformation of the kinase domain for further improvement on binding affinity and selectivity of the compounds. Collaborative approaches combining cell signaling studies, biochemistry and structural biology will help us to identify potentially very important therapeutic agent preventing non-mutational resistance to currently available drugs, and also to understand the role of conformationally regulated pseudokinase scaffold in cancer.

2.3 Experimental Procedures

2.3.1 Plasmid Construction

DNA encoding kinase domain residues 672-998 (mature protein numbering), equivalent to residues 696-1022 (precursor protein numbering) of human EGFR (NCBI reference sequence NP_005219.2) was amplified by PCR using primers that included an N-terminal hexahistidine tag and *SpeI/XhoI* restriction sites. The PCR product was subcloned into pFastBac1 (Invitrogen) for generating recombinant baculovirus with the Bac-to-Bac system (Invitrogen) for protein expression in *Spodoptera frugiperda* Sf9 cells. To generate the V924R mutation, the codon for Val^{924} (mature protein numbering) was substituted with an arginine codon using the QuikChange method (Agilent Technologies).

For wild-type ErbB3 protein, DNA encoding residues 665-1323 (mature protein numbering) of human ErbB3 intracellular region was subcloned into the pFastBac1 with N-terminal hexa-histidine tag (Shi et al., 2010).

2.3.2 Protein production and purification

Sf9 cells at 1.5-2 x 10^6/ml were infected with recombinant baculovirus, and harvested by centrifugation after 3 days. Cells expressing histidine-tagged $EGFR^{672-998}$/V924R (~3 liters of medium) were lysed by sonication in 100 ml of lysis buffer (20 mM Tris-HCl, pH 8.0, containing 500 mM NaCl, 5 mM 2-mercaptoethanol, and protease inhibitor cocktail (Roche)). After centrifugation at 40,000 x g for 30 min to remove cell debris, the supernatant was passed through a 0.45 µm filter and incubated with Ni-NTA agarose beads (Qiagen) for 1 hr at 4ºC. Beads were washed in 50 column-volumes of lysis buffer, and bound EGFR TKD protein was eluted in lysis buffer containing increasing concentrations of imidazole. Eluted protein was then further purified using an UnoQ anion exchange column (Bio-Rad) equilibrated with 20 mM Tris-HCl, pH 8.0, containing 5% glycerol, 2 mM DTT and eluting with a gradient from 75 mM to 1 M NaCl over 20 column volumes. EGFR TKD protein was then subjected to a final step of size exclusion chromatography using a Superdex 200 column (GE Healthcare) equilibrated in 20 mM Tris-HCl, pH 8.0, containing 150 mM NaCl and 2 mM DTT. 1-2 mg of purified $EGFR^{672-998}$/V924R protein was typically obtained per liter of Sf9 cell culture.

ErbB3-$ICD^{665-1323}$ wild-type protein expression and purification was performed exactly as described by Shi et al. (2010).

2.3.3 Crystallization and structure determination

Crystals were obtained using the hanging drop vapor diffusion method, by mixing equal volumes of protein and reservoir solutions and equilibrating over the reservoir solution at 21˚C. For the EGFR TKD^{V924R}/erlotinib structure, EGFR TKD protein was concentrated to 6 mg/ml in 20 mM Tris-HCl, pH 8.0, containing 150 mM NaCl and 2 mM DTT. Crystals were obtained with a

reservoir solution of 0.25 M NaSCN pH 6.9, 27% (w/v) PEG3350, and when 10 mM taurine had been included as 'additive' in the hanging drop, and were soaked for 2 hours at 21˚C in mother liquor containing 1 mM erlotinib. Crystals were cryo-protected in reservoir solution with added 20% (w/v) glycerol, and were flash frozen in liquid nitrogen. Diffraction data were collected at beamline 23ID-D of GM/CA@APS (Advanced Photon Source), where crystals diffracted to 2.75 Å, and were processed using HKL2000 (see Table 2.2). The structure was solved by molecular replacement using Phaser with the inactive EGFR (V924R) TKD structure (PDB 3GT8) as search model. Repeated cycles of manual building/rebuilding using Coot were alternated with rounds of refinement employing REFMAC, plus composite omit maps calculated using CNS. PHENIX and TLS refinement were used in the later stages. Coordinates, parameter files and molecular topology of erlotinib was generated by PRODRG. Data collection and refinement statistics are shown in Table 2.2. One molecule of $EGFR^{672-998}$/V924R is present in the asymmetric unit, and the model of its structure complexed with erlotinib includes amino acids 679-709 and 714-960 (mature EGFR numbering). Structural figures were generated with PyMOL.

For the EGFR TKD^{V924R}/55A structure, EGFR TKD protein was concentrated to 8 mg/ml in 20 mM Tris-HCl, pH 8.0, containing 150 mM NaCl and 2 mM DTT. Protein was co-crystallized with excess of a drug 55A (1:2 molar ratio) in a reservoir solution of 1.34M Ammonium sulfate, 1.34% (v/v) PEG 400, and 0.1M sodium acetate/acetic acid pH 5.5 in the hanging drop at 21˚C. Crystals were cryo-protected in reservoir solution with added 20% (w/v) glycerol and were flash frozen in liquid nitrogen. Diffraction data were collected at beamline 23ID-B of GM/CA@APS (Advanced Photon Source), where crystals diffracted to 3.3 Å, and were processed using HKL2000 (see Table 2.3). The structure was solved by molecular replacement using Phaser with the active EGFR (WT) TKD structure (PDB 1M17) as search model. Repeated cycles of manual building/rebuilding using Coot were alternated with rounds of refinement employing REFMAC(Murshudov et al., 2011) and PHENIX, plus composite omit maps calculated using PHENIX. Coordinates, parameter files and molecular topology of 55A was generated by

PRODRG. Data collection and refinement statistics are shown in Table 2.3. One molecule of EGFR$^{672-998}$/V924R is present in the asymmetric unit, and the model of its structure complexed with 55A includes amino acids 675 - 978 (mature EGFR numbering). Structural figures were generated with PyMOL.

2.3.4 Analysis of autophosphorylation by western blotting

To monitor the change in autophosphorylation, 1μM ErbB3-ICD$^{665-1323}$ proteins were incubated with inhibitors (varied concentrations noted in the Figure) and DOGS-Ni-NTA (prepared as described in Zhang et al, 2006) in 100 mM MOPS pH 7.4, containing 200 mM NaCl, divalent cations (2mM $MnCl_2$ plus 5mM $MgCl_2$), 5 % glycerol, 0.1 mM DTT and 200 μM ATP for 1 hour at 25℃, and the reactions were stopped by adding 50 mM EDTA and SDS-PAGE gel-loading buffer for rapid qualitative comparison of autophosphorylation by SDS-PAGE and immunoblotting with anti-phosphotyrosine (pY20) and anti-$(His)_5$.

2.3.5 Molecular modeling: System preparation and molecular docking

Active EGFR-TKD was modeled based on PDB entries 1M17 (which also provided the initial erlotinib conformation) and 2ITX, and L834R using PDB entry 2ITV. Inactive EGFR-TKD was modeled based on PDB entries 2GS7 and 1XKK. Protein and ligand conformations were prepared using the Protein Preparation Wizard and LigPrep protocols from Schrödinger Software (New York, NY). All docking simulations employed the OPLS (Optimized Potentials for Liquid Simulations) force field, and used Schrödinger's Induced Fit Docking (IFD) package. Ligand was first docked to rigid protein using Glide XP. For the resulting top 20 complex conformations, the protein side chains within 5.0 Å of the ligand in that pose were subject to conformational search and minimized using Prime and the ligand was redocked to the 20 new receptor conformations.

2.3.6 MD simulations

Conformations generated from induced fit docking were energy minimized and subsequently equilibrated by performing MD using the CHARMM27 force field. Each system was subjected to a constant temperature and constant pressure molecular dynamics runs at 300 K and 1 atm, followed by constant temperature equilibrium at 300 K with periodic boundaries enforced and long-range electrostatics taken into consideration for 10 ns.

2.3.7 MM/PBSA (molecular mechanics/Poisson-Boltzmann surface area) calculation

We used MM/PBSA to calculate the absolute binding free energy and compared it to the Glide score based on the 10 ns MD simulation. MM/PBSA energies of each modeled complex conformation were calculated as the average of single point MM/PBSA energy of 500 snapshots taken from the 10 ns simulation. Water molecules and salt ions were removed from the trajectory before calculation. The molecular mechanics energy, U_{MM}, was evaluated by averaging energies over all structures using an infinite cutoff for non-bonded interactions. The electrostatic contribution to the solvation free energy, W_{PB}, was calculated using Poisson-Boltzmann Solver in CHARMM. The reference system had a solvent dielectric constant of 1 and salt concentration of 0 M, and the solvated system had a dielectric constant of 80 and salt concentration of 100 mM. Nonpolar contribution to the solvation free energy, W_{SA}, was approximated with the surface area model ΔW_{SA}=[0.00542 kcal/mol/Å^2] x SASA + 0.92 kcal/mol, where the surface accessible surface area (SASA) was estimated using a 1.4 Å solvent probe radius. Terms for entropy changes in the MM/PBSA score were neglected.

2.4 References

Abel, E. V., Basile, K. J., Kugel, C. H., 3rd, Witkiewicz, A. K., Le, K., Amaravadi, R. K., . . . Aplin, A. E. (2013). Melanoma adapts to RAF/MEK inhibitors through FOXD3-mediated upregulation of ERBB3. *J Clin Invest, 123*(5), 2155-2168. doi: 10.1172/JCI65780

Adams, P. D., Afonine, P. V., Bunkoczi, G., Chen, V. B., Davis, I. W., Echols, N., . . . Zwart, P. H. (2010). PHENIX: a comprehensive Python-based system for macromolecular structure solution. *Acta Crystallogr D Biol Crystallogr, 66*(Pt 2), 213-221. doi: 10.1107/S0907444909052925

Alaoui-Jamali, M. A., Song, D. J., Benlimame, N., Yen, L., Deng, X., Hernandez-Perez, M., & Wang, T. (2003). Regulation of multiple tumor microenvironment markers by overexpression of single or paired combinations of ErbB receptors. *Cancer Res, 63*(13), 3764-3774.

Amin, D. N., Sergina, N., Ahuja, D., McMahon, M., Blair, J. A., Wang, D., . . . Moasser, M. M. (2010). Resiliency and vulnerability in the HER2-HER3 tumorigenic driver. *Sci Transl Med, 2*(16), 16ra17. doi: 10.1126/scitranslmed.3000389

Anido, J., Matar, P., Albanell, J., Guzman, M., Rojo, F., Arribas, J., . . . Baselga, J. (2003). ZD1839, a specific epidermal growth factor receptor (EGFR) tyrosine kinase inhibitor, induces the formation of inactive EGFR/HER2 and EGFR/HER3 heterodimers and prevents heregulin signaling in HER2-overexpressing breast cancer cells. *Clin Cancer Res, 9*(4), 1274-1283.

Barkovich, K. J., Hariono, S., Garske, A. L., Zhang, J., Blair, J. A., Fan, Q. W., . . . Weiss, W. A. (2012). Kinetics of inhibitor cycling underlie therapeutic disparities between EGFR-driven lung and brain cancers. *Cancer Discov, 2*(5), 450-457. doi: 10.1158/2159-8290.CD-11-0287

Baselga, J., & Swain, S. M. (2009). Novel anticancer targets: revisiting ERBB2 and discovering ERBB3. *Nat Rev Cancer, 9*(7), 463-475. doi: 10.1038/nrc2656

Bedard, P. L., Cardoso, F., & Piccart-Gebhart, M. J. (2009). Stemming resistance to HER-2 targeted therapy. *J Mammary Gland Biol Neoplasia, 14*(1), 55-66. doi: 10.1007/s10911-009-9116-x

Berger, M. B., Mendrola, J. M., & Lemmon, M. A. (2004). ErbB3/HER3 does not homodimerize upon neuregulin binding at the cell surface. *FEBS Lett, 569*(1-3), 332-336. doi: 10.1016/j.febslet.2004.06.014

Cancer Genome Atlas Research, N. (2008). Comprehensive genomic characterization defines human glioblastoma genes and core pathways. *Nature, 455*(7216), 1061-1068. doi: 10.1038/nature07385

Chakrabarty, A., Sanchez, V., Kuba, M. G., Rinehart, C., & Arteaga, C. L. (2012). Feedback upregulation of HER3 (ErbB3) expression and activity attenuates antitumor effect of PI3K inhibitors. *Proc Natl Acad Sci U S A, 109*(8), 2718-2723. doi: 10.1073/pnas.1018001108

Chen, F. L., Xia, W., & Spector, N. L. (2008). Acquired resistance to small molecule ErbB2 tyrosine kinase inhibitors. *Clin Cancer Res, 14*(21), 6730-6734. doi: 10.1158/1078-0432.CCR-08-0581

Chen, H. Y., Yu, S. L., Chen, C. H., Chang, G. C., Chen, C. Y., Yuan, A., . . . Yang, P. C. (2007). A five-gene signature and clinical outcome in non-small-cell lung cancer. *N Engl J Med, 356*(1), 11-20. doi: 10.1056/NEJMoa060096

Citri, A., Skaria, K. B., & Yarden, Y. (2003). The deaf and the dumb: the biology of ErbB-2 and ErbB-3. *Exp Cell Res, 284*(1), 54-65.

Eck, M. J., & Yun, C. H. (2010). Structural and mechanistic underpinnings of the differential drug sensitivity of EGFR mutations in non-small cell lung cancer. *Biochim Biophys Acta, 1804*(3), 559-566. doi: 10.1016/j.bbapap.2009.12.010

Emsley, P., & Cowtan, K. (2004). Coot: model-building tools for molecular graphics. *Acta Crystallogr D Biol Crystallogr, 60*(Pt 12 Pt 1), 2126-2132. doi: 10.1107/S0907444904019158

Engelman, J. A., Zejnullahu, K., Mitsudomi, T., Song, Y., Hyland, C., Park, J. O., . . . Janne, P. A. (2007). MET amplification leads to gefitinib resistance in lung cancer by activating ERBB3 signaling. *Science, 316*(5827), 1039-1043. doi: 10.1126/science.1141478

Fabian, M. A., Biggs, W. H., 3rd, Treiber, D. K., Atteridge, C. E., Azimioara, M. D., Benedetti, M. G., . . . Lockhart, D. J. (2005). A small molecule-kinase interaction map for clinical kinase inhibitors. *Nat Biotechnol, 23*(3), 329-336. doi: 10.1038/nbt1068

Ferguson, K. M., Darling, P. J., Mohan, M. J., Macatee, T. L., & Lemmon, M. A. (2000). Extracellular domains drive homo- but not hetero-dimerization of erbB receptors. *EMBO J, 19*(17), 4632-4643. doi: 10.1093/emboj/19.17.4632

Friesner, R. A., Murphy, R. B., Repasky, M. P., Frye, L. L., Greenwood, J. R., Halgren, T. A., . . . Mainz, D. T. (2006). Extra precision glide: docking and scoring incorporating a model of hydrophobic enclosure for protein-ligand complexes. *J Med Chem, 49*(21), 6177-6196. doi: 10.1021/jm051256o

Hanks, S. K., Quinn, A. M., & Hunter, T. (1988). The protein kinase family: conserved features and deduced phylogeny of the catalytic domains. *Science, 241*(4861), 42-52.

Holbro, T., Beerli, R. R., Maurer, F., Koziczak, M., Barbas, C. F., 3rd, & Hynes, N. E. (2003). The ErbB2/ErbB3 heterodimer functions as an oncogenic unit: ErbB2 requires ErbB3 to drive breast tumor cell proliferation. *Proc Natl Acad Sci U S A, 100*(15), 8933-8938. doi: 10.1073/pnas.1537685100

Janne, P. A., Gray, N., & Settleman, J. (2009). Factors underlying sensitivity of cancers to small-molecule kinase inhibitors. *Nat Rev Drug Discov, 8*(9), 709-723. doi: 10.1038/nrd2871

Jura, N., Endres, N. F., Engel, K., Deindl, S., Das, R., Lamers, M. H., . . . Kuriyan, J. (2009). Mechanism for activation of the EGF receptor catalytic domain by the juxtamembrane segment. *Cell, 137*(7), 1293-1307. doi: 10.1016/j.cell.2009.04.025

Kraus, M. H., Issing, W., Miki, T., Popescu, N. C., & Aaronson, S. A. (1989). Isolation and characterization of ERBB3, a third member of the ERBB/epidermal growth factor receptor family: evidence for overexpression in a subset of human mammary tumors. *Proc Natl Acad Sci U S A, 86*(23), 9193-9197.

Lee, J. C., Vivanco, I., Beroukhim, R., Huang, J. H., Feng, W. L., DeBiasi, R. M., . . . Mellinghoff, I. K. (2006). Epidermal growth factor receptor activation in glioblastoma through novel missense mutations in the extracellular domain. *PLoS Med, 3*(12), e485. doi: 10.1371/journal.pmed.0030485

Lee-Hoeflich, S. T., Crocker, L., Yao, E., Pham, T., Munroe, X., Hoeflich, K. P., . . . Stern, H. M. (2008). A central role for HER3 in HER2-amplified breast cancer: implications for targeted therapy. *Cancer Res, 68*(14), 5878-5887. doi: 10.1158/0008-5472.CAN-08-0380

Lemmon, M. A., & Schlessinger, J. (2010). Cell signaling by receptor tyrosine kinases. *Cell, 141*(7), 1117-1134. doi: 10.1016/j.cell.2010.06.011

Libermann, T. A., Nusbaum, H. R., Razon, N., Kris, R., Lax, I., Soreq, H., . . . Schlessinger, J. (1985). Amplification, enhanced expression and possible rearrangement of EGF receptor gene in primary human brain tumours of glial origin. *Nature, 313*(5998), 144-147.

Littlefield, P., Liu, L., Mysore, V., Shan, Y., Shaw, D. E., & Jura, N. (2014). Structural analysis of the EGFR/HER3 heterodimer reveals the molecular basis for activating HER3 mutations. *Sci Signal, 7*(354), ra114. doi: 10.1126/scisignal.2005786

Liu, Y., & Gray, N. S. (2006). Rational design of inhibitors that bind to inactive kinase conformations. *Nat Chem Biol, 2*(7), 358-364. doi: 10.1038/nchembio799

Lu, C., Mi, L. Z., Schurpf, T., Walz, T., & Springer, T. A. (2012). Mechanisms for kinase-mediated dimerization of the epidermal growth factor receptor. *J Biol Chem, 287*(45), 38244-38253. doi: 10.1074/jbc.M112.414391

Lynch, T. J., Bell, D. W., Sordella, R., Gurubhagavatula, S., Okimoto, R. A., Brannigan, B. W., . . . Haber, D. A. (2004). Activating mutations in the epidermal growth factor receptor underlying responsiveness of non-small-cell lung cancer to gefitinib. *N Engl J Med, 350*(21), 2129-2139. doi: 10.1056/NEJMoa040938

Mi, L. Z., Lu, C., Li, Z., Nishida, N., Walz, T., & Springer, T. A. (2011). Simultaneous visualization of the extracellular and cytoplasmic domains of the epidermal growth factor receptor. *Nat Struct Mol Biol, 18*(9), 984-989. doi: 10.1038/nsmb.2092

Murshudov, G. N., Skubak, P., Lebedev, A. A., Pannu, N. S., Steiner, R. A., Nicholls, R. A., . . . Vagin, A. A. (2011). REFMAC5 for the refinement of macromolecular crystal structures. *Acta Crystallogr D Biol Crystallogr, 67*(Pt 4), 355-367. doi: 10.1107/S0907444911001314

Pao, W., & Chmielecki, J. (2010). Rational, biologically based treatment of EGFR-mutant non-small-cell lung cancer. *Nat Rev Cancer, 10*(11), 760-774. doi: 10.1038/nrc2947

Park, J. H., Liu, Y., Lemmon, M. A., & Radhakrishnan, R. (2012). Erlotinib binds both inactive and active conformations of the EGFR tyrosine kinase domain. *Biochem J, 448*(3), 417-423. doi: 10.1042/BJ20121513

Park, J. W., Neve, R. M., Szollosi, J., & Benz, C. C. (2008). Unraveling the biologic and clinical complexities of HER2. *Clin Breast Cancer, 8*(5), 392-401. doi: 10.3816/CBC.2008.n.047

Sala, G., Traini, S., D'Egidio, M., Vianale, G., Rossi, C., Piccolo, E., . . . Consorzio Interuniversitario Nazionale per la, B.-O. (2012). An ErbB-3 antibody, MP-RM-1, inhibits tumor growth by blocking ligand-dependent and independent activation of ErbB-3/Akt signaling. *Oncogene, 31*(10), 1275-1286. doi: 10.1038/onc.2011.322

Schaefer, G., Haber, L., Crocker, L. M., Shia, S., Shao, L., Dowbenko, D., . . . Eigenbrot, C. (2011). A two-in-one antibody against HER3 and EGFR has superior inhibitory activity compared with monospecific antibodies. *Cancer Cell, 20*(4), 472-486. doi: 10.1016/j.ccr.2011.09.003

Schoeberl, B., Faber, A. C., Li, D., Liang, M. C., Crosby, K., Onsum, M., . . . Wong, K. K. (2010). An ErbB3 antibody, MM-121, is active in cancers with ligand-dependent activation. *Cancer Res, 70*(6), 2485-2494. doi: 10.1158/0008-5472.CAN-09-3145

Schuttelkopf, A. W., & van Aalten, D. M. (2004). PRODRG: a tool for high-throughput crystallography of protein-ligand complexes. *Acta Crystallogr D Biol Crystallogr, 60*(Pt 8), 1355-1363. doi: 10.1107/S0907444904011679

Sergina, N. V., & Moasser, M. M. (2007). The HER family and cancer: emerging molecular mechanisms and therapeutic targets. *Trends Mol Med, 13*(12), 527-534. doi: 10.1016/j.molmed.2007.10.002

Sergina, N. V., Rausch, M., Wang, D., Blair, J., Hann, B., Shokat, K. M., & Moasser, M. M. (2007). Escape from HER-family tyrosine kinase inhibitor therapy by the kinase-inactive HER3. *Nature, 445*(7126), 437-441. doi: 10.1038/nature05474

Sharma, S. V., Bell, D. W., Settleman, J., & Haber, D. A. (2007). Epidermal growth factor receptor mutations in lung cancer. *Nat Rev Cancer, 7*(3), 169-181. doi: 10.1038/nrc2088

Shi, F., Telesco, S. E., Liu, Y., Radhakrishnan, R., & Lemmon, M. A. (2010). ErbB3/HER3 intracellular domain is competent to bind ATP and catalyze autophosphorylation. *Proc Natl Acad Sci U S A, 107*(17), 7692-7697. doi: 10.1073/pnas.1002753107

Sithanandam, G., & Anderson, L. M. (2008). The ERBB3 receptor in cancer and cancer gene therapy. *Cancer Gene Ther, 15*(7), 413-448. doi: 10.1038/cgt.2008.15

Stamos, J., Sliwkowski, M. X., & Eigenbrot, C. (2002). Structure of the epidermal growth factor receptor kinase domain alone and in complex with a 4-anilinoquinazoline inhibitor. *J Biol Chem, 277*(48), 46265-46272. doi: 10.1074/jbc.M207135200

Sugawa, N., Ekstrand, A. J., James, C. D., & Collins, V. P. (1990). Identical splicing of aberrant epidermal growth factor receptor transcripts from amplified rearranged genes in human glioblastomas. *Proc Natl Acad Sci U S A, 87*(21), 8602-8606.

Tanner, B., Hasenclever, D., Stern, K., Schormann, W., Bezler, M., Hermes, M., . . . Hengstler, J. G. (2006). ErbB-3 predicts survival in ovarian cancer. *J Clin Oncol, 24*(26), 4317-4323. doi: 10.1200/JCO.2005.04.8397

Vaught, D. B., Stanford, J. C., Young, C., Hicks, D. J., Wheeler, F., Rinehart, C., . . . Cook, R. S. (2012). HER3 is required for HER2-induced preneoplastic changes to the breast epithelium and tumor formation. *Cancer Res, 72*(10), 2672-2682. doi: 10.1158/0008-5472.CAN-11-3594

Vivanco, I., Robins, H. I., Rohle, D., Campos, C., Grommes, C., Nghiemphu, P. L., . . . Mellinghoff, I. K. (2012). Differential sensitivity of glioma- versus lung cancer-specific EGFR mutations to EGFR kinase inhibitors. *Cancer Discov, 2*(5), 458-471. doi: 10.1158/2159-8290.CD-11-0284

Wang, Z., Longo, P. A., Tarrant, M. K., Kim, K., Head, S., Leahy, D. J., & Cole, P. A. (2011). Mechanistic insights into the activation of oncogenic forms of EGF receptor. *Nat Struct Mol Biol, 18*(12), 1388-1393. doi: 10.1038/nsmb.2168

Wood, E. R., Truesdale, A. T., McDonald, O. B., Yuan, D., Hassell, A., Dickerson, S. H., . . . Shewchuk, L. (2004). A unique structure for epidermal growth factor receptor bound to GW572016 (Lapatinib): relationships among protein conformation, inhibitor off-rate, and receptor activity in tumor cells. *Cancer Res, 64*(18), 6652-6659. doi: 10.1158/0008-5472.CAN-04-1168

Yoshikawa, S., Kukimoto-Niino, M., Parker, L., Handa, N., Terada, T., Fujimoto, T., . . . Yokoyama, S. (2013). Structural basis for the altered drug sensitivities of non-small cell lung cancer-associated mutants of human epidermal growth factor receptor. *Oncogene, 32*(1), 27-38. doi: 10.1038/onc.2012.21

Yun, C. H., Boggon, T. J., Li, Y., Woo, M. S., Greulich, H., Meyerson, M., & Eck, M. J. (2007). Structures of lung cancer-derived EGFR mutants and inhibitor complexes: mechanism of activation and insights into differential inhibitor sensitivity. *Cancer Cell, 11*(3), 217-227. doi: 10.1016/j.ccr.2006.12.017

Yun, C. H., Mengwasser, K. E., Toms, A. V., Woo, M. S., Greulich, H., Wong, K. K., . . . Eck, M. J. (2008). The T790M mutation in EGFR kinase causes drug resistance by increasing the affinity for ATP. *Proc Natl Acad Sci U S A, 105*(6), 2070-2075. doi: 10.1073/pnas.0709662105

Zhang, X., Gureasko, J., Shen, K., Cole, P. A., & Kuriyan, J. (2006). An allosteric mechanism for activation of the kinase domain of epidermal growth factor receptor. *Cell, 125*(6), 1137-1149. doi: 10.1016/j.cell.2006.05.013

Zhang, X., Pickin, K. A., Bose, R., Jura, N., Cole, P. A., & Kuriyan, J. (2007). Inhibition of the EGF receptor by binding of MIG6 to an activating kinase domain interface. *Nature, 450*(7170), 741-744. doi: 10.1038/nature05998

CHAPTER 3:

Activation and Inhibition of Anaplastic lymphoma kinase (ALK) in neuroblastoma

N.B. This is collaborative work with Scott C. Bresler from the Lemmon Lab, Peter J. Huwe from the Radhakrishnan lab, Daniel A. Weiser and Nicole R. Infarinato from the Mossé lab; and can be found published in Bresler *et al.* (2014) *Cancer Cell* 26(5): 682-94 and Infarinato et al. (2016) *Cancer Discovery* 6(1): 96-107. Works contributed are marked accordingly in tables and figures.

3.1 Introduction

Neuroblastoma (NB) is a devastating pediatric cancer of the autonomic nervous system, accounting for 12% of childhood cancer deaths (Maris, 2010). Despite major enhancements in treatment approaches, such as dose-intensive chemotherapy, radiation therapy and integration of immunotherapeutic strategies, the cure rate for patients with high-risk neuroblastoma remains unsatisfactory (Maris, 2010; Yu et al., 2010). Recent clinical studies have focused on increasing dose intensity of those therapies that showed improved response (Pearson et al., 2008); however, potential long-term side effects still remain a major concern (Hobbie et al., 2008; Smith et al., 2010). The most important clinical prognostic marker for neuroblastoma, MYCN copy number status, is not sufficient alone to guide optimal treatment.

Genetic studies have established the anaplastic lymphoma kinase (ALK), a cell surface receptor tyrosine kinase, as the only tractable oncogenic product for targeted therapy in neuroblastoma. Germline and somatic aberrations in the gene encoding ALK are implicated in approximately 8% of all neuroblastomas (Chen et al., 2008; George et al., 2008; Janoueix-Lerosey et al., 2008; Mosse et al., 2008). Within the high-risk subset of neuroblastoma patients, the overall frequency of *ALK* aberration at diagnosis is 14% (10% point mutations and 4% amplification) and correlates with inferior outcome (Bresler et al., 2014). Additional *ALK* mutations at relapse have also been reported (Eleveld et al., 2015; Schleiermacher et al., 2014). The activating mutations are found at several sites in the tyrosine kinase domain of full-length ALK (Bresler et al., 2014) (Figure 3.1), including three hotspots, R1275, F1174, and F1245. These findings motivated a phase I trial of the ATP-competitive ALK/MET/ROS1 inhibitor crizotinib in children with refractory neuroblastoma or other malignancies driven by *ALK* rearrangements, such as anaplastic large cell lymphoma (ALCL) and inflammatory myofibroblastic tumors (IMT)

(Mosse et al., 2013). Results from this trial underscored the importance of *ALK* across histologically diverse tumors, but recorded less frequent responses in neuroblastoma than in *ALK*-rearranged tumors – highlighting likely differences between therapeutic targeting of full-length ALK in neuroblastoma and of cytoplasmic ALK fusion proteins in ALCL, IMTs, and lung cancer. Results also underlined the need for detailed analysis of the spectrum of ALK mutations and how it relates to tumor biology and patient outcome, thus fully categorizing aberrations in ALK for optimal clinical application of ALK inhibitors in neuroblastoma. The findings from such studies will lay the groundwork for opportunities to refine treatment, to identify patients likely to benefit from ALK inhibition and to predict which newly emerged mutations are clinically relevant and 'actionable'.

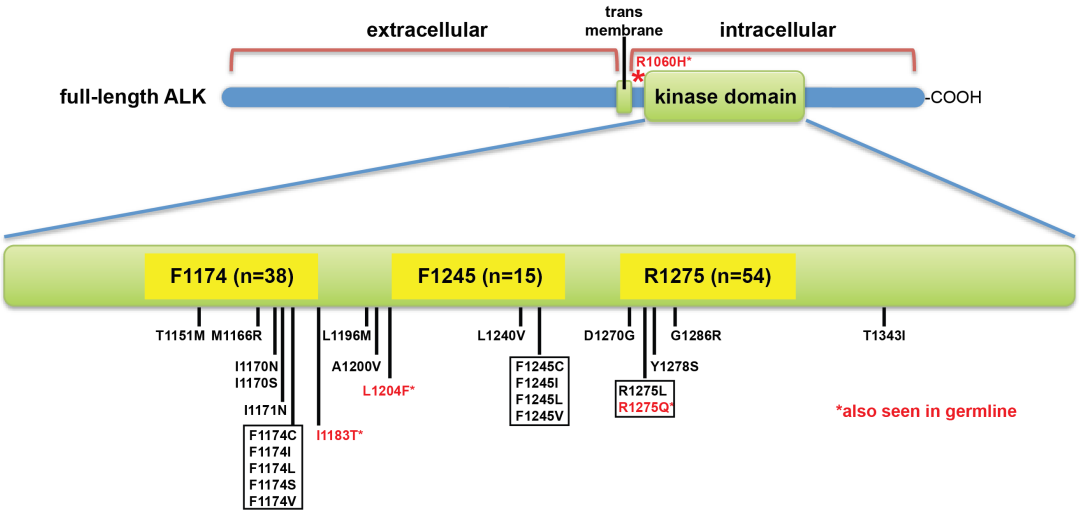

Figure 3.1 Distribution of ALK mutations in tumor samples from neuroblastoma patients

The 126 potentially disease-related mutations observed were distributed over the 16 positions marked in the ALK TKD plus R1060 (between the TKD and the transmembrane domain, upper part of the figure). Variants with red asterisks (in red text) were also found in germline DNA. (Bresler et al., 2014)

Parallel preclinical work has further revealed differential sensitivity to crizotinib for the most common ALK variants observed in neuroblastoma (Bresler et al., 2011b; Hallberg and Palmer, 2013; Tucker et al., 2015), with cells harboring the F1174L *ALK* mutation being resistant when compared with those expressing R1275Q-mutated ALK. Despite real-time integration of these findings in the clinic, and a recommended phase II dose of crizotinib in pediatric patients that is nearly twice the adult maximum tolerated dose (Mosse et al., 2013), these studies emphasize the need to identify an optimal inhibitor for direct ALK kinase inhibition in neuroblastoma in order to maximize clinical benefit.

3.2 Activity of mutated ALK-TKD in its non-phosphorylated form is an excellent predictor of transforming ability in NIH 3T3 cells

Our collaborator, Yael Mossé and colleagues analyzed somatic and germline *ALK* DNA alterations of primary tumor samples from neuroblastoma patients in order to examine the full spectrum of *ALK* mutations. The analytic cohort of 1596 patients was representative of the natural spectrum of disease in neuroblastoma. After comprehensive genomic studies of *ALK* mutations across 1596 diagnostic neuroblastoma samples, 8% of samples were found to contain ALK-TKD mutations (at 3 hot spots and 13 minor sites, Figure 3.1), which correlated significantly with poor survival in high- and intermediate- risk neuroblastoma. It seems highly unlikely that all of the mutations observed are activating and oncogenic, and it is very important from a clinical perspective to know which *ALK* mutations observed in neuroblastoma patients are likely to be oncogenic drivers. Ideally, we would like to be able to predict – as they are observed – which mutations are true drivers that cause ligand-independent ALK signaling and which should be considered passengers or variants of unknown significance. Comprehensive information of this sort will be important in refining therapeutic *ALK* mutation-based patient stratification in the clinic. In efforts to define the relationship between *ALK* DNA aberrations, tumor phenotype, and prognosis, we assessed both the biochemical effects of clinically observed ALK TKD mutations *in vitro* and the transforming ability of ALK molecules harboring those mutations.

First, we analyzed the differential effects of patient-derived mutations on the activity of the purified ALK TKD in peptide phosphorylation assays *in vitro* that used peptide mimics of the ALK activation loop as substrate. Protein kinases exist in a dynamic equilibrium between a non-phosphorylated inactive form and a phosphorylated active form. Oncogenic mutations could activate the receptor either by rendering the phosphorylated (activated) kinase even more active than wild-type, causing excessive signaling. Alternatively, the mutations could shift the equilibrium between active and inactive states so that the non-phosphorylated kinase has greatly increased basal activity and signals in the absence of normal activation. Or, both effects could be important. We assayed the activity of recombinant ALK kinase domains in both their non-phosphorylated ('basal') and fully autophosphorylated ('activated') states, determining the kinetic parameters k_{cat}, and $K_{m,\ ATP}$. As shown in Figure 3.2, the effects of mutations on the basal activity of non-phosphorylated ALK TKD vary vastly according to their locations, whereas $K_{m,\ ATP}$ values for non-phosphorylated ALK TKD variants all fell within a narrow range (0.12-0.39 mM), suggesting that all ALK TKD variants are saturated with ATP under physiological conditions (where [ATP] is in the mM range). Compared to wild-type non-phosphorylated ALK-TKD, the catalytic rate (k_{cat}) increased about 40-fold for mutations in Phe core (F1174, F1245: red in Figure 3.2), more than 10-fold for mutations in αC helix (M1166, I1170, I1171: blue in Figure 3.2) and the short helix in activation loop (R1275, Y1278: also blue in Figure 3.2), and only slightly for mutations in the P-loop, N-lobe (except the germline mutation R1192P), active site (except the gatekeeper mutation L1196M), and C-lobe. By contrast, none of the mutations increased k_{cat} for the phosphorylated ALK TKD by more than approximately 2-fold (except I1170N, which actually decreased k_{cat} by slightly more than 2-fold.

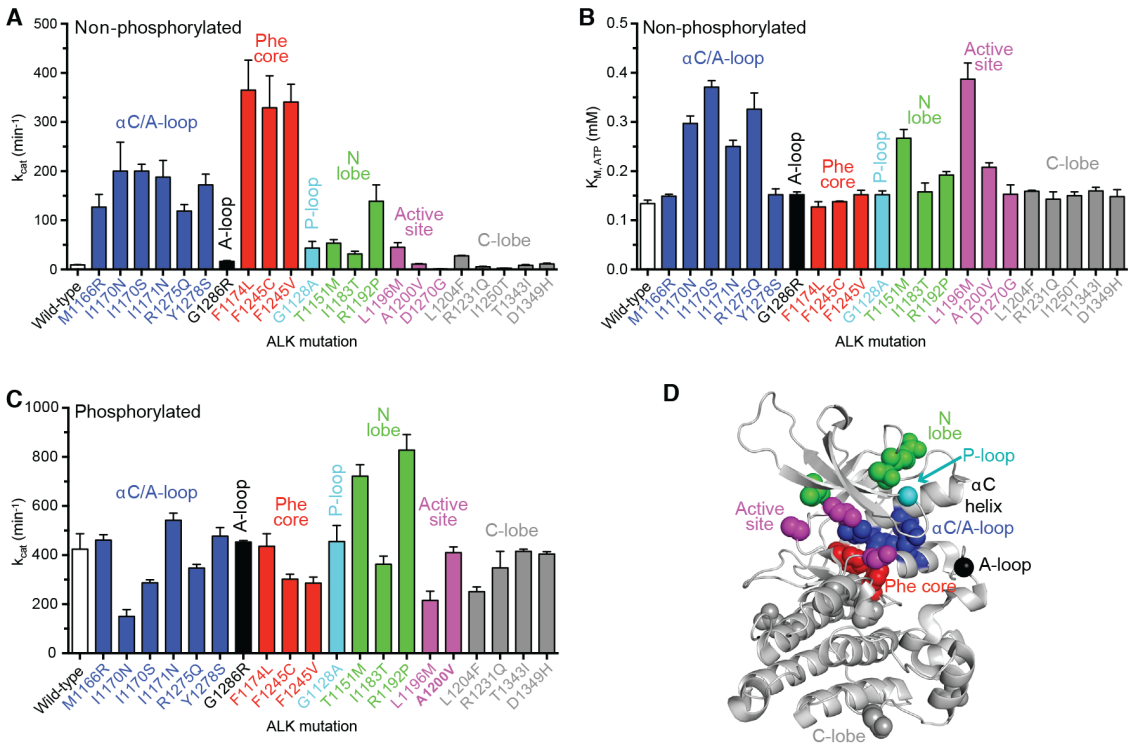

Figure 3.2 Effects of neuroblastoma mutations on the activity of non-phosphorylated and fully autophosphorylated ALK-TKD variants

(A) k_{cat} values for non-phosphorylated ALK TKD variants at saturating (2 mM) ATP, with 2 mM YYY peptide and 10 mM $MgCl_2$. (B) $K_{M,\ ATP}$ values for non-phosphorylated ALK TKD variants, determined with YYY peptide at 1.0 mM, ATP concentrations from 0.3125–2.0 mM, and 10mM $MgCl_2$. (C) k_{cat} values for fully phosphorylated ALK TKD variants, determined as in (A). Data are shown as mean ± SEM from at least three independent experiments. (D) Location of the mutations studied in biochemical analysis are shown in the ALK TKD crystal structure (PDB ID: 3LCS) with important structural regions colored as follows: αC/activation loop interface, blue; Phe core, red; P-loop, cyan; N-lobe, green; active site, magenta; and C-lobe, gray. (Bresler et al., 2014)

To further assess the transforming properties of selected ALK variants, and to determine how our biochemical studies compare with transformation ability, we monitored focus formation in NIH 3T3 cells transiently transfected with constructs directing expression of full-length ALK harboring the same mutations (Figure 3.3A). NIH 3T3 cells are normally subject to contact inhibition, and stop growing when they come into physical contact with one another. Expression of a transforming oncogene, however, causes the cells to lose contact inhibition and form areas of densely packed cells called foci following transfection. The number of foci was normalized by the number of G418-resistant colonies in order to correct for transfection efficiency, and the value of 'foci per colony' serves as an index of transformation (Figure 3.3B). In parallel, experiments using transient transfection in NIH 3T3 and CHO cells and Western blotting showed that the levels of expression of the different ALK variants was unaffected by the mutations (not shown). The focus formation assays revealed that 11 out of 24 tested mutations were not significantly transforming, suggesting them to be silent (or near silent) mutations. Neuroblastoma cell lines expressing these mutated variants are unlikely to be responsive to targeted ALK inhibition by crizotinib. Remarkably, the focus formation assay results showed a very close correspondence between transforming potential (Figure 3.3B) and *in vitro* k_{cat} for non-phosphorylated ALK TKD variants (Figure 3.2A). When the transforming abilities of ALK TKD variants were plotted against k_{cat} for the non-phosphorylated and phosphorylated ALK TKD, yields correlation coefficients (r) of 0.95 ($p < 0.0001$) and 0.095 ($p = 0.68$) were calculated respectively (Figure 3.3C).

Taken together, the data in Figure 3.2 and 3.3 argue that the activity of the non-phosphorylated ALK-TKD is an excellent predictor of ALK's transforming ability in NIH 3T3 cells, and likely its ability to function as an oncogenic driver. Mutated ALK-TKD variants with increases of just 4.6- to 4.8-fold in k_{cat} of the non-phosphorylated protein were transforming in NIH 3T3 cells, judging from results with the G1128A (cyan) and L1196M (magenta) variants (Figure 3.3). If k_{cat} was elevated by 4 fold or less, however, the variant appears not to be transforming in our assays.

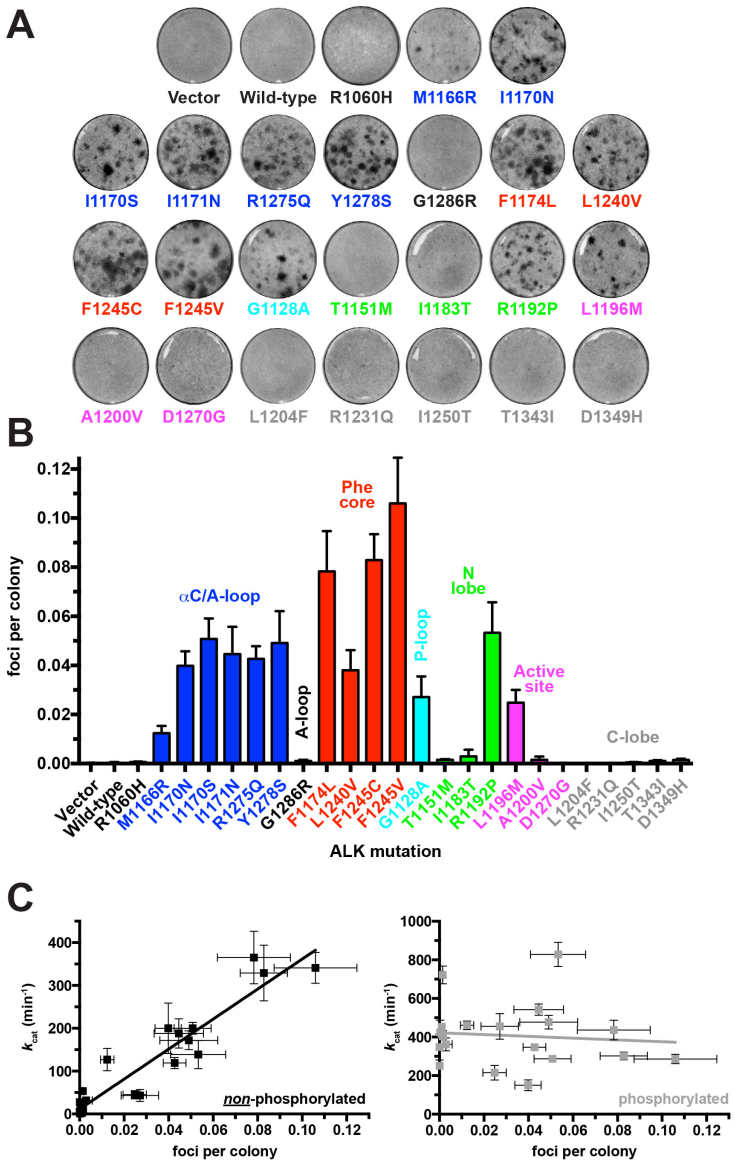

Figure 3.3 Transformation potential of ALK mutations from NIH 3T3 focus formation assays

(A) Representative focus formation assays for NIH 3T3 cells transfected with intact ALK variants or empty vector. (B) Quantitation of data presented in (A). Each independent experiment was performed in duplicate, and data are presented as mean ± SEM of at least three independent experiments. (C) Plots of the focus formation index against the *in vitro* k_{cat} for non-phosphorylated ALK TKD (left) or autophosphorylated ALK TKD (right). The lines are linear regressions to the

data. Correlation coefficients were 0.95 (non-phosphorylated) and 0.095 (phosphorylated), with a significant deviation from zero for the non-phosphorylated ALK TKD ($p < 0.0001$) but not for the phosphorylated ALK TKD ($p = 0.68$). (Bresler et al., 2014)

3.3 Computational methodology for predicting structural consequences of ALK-TKD mutations with low false positives

Our results establish ALK as an important therapeutic biomarker for patients with neuroblastoma; yet it remains a significant challenge to identify cancer-driving mutations. Biochemical and functional cellular analyses confirmed the differential effects of mutations, and thus the varied sensitivity to ALK inhibition. These findings argue that differentiating between driver mutations and the passenger mutations will be important for guiding targeted therapy, the key being able to define which *ALK* mutations observed in the clinic are likely to be activating, and therefore indications that ALK inhibitors would be of value. There are currently several available informatics tools used to predict the functional consequences of patient-derived mutations. These include PolyPhen-2 (Adzhubei et al., 2010), SIFT (Kumar et al., 2009), and the consensus classifier PredictSNP (Bendl et al., 2014), all of which estimate consequences of mutations based on sequence conservation and other criteria. Although they may have value for identifying loss-of-function mutations, these conservation-based algorithms are not logically appropriate for predicting gain-of-function in oncogenic kinase domain (Gnad et al., 2013). Indeed, a recent analysis of more than 400 activating substitutions in kinases (Molina-Vila et al., 2014) revealed that most driver mutations in oncogenic kinases are not associated with conserved residues at all. This (understandably) disappointing performance of existing computational methods in distinguishing neutral from deleterious mutations in cancer underlines a need for developing computational modeling and simulation approaches for understanding the consequences of mutations in cancer from a mechanistic point of view. The laboratory of our collaborator, Ravi Radhakrishnan, simulated molecular dynamics (MD) trajectories for ALK TKD variants in the

inactive and active conformations based on available ALK-TKD crystal structures, and analyzed the resulting MD trajectories for three key structural properties: hydrogen-bonding networks, hydrophobic interactions, and principal component analysis. A mutation is predicted to be activating overall if one or more of these analyses suggests that it is activating, as follows:

• Hydrogen-bonding network: A simple scoring function was created to analyze whether each mutation promotes distinct sets of key intramolecular hydrogen bonds network characterizing the 'active-like' or 'inactive-like' ALK TKD conformation. As mentioned in Chapter 1 (Figure 1.4), key autoinhibitory interactions between αC helix and short helix of activation loop of ALK TKD are absent in active conformations, and their relief will correlate with kinase activation.

• Hydrophobic interaction network: Disruption of the key autoinhibitory hydrophobic interactions was also assessed, by monitoring the solvent-accessible surface area (SASA) of relevant residues throughout the MD simulations. Mutations that increase SASA of the hydrophobic core are scored as activating. In order to determine whether each mutation destabilizes the inactive state relative to the active state, Free energy perturbation (FEP) simulations were also used.

• Principal component analysis (PCA): PCA revealed correlated global motions across the MD trajectory. The top 10 dominant modes for the active conformation show considerably greater motion than in the inactive ALK TKD. Each mutation with a top eigenvalue above 200$Å^2$ was scored as activating.

The computational analysis of the patient derived-mutations that we also assessed for biochemical effects and transforming capacity is summarizes in Table 3.1. In order to minimize the risk of bias, both sides of the approach – computational analysis and *in vitro* biochemical/ cellular studies – were performed without knowledge of the other. Importantly, every mutation analyzed (except R1231Q) was predicted by the PolyPhen-2 algorithm to be 'deleterious', whereas the structurally cognizant approach used by the Radhakrishnan laboratory suggests a very different functional picture. The MD-based approach predicts that only around 50% of the

mutations will be activating, and agrees quite well with our experimental studies (Table 3.1). There is still room for improvement, but these data suggest that the MD-based computational approach has significant promise for accurately predicting the biochemical effects, transforming capacity and responsiveness to targeted pharmacologic ALK inhibition, complementing traditional experiments.

Variant	*k_{cat} (min^{-1})*[a]	*Activated in vitro?*[b]	*Changes indicative of kinase activation in MD simulations of:*			*Overall prediction of activation in silico?*	*Transforming in NIH 3T3?*[c]	*PolyPhen-2 Prediction (probability)*[d]
			H-bonds	*SASA/ FEP*	*PCA*			
F1174L	365	●	●	-	●	●	●	● (0.70)
F1245V	341	●	●	-	-	●	●	● (1.00)
F1245C	329	●	-	-	-	-	●	● (1.00)
I1170N	200	●	●	●	-	●	●	● (1.00)
I1170S	200	●	-	●	-	●	●	● (1.00)
I1171N	188	●	-	-	-	-	●	● (1.00)
Y1278S	172	●	-	-	●	●	●	● (0.99)
R1192P	139	●	●	-	●	●	●	● (0.99)
M1166R	127	●	●	-	-	●	○	● (0.99)
R1275Q	119	●	●	-	-	●	●	● (1.00)
T1151M	53	●	●	-	-	●	-	● (0.98)
L1196M	45	●	-	-	-	-	○	● (1.00)
G1128A	43	●	●	-	-	●	○	● (1.00)
I1183T	32	-	-	-	-	-	-	● (0.96)
L1204F	28	-	-	-	-	-	-	● (0.99)
G1286R	16	-	-	-	-	-	-	● (0.98)
A1200V	11	-	-	-	-	-	-	● (0.67)
D1349H	11	-	-	-	-	-	-	● (0.94)
Wild-type	9	-	NA	NA	NA	NA	-	NA
T1343I	9	-	-	-	-	-	-	● (0.84)
R1231Q	5	-	-	-	-	-	-	- (0.01)
I1250T[e]	3	-	-	●	-	●[e]	-	●[e](1.00)
D1270G[e]	1	-	●	-	-	●[e]	-	●[e](1.00)

[a] k_{cat} for non-phosphorylated TKD is listed – from Figure 3.2A.
[b] A variant is considered 'activated' *in vitro* if k_{cat} for non-phosphorylated TKD exceeds 4.6 times that of wild-type (see text).
[c] Grey circles represent weak transformation.
[d] Black circles in PolyPhen-2 column indicate that this algorithm predicts that the mutation is damaging. Probabilities in parentheses taken from PolyPhen-2 batch run at http://genetics.bwh.harvard.edu/pph2/ (Adzhubei et al., 2010).
[e] D1270G and I1250T mutations are known to be inactivating (this work and Schönherr et al., 2011a). D1270G disrupts the DFG motif, I1250T expresses poorly, suggesting compromised folding.!

Table 3.1 Computational predictions of effects of ALK TKD mutations (Bresler et al., 2014)

3.4 Ongoing collaborative efforts to improve a predictive model with iteration between biochemical/cellular studies and MD-based computational analysis of mutated ALK TKDs

So far we have studied the biochemical consequences of a wide variety of ALK kinase domain mutations in parallel with studies of their transforming abilities, as well as computational studies of their structural effects. Armed with increasing number of experimental data, we are now developing a computational methodology for mechanistic profiling of ALK mutations in neuroblastoma, which facilitate the prediction of effects of new clinically emerging mutations. The approach we are taking is iteration between MD simulations and new experimental studies of a spectrum of ALK mutations in order to improve our current computational analysis – which predicts ~ 75% of transforming mutations and silent mutations – enabling future prediction of oncogenic driver mutations with low false positive rates.

Two different collections of ALK-TKD mutations are currently being studied for kinetic profiling using the peptide phosphorylation assay and for oncogenic transformation capacity using the focus formation assay (Figure 3.4) with no prior knowledge of the computational analysis to minimize bias. The preliminary data from these studies are reported here. The first collection (Figure 3.4A) is a mixture of oncogenic driver mutations with silent or passenger mutations as predicted by computational analysis: C1156Y, G1269A, F1174S, R1279Q, F1098V, Y1278E, Y1278S, Y1282E, Y1283E, E1161A (Figure 3.4A). Among these 10 tested mutations, F1174S and Y1278S are highly transforming as assessed by focus formation in NIH3T3 cells, which is consistent with their *in vitro* k_{cat} values, 364.6 min^{-1} (40-fold increase compared to WT) and 276.5 min^{-1} (31-fold increase compared to WT) respectively. Our previous experiments (Figures 3.2 and 3.3) argue that the catalytic activity of the nonphosphorylated ALK-TKD is an excellent predictor of ALK's oncogenic transformation capacity in NIH3T3 cells. And increase of 4~5-fold of the k_{cat} values of the nonphosphorylated ALK TKD appears sufficient for NIH 3T3 cell transformation. By

contrast, C1156Y has a k_{cat} value of 27.63 min^{-1}, which only represents a 3-fold increase, does not induce oncogenic transformation in NIH 3T3 cells. However it is possible that there might be a threshold of detection using this assay. Further assessment of full spectrum of ALK TKD variants comparing their biochemical and cellular studies would be helpful. The second collection includes the following 11 mutations found in Vietnamese patients and are shown in Figure 3.4B: Y1096A, C1097A, D1163N, I1170V, G1202R, R1212C, R1213C, E1242K, A1251T, F1271L, Y1278A. These mutated ALK variants exhibit different degrees of transforming ability in NIH3T3 cells which likely reflect their different catalytic activities. The experimental analysis (biochemical and cellular studies) with at least three independent experiments is near completion and will be compared to the data from the computational analysis. Our studies will provide valuable mechanistic insight into how ALK is regulated, and will also provide the groundwork for guiding more refined targeted therapy in neuroblastoma patients.

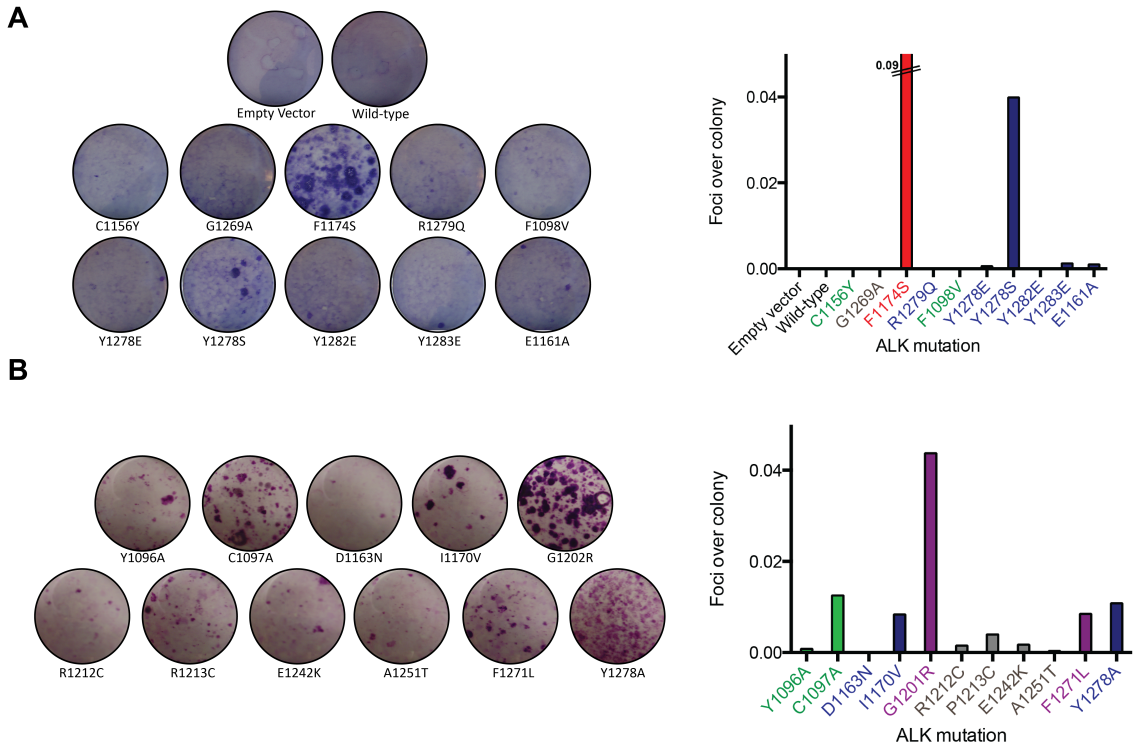

Figure 3.4 Ongoing cellular transformation studies of ALK-TKD variants using NIH3T3 focus formation assays

These are preliminary results of focus formation assays for (A) a collection of oncogenic driver and silent or passenger mutations as predicted by computational analysis and (B) mutations found in sequencing project in Vietnam. (Left) A representative focus formation assay in NIH 3T3 cells transfected with intact ALK variants or empty vector (pcDNA 3.1) is shown. For better visualization cells were stained with crystal violet. Quantitation of the data presented in (Right).

3.5 ALK variants found in neuroblastoma are differentially sensitive to the inhibitor crizotinib

Our previously published studies indicated that the relative crizotinib sensitivities of ALK variants found in neuroblastoma may simply reflect their ATP-binding affinities, with reduced $K_{M,\ ATP}$ (higher ATP-binding affinity) predicting crizotinib resistance for F1174L-mutated ALK, for example (Bresler et al., 2011b). We explored two strategies to overcome this problem. In the first, we tested a series of second-generation ALK kinase inhibitors (Figure 3.5), anticipating that their structural differences might allow some to show selective (or improved) inhibition of F1174L-mutated ALK, as has been suggested for other ALK variants (Fontana et al., 2015). As we failed to find any inhibitors that satisfied this criterion, our second approach was to investigate the impact of globally increasing the affinity of drug-binding to all ALK variants – made possible by using the highly potent ALK/ROS1 inhibitor PF-06463922 (T. W. Johnson et al., 2014; Zou et al., 2015). We hypothesized that a drug with substantially increased ALK-binding affinity might be capable of inhibiting all ALK variants at readily achievable drug concentrations, and that this feature might negate the effects of primary resistance mutations. In other words, even when some ALK variants bind the drug more weakly than others, if all have drug-binding affinities that allow them to be saturated with readily achievable drug concentrations, primary resistance will be negated. We show here that PF-06463922 does indeed have substantially greater potency than crizotinib as an ALK inhibitor *in vitro*, across all neuroblastoma mutations tested. Most importantly, PF-06463922 also showed excellent activity against full-length oncogenic ALK variants in preclinical *in vivo* models of ALK-driven neuroblastoma where crizotinib fails. Through biochemical, cell-based, xenograft and patient-derived xenograft (PDX) studies, we demonstrate that PF-06463922 has unprecedented activity as a single agent against *ALK* mutants, including those with primary crizotinib resistance, thus positioning PF-06463922 as the lead ALK inhibitor for clinical development in ALK- driven neuroblastoma.

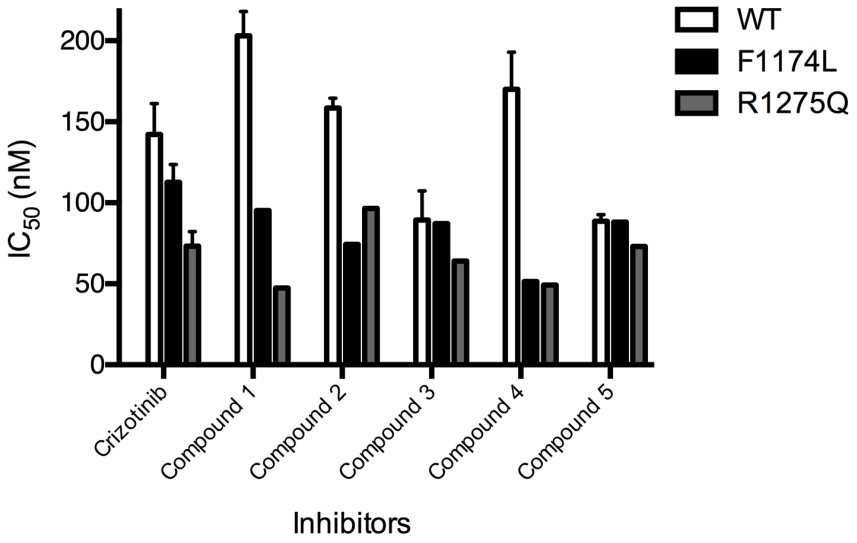

Figure 3.5 Inhibitor sensitivities of ALK-TKD WT, F1174L, and R1275Q

In order to identify which of the next-generation ALK tyrosine kinase inhibitors is most potent against the widest range of ALK mutants (to decide which should progress clinically), IC_{50} values at 2mM ATP were determined using the radioactive in vitro assay and compared side-by-side. The compounds are numbered rather than named, because the MTA agreements under which they were obtained prohibits side-by-side comparison in published work. However, since none of the five new compounds appeared dramatically different from crizotinib, we did not pursue any of them.

3.6 Identification of the next-generation ALK/ROS1 inhibitor PF-06463922 as capable of overcoming primary resistance to crizotinib in ALK-driven neuroblastoma

In our earlier studies, we were able to recapitulate the differential crizotinib sensitivity of F1174L and R1275Q ALK variants *in vitro*, using kinase assays (Bresler et al., 2011b). We also showed above (Figure 3.3) that the transforming ability of ALK variants correlates most closely with *in*

vitro k_{cat} values for the non-phosphorylated kinase domain of the receptor – implying that activation of this species is key for oncogenesis. Unfortunately, a preliminary screen through a series of second-generation ALK inhibitors (Figure 3.5) failed to identify an inhibitor that differed significantly from crizotinib in its relative ability to inhibit R1275Q, F1174L, and F1245C variants of the non-phosphorylated ALK tyrosine kinase domain (ALK-TKD) *in vitro*. The ALK/ROS1 inhibitor PF-06463922 stood out starkly in these assays, however, by yielding uniquely low IC_{50} values. As previously pointed out (Zou et al., 2015), PF-06463922 is more potent against wild-type ALK than crizotinib, alectinib, or ceritinib (included in Figure 3.5) by 4-fold or more when K_i values are compared. In our *in vitro* experiments, PF-06463922 gave IC_{50} values for inhibition of F1174L- and F1245C-mutated ALK that were significantly lower than those seen with crizotinib even for the crizotinib sensitive R1275Q variant (Figure 3.6A and 3.6B). Indeed, measured IC_{50} values for PF-06463922 were approximately 5-fold lower than those for crizotinib for all variants and were actually limited in this assay by the concentration of kinase protein required to measure activity of unphosphorylated ALK-TKD (50 nM). Estimated K_i values from our data using the equations of Cha (Cha, 1975) are less than 0.2 nM for inhibition of mutated ALK-TKD by PF-06463922, compared with 6 to 10 nM for crizotinib inhibition, K_i values consistent with previous reports using different methods and different sets of mutations (T. W. Johnson et al., 2014; Zou et al., 2015).

These data show that PF-06463922 is a very potent inhibitor for multiple mutated full-length ALK variants seen in neuroblastoma, as also reported for acquired resistance mutations seen in cytoplasmic ALK fusion proteins in lung cancer and elsewhere (T. W. Johnson et al., 2014; Mologni et al., 2015; Zou et al., 2015). We hypothesized that this significantly increased potency and/or affinity of PF-06463922, compared with other ALK inhibitors in development, might be sufficient to negate the consequences of differential sensitivity of ALK variants to kinase inhibitors.

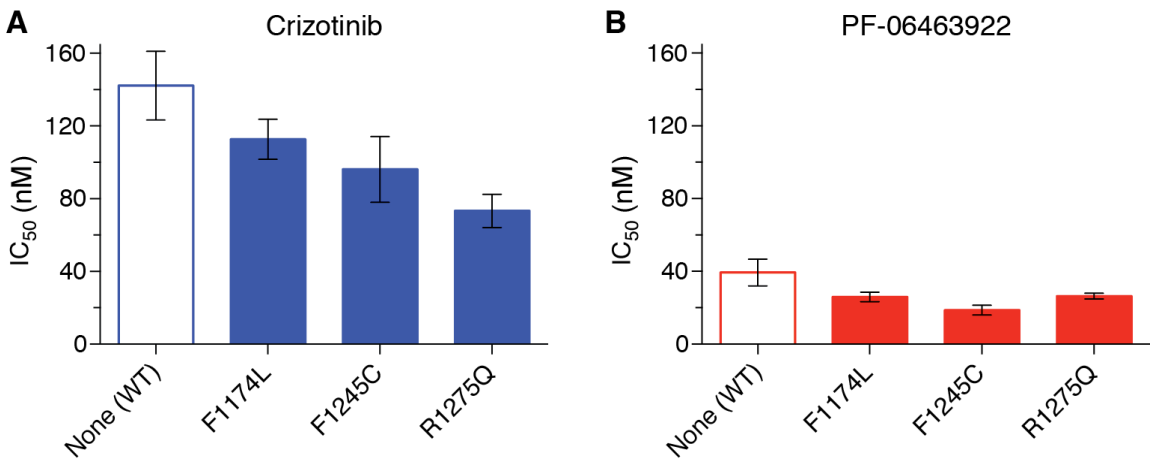

Figure 3.6 *In vitro* Inhibition profiles of non-phosphorylated ALK-TKD mutants against (A) Crizotinib and (B) PF-0643922.

PF-06463922 exhibits superior inhibitory activity against all tested ALK-TKD variants in kinase assays. *In vitro* inhibition profiles of purified non-phosphorylated ALK-TKD protein (at 50 nM) harboring the noted mutations with crizotinib (A) and PF-06463922 (B). Inhibitor concentration was varied from 0 to 25,600 nM, with ATP present at 2 mM, and substrate peptide was held at 0.5 mM, as described (Bresler et al., 2011a). Results are plotted as mean ± SD for at least three independent experiments. As discussed in the text, the IC_{50} values obtained in this experimental format correspond to K_i values in the 6-10 nM range for crizotinib, and the 0.2 nM range for PF-06463922.

3.7 PF-06463922 induces complete tumor regression in patient-derived and cell line- derived xenografts with and without primary resistance to crizotinib

The data in Figure 3.6 suggest that F1245C-mutated ALK should resemble F1174L-mutated ALK in its primary resistance to crizotinib – consistent with limited clinical data (Mosse et al., 2013) –

but that tumors driven by all three hotspot ALK variants should respond to PF-06463922. To test these hypotheses, we compared *in vivo* efficacies of PF-06463922 and crizotinib in crizotinib-naïve PDXs harboring F1174L or F1245C *ALK* mutations (COG-N-453x and Felix-PDX, respectively), as well as cell line – derived xenografts utilizing SH-SY5Y cells (F1174L) or NB-1643 cells (R1275Q). Tumor-bearing animals were treated by oral gavage with either 5 mg/kg PF-06463922 twice daily (b.i.d.) or 100 mg/kg crizotinib once daily (qd). Two of the models (Felix-PDX and SH-SY5Y) were treated for 6 weeks, whereas the new COG-N-453x PDX and NB-1643, both slightly more sensitive to crizotinib, were treated for longer (8.1 and 8.9 weeks, respectively). Crizotinib and PF-06463922 at these doses were both well tolerated. As expected, crizotinib alone at 100 mg/kg/day demonstrated limited inhibition of tumor growth in these models. Crizotinib delayed growth in both PDXs (Figure 3.7A and 3.7B), such that tumor volume at any given time was approximately 30% of that seen in vehicle-treated mice. The SH-SY5Y (F1174L) xenograft showed no response to crizotinib (Figure 3.7C). In contrast, the NB-1643 (R1275Q) xenograft showed an initial response with essentially no tumor growth for 3.5 weeks when treated with crizotinib – as previously described (Bresler et al., 2011b) – although significant tumor growth was seen after 4 weeks (Figure 3.7D).

Contrasting with these limited, or transient, responses to 100 mg/kg/day crizotinib, treatment with 10 mg/kg/day PF-06463922 (5 mg/kg b.i.d.) resulted in rapid (within 2–3 weeks) and sustained complete tumor regression for the duration of treatment in all xenografts (red curves in Figure 3.7; and Table 3.2). After PF-06463922 treatment was stopped, animals were further monitored for tumor progression by observation and palpation. Mice that had been treated with 10 mg/kg/day PF-06463922 remained in complete remission, with no discernible tumor growth for a further 4.8 weeks (COG-N-453x), 7.1 weeks (Felix-PDX), 5 weeks (SH-SY5Y), and 4 weeks (NB-1643), as shown in Figure 3.8. Thus, xenografts harboring the *de novo* crizotinib-resistant ALK F1174L mutation exhibited unprecedented antitumor responses to single-agent ALK inhibition therapy with PF-06463922, as did a PDX harboring the F1245C mutation.

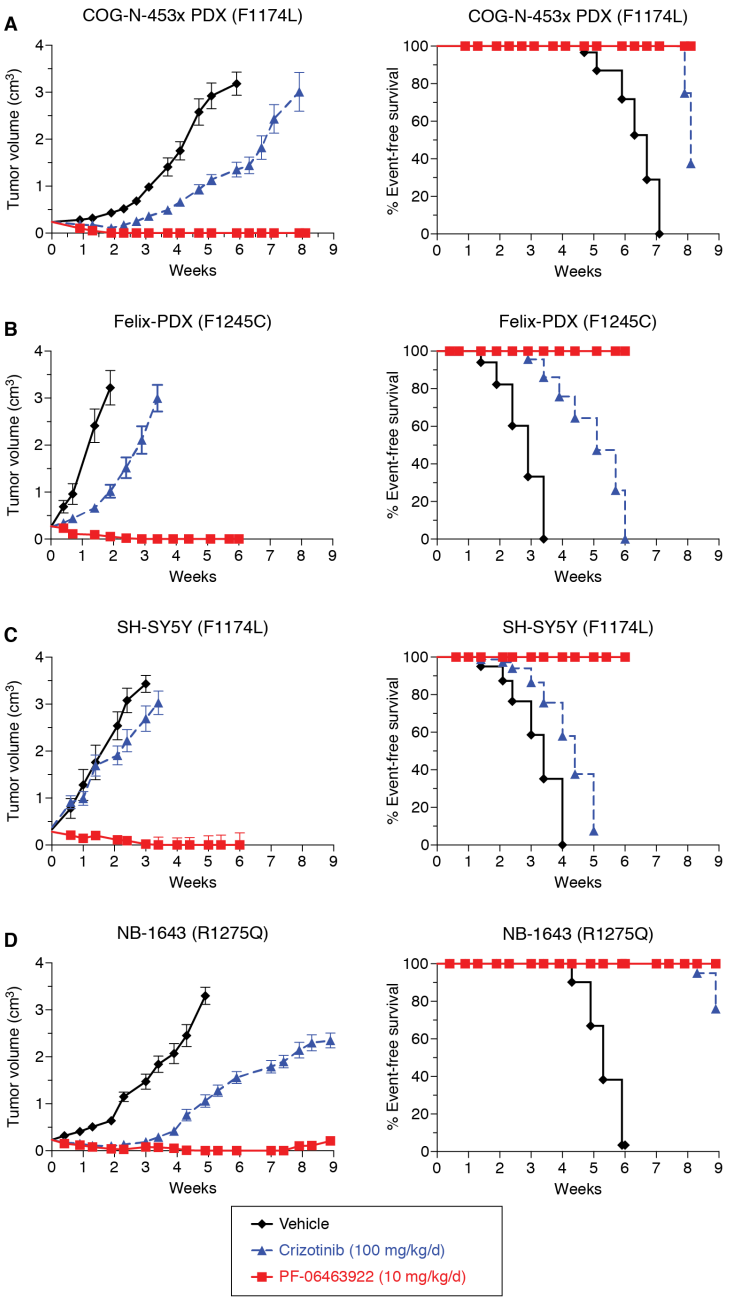

Figure 3.7 *In vivo* efficacy studies comparing PF-06463922 to crizotinib.

PF-06463922 induces complete tumor regression in PDX and xenograft models of crizotinib-resistant and crizotinib- sensitive neuroblastoma. Subcutaneously implanted neuroblastoma tumors were monitored in CB17 SCID mice treated with 10 mg/kg/day PF-06463922 (solid red

line and squares), 100 mg/kg/day crizotinib (dashed blue line and triangles), or vehicle (solid black line and diamonds). Data are shown only for the duration of treatment in each case. Study end points for survival analysis (right) are shown using Kaplan – Meier curves (median ± SEM; *n* = 10 for each data point). A mixed- effects linear model was used for analysis of statistical significance of tumor growth delay. Kaplan – Meier curves for EFS were compared using a log-rank test, with $P < 0.05$ taken as indicating significance (see Table 3.2). These experiments were performed by N.R.

PDX or xenograft (mutation)	ALK status	MYCN status	Treatment	Tumor volume		EFS	
				P value vs. vehicle control	P value vs. crizotinib	P value vs. vehicle control	P value vs. crizotinib
COG-N-453x	Mutated: F1174L	Amplified	Crizotinib	<0.0001		<0.0001	
			PF-06463922	<0.0001	<0.0001	<0.0001	0.0118
Felix-PDX	Mutated: F1245C	Nonamplified	Crizotinib	<0.0001		0.0008	
			PF-06463922	<0.0001	<0.0001	<0.0001	<0.0001
SH-SY5Y	Mutated: F1174L	Nonamplified	Crizotinib	0.0011		0.0502	
			PF-06463922	<0.0001	<0.0001	<0.0001	0.0003
NB-1643	Mutated: R1275Q	Amplified	Crizotinib	<0.0001		<0.0001	
			PF-06463922	<0.0001	<0.0001	<0.0001	0.1464

Table 3.2 Statistical analysis for in vivo efficacy studies in PDXs from COG-N-453x and Felix cells, and xenografts from SH-SY5Y and NB-1643 cells

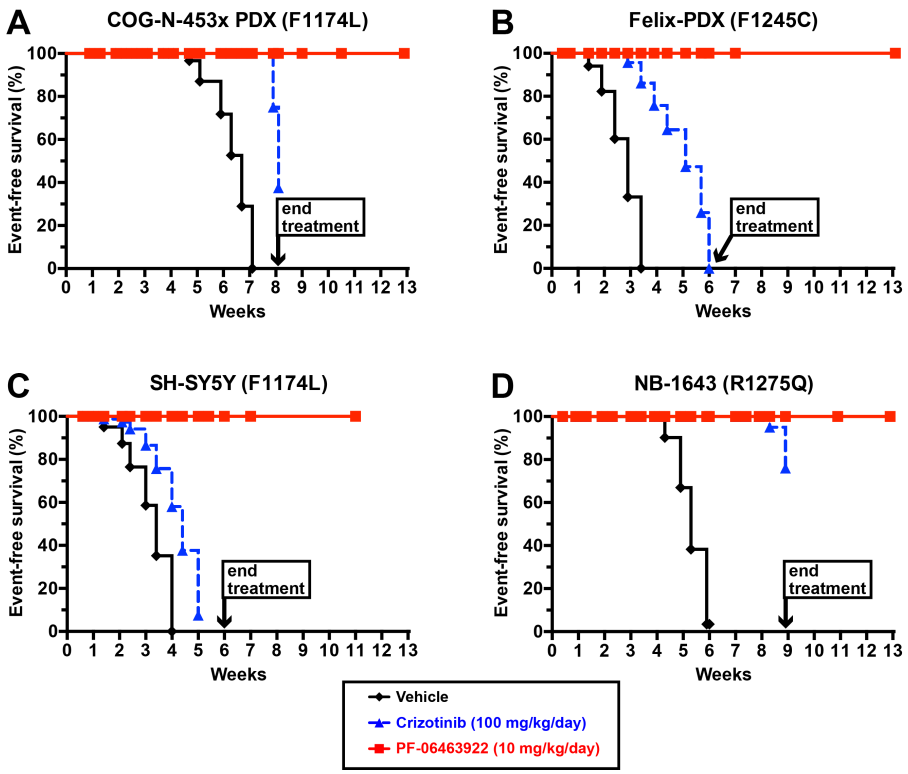

Figure 3.8 *In vivo* effects of crizotinib and PF-06463922 on event-free survival (EFS) in neuroblastoma PDX and xenograft models.

Female CB17 SCID mice bearing: (A), COG-N-453x (ALK-F1174L); (B), Felix-PDX (ALK-F1245C); (C), SH-SY5Y (ALK-F1174L); and (D), NB-1643 (ALK-R1275Q) were treated with vehicle (black curves and diamonds), 100 mg/kg/day crizotinib (blue curves and triangles), or 10 mg/kg/day PF-06463922 (red curves and squares). EFS is plotted for the period during treatment (as in Fig 3.7) and for a period of 4-7 weeks after cessation of therapy. Remarkably, no discernible tumor growth could be detected in any of the PF-06463922-treated mice during the period of monitoring. These experiments were performed by N.R.

Given these rapid and complete responses to 10mg/ kg/day PF-06463922 shown in Figure 3.7, we also evaluated a lower dose of 3 mg/kg/day (1.5 mg/kg b.i.d.) in both the Felix-PDX (F1245C) and SH-SY5Y (F1174L) xenografts. As shown in Figure 3.9 and Table 3.3, this lower PF-06463922 dose was still substantially more effective than a 33-fold higher dose of crizotinib. In the SH-SY5Y xenograft (Figure 3.9B), 3 mg/kg/day PF-06463922 induced complete regression within 6 weeks of treatment (compared with 2–3 weeks for 10 mg/kg/ day PF-06463922). The lower dose of PF-06463922 caused significant growth delay in Felix-PDX (Figure 3.9A), with tumors remaining palpable throughout treatment and showing little further growth after approximately 4 weeks. PF-06463922 at both dosing levels significantly prolonged event-free survival (EFS) relative to control and crizotinib arms in SH-SY5Y and Felix xenografts (Figure 3.9 and Table 3.3).

				Tumor volume			EFS		
Xenograft/ PDX	ALK status	MYCN status	Treatment	P value vs. vehicle control	P value vs. crizotinib	P value vs. PF-06463922 (3 mg/kg/day)	P value vs. vehicle control	P value vs. crizotinib	P value vs. PF-06463922 (3 mg/kg/ day)
Felix-PDX	Mutated: F1245C	Nonamplified	Crizotinib	<0.0001			0.0008		
			PF-06463922 (3 mg/kg/day)	<0.0001	<0.0001		<0.0001	<0.0001	
			PF-06463922 (10 mg/kg/day)	<0.0001	<0.0001	0.3247	<0.0001	<0.0001	0.3428
SH-SY5Y	Mutated: F1174L	Nonamplified	Crizotinib	0.0011			0.0502		
			PF-06463922 (3 mg/kg/day)	<0.0001	<0.0001		<0.0001	0.0003	
			PF-06463922 (10 mg/kg/day)	<0.0001	<0.0001	0.6932	<0.0001	0.0003	NA

Table 3.3 Statistical analysis for Felix-PDX and SH-SY5Y *in vivo* efficacy studies testing two doses of PF-06463922 (10 mg/kg/day and 3 mg/kg/day)

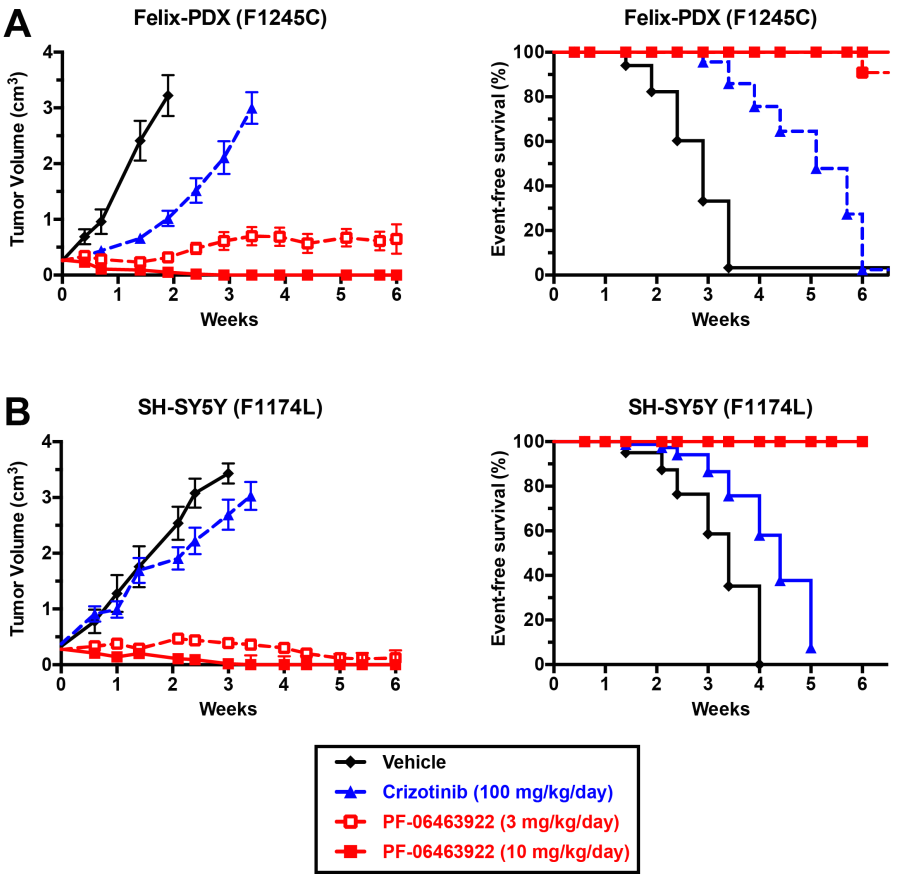

Figure 3.9 *In vivo* efficacy studies comparing PF-06463922 treatment at 10 mg/kg/day (5 mg/kg BID) and 3 mg/kg/day (1.5 mg/kg BID) with crizotinib treatment at 100 mg/kg QD in (A) Felix-PDX xenografts and (B) SH-SY5Y xenografts.

Tumor volumes are plotted over 6 weeks of continuous treatment (Median ± S.E.M., n=10 for each data point), as are Kaplan-Meier survival curves. A mixed-effects linear model was used to assess statistical significance analysis of tumor growth delay, and EFS Kaplan-Meier curves were compared by using log-rank test, * $p<0.05$ (see Table 3.2). These experiments were performed by N.R.

3.8 PF-06463922 efficiently inhibits ALK phosphorylation *in vivo*

To compare the effects of the two ALK inhibitors on ALK activity, we used immunoblotting to analyze pALK levels in tumor lysates from NB-1643 xenografts treated with vehicle, PF-06463922, or crizotinib. Tumors were harvested after 3 days of drug treatment, 1 hour after the last dose. As shown in Figure 3.10, pALK was essentially undetectable in tumors from the PF-06463922-treated mice, whereas tumors from crizotinib-treated mice retained significant ALK phosphorylation. Interestingly, crizotinib appeared to suppress ALK phosphorylation at Y1278 (Figure 3.10A), which lies in the activation loop of the TKD, more completely than at Y1604 (Figure 3.10B), which lies in the regulatory C-terminal tail of the receptor. In contrast, PF-06463922 at 10 mg/kg/day almost completely suppressed phosphorylation at both sites. Thus, consistent with its more potent inhibition of *in vivo* growth of ALK-dependent tumors, PF-06463922 appears to suppress ALK phosphorylation more effectively than crizotinib, even at a 10-fold lower daily dose.

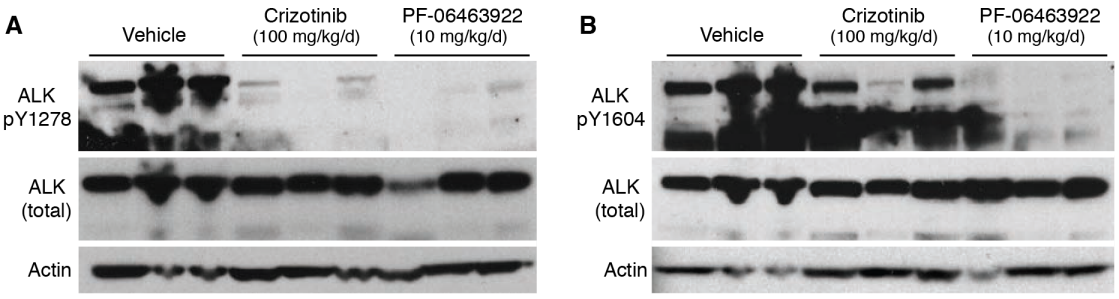

Figure 3.10 PF-06463922 abrogates ALK phosphorylation more effectively than crizotinib *in vivo*.

Mice harboring NB-1643 xenografts (*n* = 3 per arm) were treated for 3 days with vehicle, crizotinib (100 mg/kg qd), or PF-06463922 (5 mg/kg b.i.d., 10 mg/kg/day). Tumors were harvested 1 hour after the final drug treatment, and subjected to immunoblotting, using antibodies against pY1278 in the activation loop of the kinase (A) or pY1604 in the C-terminal regulatory tail (B), alongside control blots for total ALK and β-actin (lower panels). These experiments were performed by N.R.

3.9 PF-06463922 inhibits growth of ALK-mutated neuroblastoma cell lines at approximately 20- to 125- fold lower concentrations than crizotinib

To compare PF-06463922 and crizotinib over a broader range of ALK-driven tumors, we assessed their abilities to inhibit growth of a range of cell lines *in vitro*, employing a CellTiter-Glo luminescent cell viability assay. As shown in Figure 3.11 and Table 3.4, IC_{50} values measured for PF-06463922 in neuroblastoma cell lines dependent on R1275Q-mutated ALK were 51-fold (NB-1643) and 19-fold (LAN-5) lower than those measured for crizotinib (Figures 3.11A and 3.11B), which themselves were approximately 310 nM. Importantly, IC_{50} values for PF-06463922 inhibition of cell lines driven by the ALK-resistant F1174L ALK variant were also much lower – falling in the range of 12.7 nM to 26.6 nM, which is approximately 30-fold lower than measured for crizotinib (Figure 3.11C–F and Table 3.4). A similar difference was also seen for Felix cells, driven by the F1245C variant (Figure 3.11G). Whereas a small (~3-fold) difference in IC_{50} appeared to be sufficient to explain the relative crizotinib resistance of tumors and cell lines driven by F1174L-mutated ALK in neuroblastoma compared with those driven by R1275Q (Bresler et al., 2011b), the overall higher potency of PF-06463922 appears to render such differences irrelevant, so that both tumor cell lines (Figure 3.11) and xenografts (Figure 3.7) driven by the F1174L variant are sensitive to PF-06463922. The same appears to be true for the F1245C variant. Similar results were seen for NB-1 cells, driven by amplified wild-type ALK, with IC_{50} values of 256 nM and 5.2 nM for crizotinib and PF-06463922, respectively (Figure 3.11H).

Three other interesting observations emerge from this study. First, the difference in IC_{50} values for crizotinib and PF-06463922 was even greater (>100-fold) for the NCI-H3122 lung cancer cell line driven by the EML4–ALK fusion (Figure 3.11I and Table 3.4), suggesting that the presence of the TKD in the intact receptor might slightly limit the potency of PF-06463922. Second, in agreement with previous studies (Zou et al., 2015), PF-06463922 was less toxic than crizotinib in cell lines that are not dependent on ALK for growth (Figure 3.11J and 3.11K),

consistent with its high selectivity (T. W. Johnson et al., 2014). Third, PF-06463922 treatment did not cause complete growth inhibition in cell lines with R1275Q, F1174L, or F1245C mutations, whereas crizotinib did. One possible explanation for the plateau in PF-06463922 activity might be its higher specificity for ALK and ROS1 (K. Johnson et al., 2011), with limited off-target effects. The additional diminution of cell viability with crizotinib might arise from its ability to inhibit other kinases, including c-Met and RON (Cui et al., 2011), which could possibly contribute to tumor cell growth. A similar phenomenon was seen in several lung cancer cell lines driven by ALK fusion proteins harboring resistance mutations (Zou et al., 2015).

Cell Line	***ALK* Status**	***MYCN* status**	**IC_{50} (nM)**		
			Crizotinib	**PF-06463922**	**Fold**
NB-1643	R1275Q	Amplified	**308.4** ± 80.7	**6.1** ± 0.3	51
LAN-5	R1275Q	Amplified	**320.4** ± 38.5	**16.8** ± 4.3	19
SH-SY5Y	F1174L	Non-amplified	**625.1** ± 55.7	**16.5** ± 1.2	38
NB-SD	F1174L	Amplified	**473.6** ± 119	**12.7** ± 1.3	38
COG-N-415	F1174L	Amplified	**379.5** ± 27.3	**14.6** ± 6.2	26
KELLY	F1174L	Amplified	**898.8** ± 33.5	**26.6** ± 1.2	34
Felix	F1245C	Non-amplified	**814.0** ± 119	**21.8** ± 3.2	37
NB-1	Amplified wt	Amplified	**256.4** ± 73.3	**5.2** ± 1.4	49
NCI-H3122	EML4-ALK, v1	Unknown	**349.5** ± 25.3	**2.8** ± 0.4	125
NB-EBc1	Wild-type	Non-amplified	**3,841** ± 1081	**>3,841**	-
SK-N-BE(2)-C	Wild-type	Amplified	**4,503** ± 58.6	**>4,503**	-

Table 3.4 PF-06463922 is potent against ALK-mutated NB cell lines *in vitro*.

Mean (n=3) IC_{50} values (± SD) for crizotinib and PF-06463922 are listed for 10 NB cell lines harboring the indicated ALK aberrations, plus one NSCLC cell line (NCI-H3122). Fold increases in the IC_{50} values with crizotinib over those measured for PF-06463922 are also listed in the right-most column.

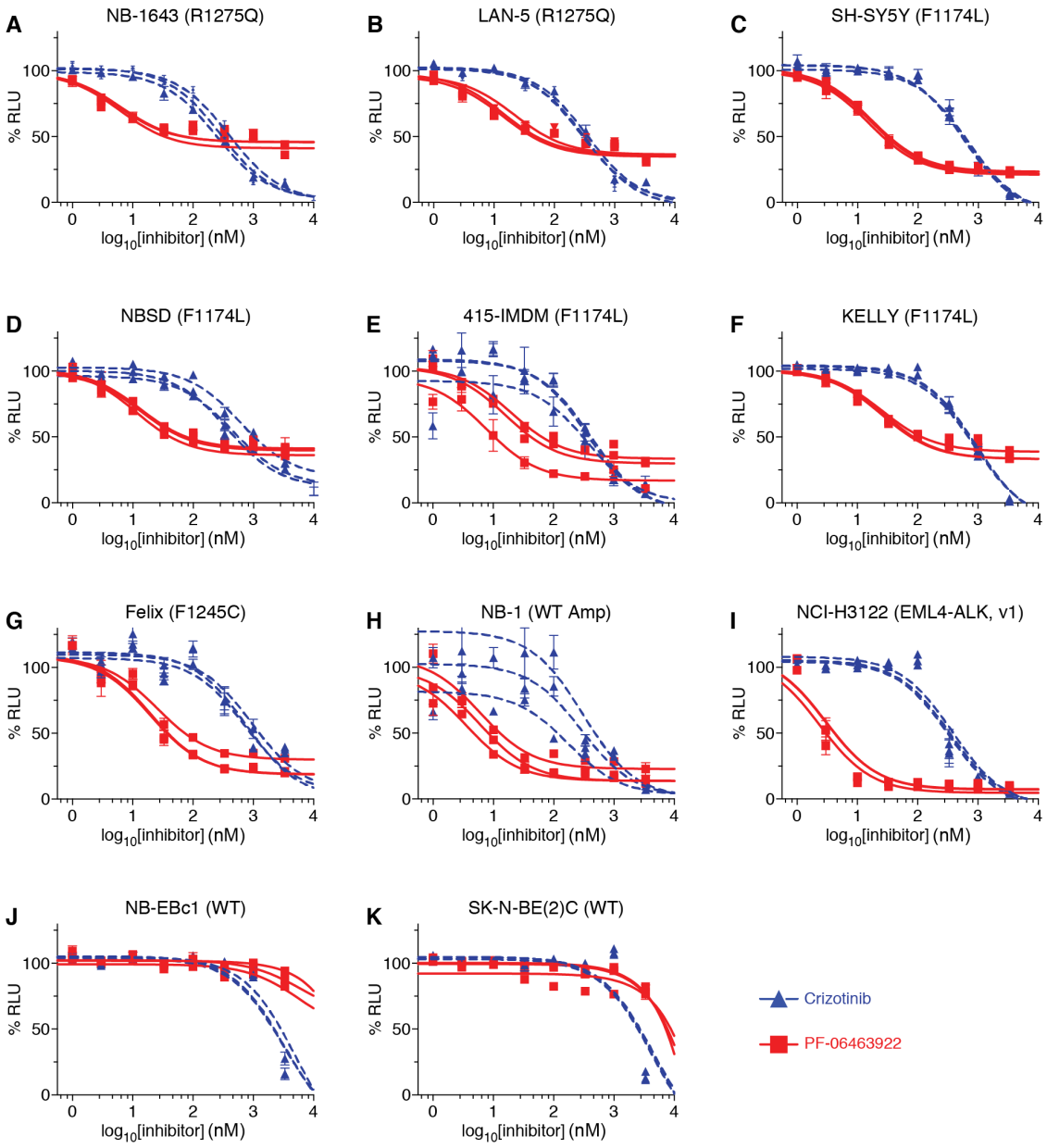

Figure 3.11 PF-06463922 inhibits viability of neuroblastoma cell lines at concentrations corresponding to clinically relevant doses (≤100 nM).

Dose response curves for the effects of crizotinib (dashed blue curves) and PF-06463922 (red curves) on cell viability are shown for a series of neuroblastoma cell lines driven by R1275Q-mutated ALK (A and B), F1174L-mutated ALK (C–F), F1245C-mutated ALK (G), and amplified

wild-type ALK (H). NCI-H3122 cells, driven by an ALK translocation, are shown for comparison (I), as well as two cell lines that are not ALK dependent (J and K). Data points are plotted as means ± SD for at least three different experiments, with blue triangles for crizotinib and red squares for PF-06463922. The IC_{50} curves for individual experiments are also plotted, with mean IC_{50} values obtained over the three experiments listed in Table 3.4. RLU, relative light unit. These experiments were performed by N.R.

3.10 Comparison of effects on ALK phosphorylation in cell lines

In an effort to correlate the lower IC_{50} values seen for PF-06463922 in cell viability studies in Figure 3.11 with ALK inhibition, we also compared the effects of PF-06463922 and crizotinib on ALK phosphorylation in neuroblastoma cell lines harboring different ALK variants (Figure 3.12A and B). Both inhibitors substantially diminished ALK phosphorylation at Y1278 (in the activation loop of the kinase). Consistent with the lower IC_{50} values observed for PF-06463922 for effects on viability of R1275Q-expressing NB-1643 cells, the pALK signal was almost completely abolished at 100 nM PF-06463922, although some signal remained with the equivalent concentration of crizotinib (Figure 3.12A). Similarly, at any given concentration of drug, PF-06463922 treatment appeared to promote greater diminution of the pALK signal than crizotinib in F1174L-expressing SH-SY5Y cells (Figure 3.12B). It is interesting, however, that the difference between PF-06463922 and crizotinib was more stark for the EML4–ALK-driven NCI-H3122 lung cancer cell line (Figure 3.12C), as also seen in the cell viability studies. Indeed, across the board, as listed in Table 3.4, IC_{50} values for PF-06463922 in cell viability studies were approximately 10-fold higher for the ALK-dependent neuroblastoma cell lines (10–30 nM) than for the *ALK*-translocated lung cancer line (IC_{50} = 2.8 nM). Zou and colleagues(Zou et al., 2015) recently reported PF-06463922 IC_{50} values in the 2 to 3 nM range for cells driven by EML4–ALK fusions, but higher values (similar to those seen for neuroblastoma cells) in the cells expressing mutated EML4–ALK. In all cases, however, the superior potency of PF-06463922 was such that the IC_{50} values were sufficient to predict clinical efficacy.

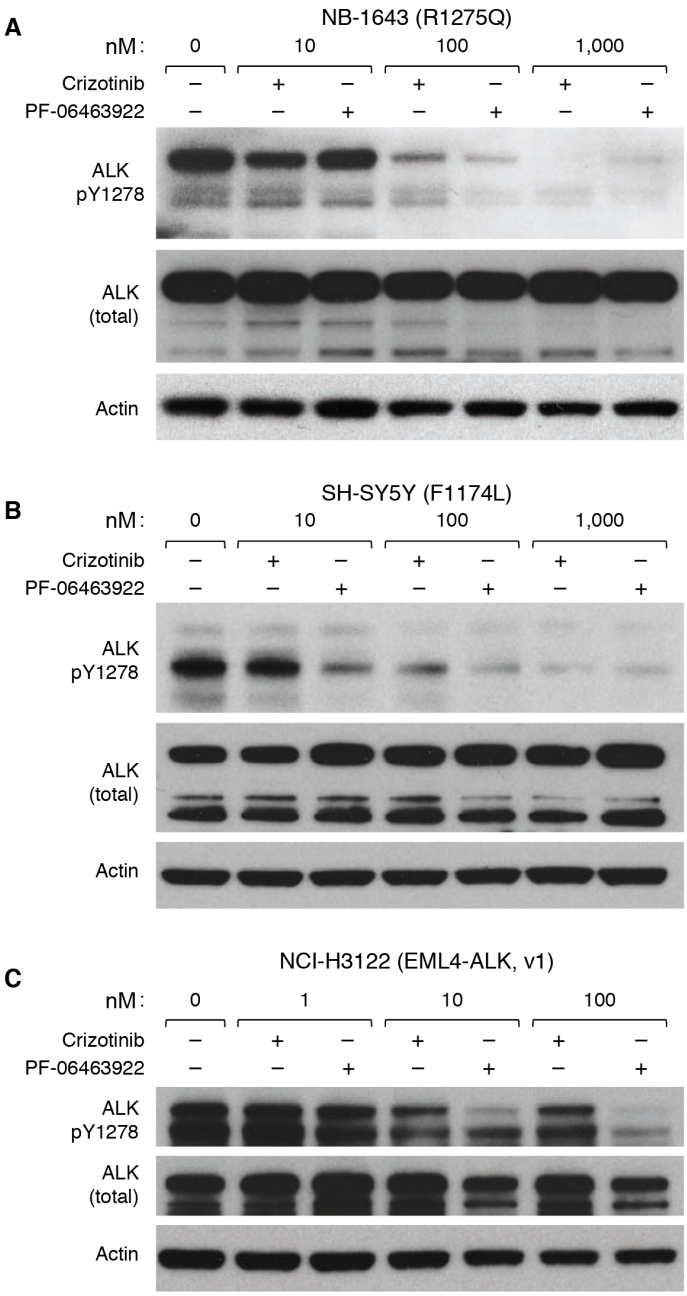

Figure 3.12 PF-06463922 displays on-target activity in neuroblastoma and NSCLC cells.

(A) NB-1643, (B) SH-SY5Y, and (C) NCI-H3122 cells were treated with increasing concentrations of crizotinib or PF-06463922. Levels of ALK autophosphorylation at Y1278 in the kinase activation loop were analyzed by Western blotting 24 hours after treatment, as described in Methods.

3.11 Inhibition of NIH 3T3 cell transformation by mutated ALK

To compare the effects of the two ALK inhibitors on mutated ALK variants all in a common cell background, we also analyzed their ability to inhibit ALK-mediated transformation of NIH 3T3 cells in focus formation assays, as described previously (Bresler et al., 2014). As shown in Figure 3.13A–C, PF-06463922 was substantially more effective than crizotinib at blocking transformation/focus formation induced by ALK with any of the three hotspot mutations. IC_{50} values were consistently 5- to 10-fold lower for PF-06463922 than for crizotinib, consistent with experiments in all other *in vitro* and *in vivo* contexts described here. It is interesting, however, that NIH 3T3 cells expressing the R1275Q variant were significantly more sensitive to both drugs than cells expressing F1174L- or F1245C- mutated ALK. Indeed, the IC_{50} values for inhibition of focus formation in R1275Q-expressing cells (Figure 3.13A) were lower than in F1174L-expressing cells (Figure 3.13B) by 3.1-fold and 4.3- fold for crizotinib and PF-06463922, respectively. These numbers are greater than can be explained based on *in vitro* IC_{50} values or K_i values for the two variants (Figure 3.6) or on their relative $K_{m,\ ATP}$ values (Bresler et al., 2011b). In turn, these data suggest that there is an additional characteristic of R1275Q-mutated ALK that may render tumors driven by it more sensitive to ALK inhibitors. Possibilities would include altered trafficking rates and/or signaling specificity, for example (Mazot et al., 2011). A key finding, however, is that the IC_{50} values measured with PF-06463922 for all variants were lower than those measured for crizotinib with the crizotinib-sensitive R1275Q variant.

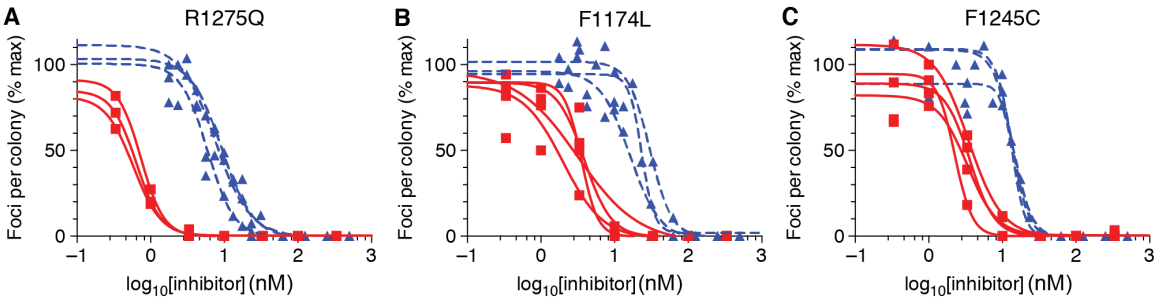

Figure 3.13 PF-06463922 is more effective than crizotinib in inhibiting NIH 3T3 cell transformation by mutated ALK variants.

Inhibition of NIH-3T3 cell transformation in focus formation assays is shown for transfections with ALK harboring: the R1275Q mutation (A), the F1174L mutation (B), and the F1245C mutation (C). The individual inhibition curves are shown for 3 to 4 experiments in each case for both crizotinib (blue dashed curves) and PF-06463922 (red solid curves), with data points from all experiments superimposed on the plots. Mean IC_{50} values (±SD) for crizotinib and PF-06463922, respectively, were 7.5 nM and 0.6 nM for R1275Q, 23.2 nM and 2.8 nM for F1174L, and 13.8 nM and 3.0 nM for F1245C.

3.12 Conclusions

Although our work, and that of others, has positioned ALK as the first tractable oncogene for targeted therapy in neuroblastoma, it is now clear that not all *ALK* mutations impart oncogenic dependency (Bresler et al., 2014; Tucker et al., 2015). Moreover, susceptibility of ALK-driven tumors and cell lines to crizotinib differs according to the underlying mutation (Bresler et al., 2011b; Chand et al., 2013), with mutations at two of the three hotspots (F1174 and F1245) apparently causing primary resistance to ALK kinase inhibition with crizotinib (Bresler et al., 2014; Bresler et al., 2011b). Consistent with this, whereas marked antitumor activity was observed in the Children's Oncology Group (COG) phase I trial of crizotinib in pediatric patients with diseases caused by *ALK* translocations, far fewer objective responses were seen in patients with *ALK*-

mutated neuroblastoma (Mosse et al., 2013). We therefore sought alternative ALK inhibition strategies to overcome this intrinsic resistance. Here, we report that the superior potency of PF-06463922 as an ALK kinase inhibitor delivers impressive activity across a range of *in vitro* and *in vivo* preclinical studies in which significant resistance is detected with all other inhibitors that we have tested, including crizotinib (Bresler et al., 2011b). Effective doses of PF-06463922 were 10- to 30-fold lower than those required for crizotinib in these preclinical studies. In particular, we show that PF-06463922 has notable and unparalleled single agent antitumor activity (even at 3 mg/kg/day) in PDX models of *ALK*-mutated neuroblastoma for which the underlying ALK mutations were known to be associated with primary resistance to crizotinib. Moreover, treatment with PF-06463922 abrogates pALK more completely than crizotinib in xenograft tumors harboring the crizotinib-sensitive R1275Q mutation (in NB-1643 xenografts), and promotes sustained complete regressions without subsequent tumor regrowth. With the caveat that the mouse models used here are xenografts, rather than transgenic or orthotopic models, these data indicate that PF-06463922 will have much broader utility against ALK-driven neuroblastoma than any other ALK inhibitor that we have investigated, largely as a result of the substantially increased affinity for its target.

PF-06463922 is currently being investigated in a phase I/ II clinical trial (NCT01970865) for patients with advanced non–small cell lung carcinoma (NSCLC) harboring ALK or ROS1 molecular alterations (Zou et al., 2015). Although most patients with ALK-translocated NSCLC derive substantial clinical benefit from crizotinib, some of these patients derive no benefit due to intrinsic resistance, and others derive initial benefit but subsequently acquire resistance through secondary *ALK* mutations or other mechanisms (Solomon et al., 2014). PF-06463922 was discovered using structure-guided efforts to maintain potency across a range of resistance mutations and to optimize physicochemical properties (T. W. Johnson et al., 2014). It is a potent macrocyclic ALK inhibitor with good absorption, distribution, metabolism, and excretion, as well as a low propensity for P-glycoprotein–mediated efflux and considerably improved central

nervous system penetration. PF-06463922 was also designed and optimized to penetrate the blood–brain barrier and has shown strong distribution in the central nervous sys- tem in preclinical studies (K. Johnson et al., 2011). This is also likely to be a highly favorable attribute for use of PF-06463922 in neuroblastoma that recurs at this site (Kramer et al., 2001).

Our results show that PF-06463922 inhibits various oncogenically mutated ALK variants with subnanomolar K_i values *in vitro*, and with IC_{50} values in the 10 nM range in cell viability assays. As in very recently reported preclinical studies of ALK-driven lung cancers (Zou et al., 2015), the activity of PF-06463922 did not vary significantly depending on the underlying *ALK* mutation – arguing that it will have a very broad potency in ALK-driven neuroblastomas, as well as in lung cancer. The *in vivo* responses to PF-06463922 that we report are unprecedented in ALK-driven neuroblastoma models and argue for the expedited clinical development of PF-06463922 in this disease. As is typically the case with single-agent therapies against oncogene-addicted cancers, acquired resistance to PF-06463922 is likely to arise, and future studies will need to identify the mechanisms of resistance. It is important to note, however, that the major challenge for targeted therapy in ALK-driven neuroblastoma has been overcoming *de novo* resistance, and our data show that this is achieved with PF-06463922. We are therefore now poised to fast-track the development of PF-06463922 to maximize clinical benefit in the subset of patients with ALK-driven neuroblastoma.

3.13 Experimental Procedures

3.13.1 Plasmid Construction

DNA encoding kinase domain residues 1090-1416 of human ALK was amplified by using primers that included an N-terminal hexahistidine tag and *SpeI/NotI* restriction sites. Mutations were introduced using the QuickChange method (Stratagene), and the PCR product was subcloned

into pFastBac1 for protein expression in Sf9 cells. For focus formation assays, full-length ALK variants were subcloned into the MigR1 vector (BioPioneer, Inc.).

3.13.2 Recombinant protein expression and purification

Spodoptera frugiperda Sf9 cells at 1.5-2 x 10^6 /ml were infected with recombinant baculovirus, and harvested by centrifugation after 3 days. Cells expressing histidine-tagged ALK variants were lysed by sonication in 100ml of lysis buffer (50mM Na phosphate buffer, pH 8.0, 300 mM NaCl, 10mM imidazole, 4mM β-mercaptoethanol, and protease inhibitor cocktail (Roche)). After centrifugation at 40,000 x g for 30 minutes to remove insoluble cell debris, the supernatant was incubated with Ni-NTA agarose beads (Qiagen) for 1 hour at 4^oC. The Ni-NTA beads were washed with 50 column volumes of lysis buffer, pH 8.0 containing 20mM imidazole and bound ALK TKD protein was eluted in lysis buffer, pH 8.0 containing 300mM imidazole. Eluted ALK TKD protein was incubated with 1mM YopH phosphatase for 12 hours at 4^oC to reverse autophosphorylation occurred during expression, and purified as described (Zhang et al., 1992). YopH was removed using a cation exchange column after reducing NaCl concentration to 100 mM. Eluted protein was then further purified using a butyl sepharose HP column (GE Healthcare) equilibrated with 1M $(NH_4)_2SO_4$, 25mM HEPES pH 7.0, 150 mM NaCl and 2mM DTT (HIC buffer A) and eluting with a 20 column volume linear gradient to 0 M $(NH_4)_2SO_4$, 25mM HEPES pH 7.0, 150 mM NaCl and 2mM DTT (HIC buffer B). ALK TKD protein was then subjected to a final step of size exclusion chromatography using a Superdex 200 or Superose 6 column (GE Healthcare) equilibrated in 25 mM HEPES pH 7.4m 150 mM NaCl, 4 mM DTT.

3.13.3 Peptide phosphorylation assays

In vitro kinase assay measuring γ-^{32}P incorporation into substrate was performed as described (Bresler et al., 2011b) with peptide mimic of ALK activation loop with sequence: biotin-ARDIYRASYYRKGGCAMLPVK (CanPeptide). Enzyme concentrations for unphosphorylated ALK-TKD variants were fixed at 50nM. Under the assay condition, reaction rates were linear with

respect to enzyme concentration and time. Assays were performed in 100 mM HEPES pH 7.4, 150 mM NaCl, 2mM DTT, 10 mM $MgCl_2$ and 0.5 mg/ml BSA at 25°C. $K_{m,\ ATP}$ was measured by varying ATP concentration from 0.015625 mM to 2mM at saturating peptide condition (1mM), $K_{m,\ peptide}$ and k_{cat} were measure by varying peptide concentration from 0.015625 mM to 2mM at excess ATP (2mM). Samples were taken at each time point, spotted onto phosphocellulose paper (Upstate Biotechnology) and quenched with 0.5 % phosphoric acid. Liquid scintillator was used to measure incorporated radioactivity of each phosphocellulose paper. Initial rates were determined for linear portion of the enzyme reaction (when < 10% substrate depletion or product formation), normalized for enzyme concentration, and fit to the Michaelis-Menten equation ($v_O = v_{max}[S]/(K_m+[S])$) using GraphPad Prism 5.0.

3.13.4 *In vitro* analysis of ALK-TKD variants Inhibition

Inhibition profiling of ALK kinase inhibitors was assessed by radioactive peptide phosphorylation assay using a peptide mimic of the ALK activation loop with sequence: biotin-ARDIYRASYYRKGGCAMLPVK (CanPeptide) as described (Bresler et al., 2011b). *In vitro* inhibition assays monitored incorporation of P^{32} from γ-^{32}P ATP and enzyme concentration for proteins was fixed at 50 nM. Assays were performed in 100 mM HEPES pH 7.4, 150 mM NaCl, 2mM DTT, 10 mM $MgCl_2$ and 0.5 mg/ml BSA at 25°C, and initiated by mixing equal volumes of solutions containing ALK-TKD (2X protein mix) and substrates (2X substrate mix). Substrate mix was prepared with inhibitor (2-fold serial dilution) prior to mixing so that final concentration of inhibitor covers broad range between 0 and 25,600 nM. Concentrations of peptide and ATP were held fixed at 0.5 mM and 2 mM respectively. After 1 hour of phosphorylation reaction at RT, aliquots were taken and spotted onto phosphocellulose paper (Upstate Biotechnology) to capture peptide followed by immediate quenching with 0.5 % phosphoric acid. Incorporated radioactivity was measured by scintillation counter after extensive washing and drying of each phosphocellulose paper. All data were normalized to the no-inhibitor reaction after subtracting background counts from no-enzyme reaction, and were fitted to Log (inhibitor) vs. response

nonlinear regression curve to find the absolute IC_{50} in GraphPad Prism 5.0. Triplicate experiments were run, and mean values were reported with standard deviation.

3.13.5 *In vivo* efficacy studies

The Felix and COG-N-453x PDXs and the SH-SY5Y and NB-1643 cell line – derived xenografts were implanted subcutaneously into the right flanks of female CB17 SCID mice (Taconic Biosciences). PDX tumors were established in the laboratory of Dr. C. Patrick Reynolds and obtained through the Children's Oncology Group Cell Culture and Xenograft Repository. For single-agent treatment arms, mice were randomized into statistically identical cohorts at a median starting tumor volume of 200 to 300 mm^3 with 10 mice per group. Crizotinib (100 mg/kg qd), PF-06463922 (10 mg/kg/day, 5 mg/kg b.i.d. or 3 mg/kg/day, 1.5 mg/kg b.i.d.), and their respective vehicles were administered by oral gavage at 100 µL/10 g of body weight for a minimum of 6 weeks. Vehicle control mice were given 0.5% methylcellulose and 0.5% Tween-80 in water every day, and hydrochloric acid vehicle in water equimolar to the highest PF-06463922 concentration twice daily. Tumor size was measured two to three times a week by a digital caliper, and volume was calculated by spheroid formula $(p/6) \times d^3$, where d represents the mean diameter. According to the Institutional Animal Care and Use Committee (IACUC) protocol, mice were removed from the study and euthanized once tumors reached 3 cm^3. This study was approved by The Children's Hospital of Philadelphia (CHOP) IACUC protocol #IAC-15-000643.

3.13.6 Statistical analysis of *in vivo* efficacy studies

A linear mixed-effects model was used to test the difference in the rate of tumor volume change over time between different groups. The model included group, day, and group-by-day interaction as fixed effects and included a random intercept and a random slope for each mouse. A significant group-by-day interaction would suggest that the tumor volume changes at different rates for the comparison groups. The model used vehicle group as the reference group and created separate group indicators and interaction terms for other groups. Appropriate contrast

statements were created to compare the two groups other than the vehicle group. If a mouse was sacrificed or removed for biologic or biochemical analysis, the tumor volume was considered missing on the days afterward. EFS curves were estimated using the Kaplan–Meier method and were compared using the log-rank test. Event includes death and tumor size exceeding 3 cm^3 (mouse sacrificed). Mice that were removed for biologic or biochemical analysis were considered censored at the time of removal.

3.13.7 Cell line and reagents

All neuroblastoma cell lines [SH-SY5Y, KELLY, 415-IMDM, NBSD, Felix, NB-1643, LAN-5, NB-1, NB-EBc1, and SK-N-BE(2)C] were obtained in March 2013 from the CHOP cell bank, which is routinely genotyped by short tandem repeat (STR) analysis and tested for *Mycoplasma*. Annual genotyping (AmpFLSTR Identifiler Kit) of these lines and a single nucleotide polymorphism array analysis (Illumina H550) were performed to ensure maintenance of cell identity. The NSCLC cell line NCI-H3122 was generously provided by Jeffrey Engelman (Massachusetts General Hospital, Boston, MA) in March 2014. Cell lines were maintained at 37°C and 5% CO_2 and cultured in RPMI-1640 media supplemented with 10% FBS, 1% l-glutamine, 1% penicillin/streptomycin, and 0.1% gentamycin (as per provider protocol, gentamycin was not used for NCI-H3122). Felix, which was established from the same postmortem sample as Felix-PDX, was grown in Iscove's modified Dulbecco's medium (IMDM) base media with 20% FBS, 1% l-glutamine, and 1% insulin, transferrin, and selenium (ITS; Sigma Aldrich).

3.13.8 *In vitro* pharmacologic growth inhibition

Crizotinib and PF-06463922 were provided by Pfizer, Inc. The drugs were reconstituted in 100% DMSO to a stock concentration of 10 mM and stored at −80°C. Pfizer, Inc., verified the concentrations of the stocks by mass spectrometry. Cells were plated at a density of 3,000 cells per well in triplicate in black clear-bottom tissue culture–treated 96-well plates (VWR) and treated 24 hours later with a 4-log dose range of inhibitor and a DMSO control. To ensure optimal

solvation, serial drug dilutions were performed in DMSO and then diluted further in starving media (0.04% FBS in RPMI or IMDM base media) before treatment. Plates were incubated for 120 hours before measuring ATP levels using the CellTiter-Glo luminescent cell viability assay (Promega) according to the manufacturer's protocol. Luminescence was measured three times per plate with a GloMax-Multi Microplate Multimode Reader (Promega) to produce an average reading for each well. Viability assays were repeated three times per cell line. To generate IC_{50} values, the data were analyzed as follows: luminescence readings were normalized to media-only background wells and expressed as percentages of the DMSO-treated control wells. GraphPad Prism 5.0 was used to plot percent luminescence against inhibitor concentration (logarithmic scale). IC_{50} values and dose–response curves were then generated using the $\log_{10}$(inhibitor) versus response nonlinear regression, defining IC_{50} as the concentration that achieves half-maximal effect where complete killing was not observed.

3.13.9 Focus formation assays

For focus-formation assays, full-length ALK variants were subcloned into the MigR1 vector (BioPioneer, Inc.). Low-passage NIH 3T3 cells (typically <15) at approximately 60% to 70% confluence were transfected with full-length mutated ALK constructs using Lipofectamine 2000 (Invitrogen) according to the manufacturer's protocol. Cells were then allowed to recover for 2 days and were transferred to 6-well plates. Each well was then topped off with medium containing DMSO as vehicle control or the appropriate concentration of the inhibitor in DMSO (covering 4–5 logs). Medium (DMEM with GlutaMAX with 5% calf serum) was then changed every 3 days with a fresh inhibitor. Focus formation typically took 10 to 14 days. Cells were fixed in 3.7% formaldehyde in phosphate-buffered saline (PBS) for 5 minutes and then stained with 0.05% crystal violet in distilled water for 30 minutes in order to count foci. The number of foci per well was normalized to the result seen in the DMSO control well. The half-maximal inhibitory concentration (IC_{50}) was then determined from nonlinear regression analysis of a $\log_{10}$(inhibitor) versus response curve using GraphPad Prism 5.0. Each independent experiment was performed

in triplicate at least, and mean values are reported with standard deviation. Western blot analysis in parallel with transfections showed similar levels of expression for the different mutants.

3.13.10 Western blot analysis

Between 2×10^6 and 3×10^6 cells were plated in 100 × 20 mm tissue culture dishes, allowed to attach for 24 hours, treated, and harvested on ice. Pellets were washed twice with ice-cold PBS and stored at −80°C until lysis. Cells were lysed with hypotonic lysis (10 mM Tris/HCl, 10 mM NaCl, 1% Triton, 1 mM EGTA, pH 7.4) buffer with 1% protease/phosphatase inhibitor cocktail (Cell Signaling Technology), incubated on ice for at least 15 minutes, and then spun in a microcentrifuge at top speed at 4°C for 5 minutes. Protein from the supernatant was quantified using the Bicinchoninic Acid (BCA) Assay (Thermo Scientific). Lysates (50 µg protein) were separated on NuPAGE Novex 4% to 12% Bis-Tris gels (Life Technologies) at 130 volts, then transferred to polyvinylidene difluoride membranes (Millipore) at 4°C at 30 volts. Membranes were blocked in 5% milk or 5% bovine serum albumin fraction V, heat shock (Roche) for phospho-proteins in 1xTris-buffered saline and Tween 20 (TBST) for 45 minutes at room temperature, and then incubated with primary anti- bodies overnight at 4°C. All primary antibodies were diluted 1:1,000, except for the β-actin antibodies (1:5,000). ALK pY1604, ALK pY1278, and ALK antibodies were purchased from Cell Signaling Technology, and the β-actin antibody was purchased from Santa Cruz Biotechnology. Membranes were washed for 10 minutes three times in 1× TBST before a 45-minute incubation at room temperature with the secondary antibody. Goat anti-rabbit and goat anti-mouse secondary antibodies were purchased from Cell Signaling Technology and diluted 1:5,000 in 5% milk in 1× TBST. Membranes were washed again three times before developing. If necessary, membranes were stripped with a 0.1 M glycine, 0.5% Tween 20 (pH 2.5) buffer for two 15-minute incubations.

3.13.11 Western blot analysis of xenograft tumors

At a median starting tumor volume of 200 to 300 mm^3, NB-1643– engrafted mice were randomized into groups of three and treated with either vehicle, crizotinib (100 mg/kg qd), or PF-06463922 (10 mg/kg/day, 5 mg/kg b.i.d.). Tumors were collected and snap-frozen in liquid nitrogen after 3 days of treatment, 1 hour after the final dose was administered. Tumors were homogenized in hypotonic lysis buffer with 10% protease phosphatase inhibitor cocktail in a ratio of 2,000 µL lysis buffer: 0.5 g tumor. Protein (150 µg), as assessed using the BCA assay, was loaded onto gels to detect pALK.

3.14 References

Adzhubei, I. A., Schmidt, S., Peshkin, L., Ramensky, V. E., Gerasimova, A., Bork, P., Kondrashov, A. S., & Sunyaev, S. R. (2010). A method and server for predicting damaging missense mutations. *Nat Methods, 7*(4), 248-249. doi: 10.1038/nmeth0410-248

Bendl, J., Stourac, J., Salanda, O., Pavelka, A., Wieben, E. D., Zendulka, J., Brezovsky, J., & Damborsky, J. (2014). PredictSNP: robust and accurate consensus classifier for prediction of disease-related mutations. *PLoS Comput Biol, 10*(1), e1003440. doi: 10.1371/journal.pcbi.1003440

Bresler, S. C., Weiser, D. A., Huwe, P. J., Park, J. H., Krytska, K., Ryles, H., Laudenslager, M., Rappaport, E. F., Wood, A. C., McGrady, P. W., Hogarty, M. D., London, W. B., Radhakrishnan, R., Lemmon, M. A., & Mosse, Y. P. (2014). ALK mutations confer differential oncogenic activation and sensitivity to ALK inhibition therapy in neuroblastoma. *Cancer Cell, 26*(5), 682-694. doi: 10.1016/j.ccell.2014.09.019

Bresler, S. C., Wood, A. C., Haglund, E. A., Courtright, J., Belcastro, L. T., Plegaria, J. S., Cole, K., Toporovskaya, Y., Zhao, H., Carpenter, E. L., Christensen, J. G., Maris, J. M., Lemmon, M. A., & Mosse, Y. P. (2011a). Differential inhibitor sensitivity of anaplastic lymphoma kinase variants found in neuroblastoma. *Science Trans. Med., 3*(108), 108ra114. doi: 10.1126/scitranslmed.3002950

Bresler, S. C., Wood, A. C., Haglund, E. A., Courtright, J., Belcastro, L. T., Plegaria, J. S., Cole, K., Toporovskaya, Y., Zhao, H., Carpenter, E. L., Christensen, J. G., Maris, J. M., Lemmon, M. A., & Mosse, Y. P. (2011b). Differential inhibitor sensitivity of anaplastic lymphoma kinase variants found in neuroblastoma. *Sci Transl Med, 3*(108), 108ra114. doi: 10.1126/scitranslmed.3002950

Cha, S. (1975). Tight-binding inhibitors-I. Kinetic behavior. *Biochem Pharmacol, 24*(23), 2177-2185.

Chand, D., Yamazaki, Y., Ruuth, K., Schonherr, C., Martinsson, T., Kogner, P., Attiyeh, E. F., Maris, J., Morozova, O., Marra, M. A., Ohira, M., Nakagawara, A., Sandstrom, P. E., Palmer, R. H., & Hallberg, B. (2013). Cell culture and Drosophila model systems define three classes of anaplastic lymphoma kinase mutations in neuroblastoma. *Dis Model Mech, 6*(2), 373-382. doi: 10.1242/dmm.010348

Chen, Y., Takita, J., Choi, Y. L., Kato, M., Ohira, M., Sanada, M., Wang, L., Soda, M., Kikuchi, A., Igarashi, T., Nakagawara, A., Hayashi, Y., Mano, H., & Ogawa, S. (2008). Oncogenic mutations of ALK kinase in neuroblastoma. *Nature, 455*(7215), 971-974. doi: 10.1038/nature07399

Cui, J. J., Tran-Dube, M., Shen, H., Nambu, M., Kung, P. P., Pairish, M., Jia, L., Meng, J., Funk, L., Botrous, I., McTigue, M., Grodsky, N., Ryan, K., Padrique, E., Alton, G., Timofeevski, S., Yamazaki, S., Li, Q., Zou, H., Christensen, J., Mroczkowski, B., Bender, S., Kania, R. S., & Edwards, M. P. (2011). Structure based drug design of crizotinib (PF-02341066), a potent and selective dual inhibitor of mesenchymal-epithelial transition factor (c-MET) kinase and anaplastic lymphoma kinase (ALK). *J Med Chem, 54*(18), 6342-6363. doi: 10.1021/jm2007613

Eleveld, T. F., Oldridge, D. A., Bernard, V., Koster, J., Daage, L. C., Diskin, S. J., Schild, L., Bentahar, N. B., Bellini, A., Chicard, M., Lapouble, E., Combaret, V., Legoix-Ne, P., Michon, J., Pugh, T. J., Hart, L. S., Rader, J., Attiyeh, E. F., Wei, J. S., Zhang, S., Naranjo, A., Gastier-Foster, J. M., Hogarty, M. D., Asgharzadeh, S., Smith, M. A., Guidry Auvil, J. M., Watkins, T. B., Zwijnenburg, D. A., Ebus, M. E., van Sluis, P., Hakkert, A., van Wezel, E., van der Schoot, C. E., Westerhout, E. M., Schulte, J. H., Tytgat, G. A., Dolman, M. E., Janoueix-Lerosey, I., Gerhard, D. S., Caron, H. N., Delattre, O., Khan, J., Versteeg, R., Schleiermacher, G., Molenaar, J. J., & Maris, J. M. (2015). Relapsed neuroblastomas show frequent RAS-MAPK pathway mutations. *Nat Genet, 47*(8), 864-871. doi: 10.1038/ng.3333

Fontana, D., Ceccon, M., Gambacorti-Passerini, C., & Mologni, L. (2015). Activity of second-generation ALK inhibitors against crizotinib-resistant mutants in an NPM-ALK model compared to EML4-ALK. *Cancer Med, 4*(7), 953-965. doi: 10.1002/cam4.413

George, R. E., Sanda, T., Hanna, M., Frohling, S., Luther, W., 2nd, Zhang, J., Ahn, Y., Zhou, W., London, W. B., McGrady, P., Xue, L., Zozulya, S., Gregor, V. E., Webb, T. R., Gray, N. S., Gilliland, D. G., Diller, L., Greulich, H., Morris, S. W., Meyerson, M., & Look, A. T. (2008). Activating mutations in ALK provide a therapeutic target in neuroblastoma. *Nature, 455*(7215), 975-978. doi: 10.1038/nature07397

Gnad, F., Baucom, A., Mukhyala, K., Manning, G., & Zhang, Z. (2013). Assessment of computational methods for predicting the effects of missense mutations in human cancers. *BMC Genomics, 14 Suppl 3*, S7. doi: 10.1186/1471-2164-14-S3-S7

Hallberg, B., & Palmer, R. H. (2013). Mechanistic insight into ALK receptor tyrosine kinase in human cancer biology. *Nat Rev Cancer, 13*(10), 685-700. doi: 10.1038/nrc3580

Hobbie, W. L., Moshang, T., Carlson, C. A., Goldmuntz, E., Sacks, N., Goldfarb, S. B., Grupp, S. A., & Ginsberg, J. P. (2008). Late effects in survivors of tandem peripheral blood stem cell transplant for high-risk neuroblastoma. *Pediatr Blood Cancer, 51*(5), 679-683. doi: 10.1002/pbc.21683

Janoueix-Lerosey, I., Lequin, D., Brugieres, L., Ribeiro, A., de Pontual, L., Combaret, V., Raynal, V., Puisieux, A., Schleiermacher, G., Pierron, G., Valteau-Couanet, D., Frebourg, T., Michon, J., Lyonnet, S., Amiel, J., & Delattre, O. (2008). Somatic and germline activating mutations of the ALK kinase receptor in neuroblastoma. *Nature, 455*(7215), 967-970. doi: 10.1038/nature07398

Johnson, K., McGlynn, B., Saggio, J., Baniewicz, D., Zhuang, H., Maris, J. M., & Mosse, Y. P. (2011). Safety and efficacy of tandem 131I-metaiodobenzylguanidine infusions in relapsed/refractory neuroblastoma. *Pediatr Blood Cancer, 57*(7), 1124-1129. doi: 10.1002/pbc.23062

Johnson, T. W., Richardson, P. F., Bailey, S., Brooun, A., Burke, B. J., Collins, M. R., Cui, J. J., Deal, J. G., Deng, Y. L., Dinh, D., Engstrom, L. D., He, M., Hoffman, J., Hoffman, R. L., Huang, Q., Kania, R. S., Kath, J. C., Lam, H., Lam, J. L., Le, P. T., Lingardo, L., Liu, W., McTigue, M., Palmer, C. L., Sach, N. W., Smeal, T., Smith, G. L., Stewart, A. E., Timofeevski, S., Zhu, H., Zhu, J., Zou, H. Y., & Edwards, M. P. (2014). Discovery of (10R)-7-amino-12-fluoro-2,10,16-trimethyl-15-oxo-10,15,16,17-tetrahydro-2H-8,4-(m etheno)pyrazolo[4,3-h][2,5,11]-benzoxadiazacyclotetradecine-3-carbonitrile (PF-06463922), a macrocyclic inhibitor of anaplastic lymphoma kinase (ALK) and c-ros oncogene 1 (ROS1) with preclinical brain exposure and broad-spectrum potency against ALK-resistant mutations. *J Med Chem, 57*(11), 4720-4744. doi: 10.1021/jm500261q

Kramer, K., Kushner, B., Heller, G., & Cheung, N. K. (2001). Neuroblastoma metastatic to the central nervous system. The Memorial Sloan-kettering Cancer Center Experience and A Literature Review. *Cancer, 91*(8), 1510-1519.

Kumar, P., Henikoff, S., & Ng, P. C. (2009). Predicting the effects of coding non-synonymous variants on protein function using the SIFT algorithm. *Nat Protoc, 4*(7), 1073-1081. doi: 10.1038/nprot.2009.86

Maris, J. M. (2010). Recent advances in neuroblastoma. *N Engl J Med, 362*(23), 2202-2211. doi: 10.1056/NEJMra0804577

Mazot, P., Cazes, A., Boutterin, M. C., Figueiredo, A., Raynal, V., Combaret, V., Hallberg, B., Palmer, R. H., Delattre, O., Janoueix-Lerosey, I., & Vigny, M. (2011). The constitutive activity of the ALK mutated at positions F1174 or R1275 impairs receptor trafficking. *Oncogene, 30*(17), 2017-2025. doi: 10.1038/onc.2010.595

Molina-Vila, M. A., Nabau-Moreto, N., Tornador, C., Sabnis, A. J., Rosell, R., Estivill, X., Bivona, T. G., & Marino-Buslje, C. (2014). Activating mutations cluster in the "molecular brake" regions of protein kinases and do not associate with conserved or catalytic residues. *Hum Mutat, 35*(3), 318-328. doi: 10.1002/humu.22493

Mologni, L., Ceccon, M., Pirola, A., Chiriano, G., Piazza, R., Scapozza, L., & Gambacorti-Passerini, C. (2015). NPM/ALK mutants resistant to ASP3026 display variable sensitivity to alternative ALK inhibitors but succumb to the novel compound PF-06463922. *Oncotarget, 6*(8), 5720-5734. doi: 10.18632/oncotarget.3122

Mosse, Y. P., Laudenslager, M., Longo, L., Cole, K. A., Wood, A., Attiyeh, E. F., Laquaglia, M. J., Sennett, R., Lynch, J. E., Perri, P., Laureys, G., Speleman, F., Kim, C., Hou, C., Hakonarson, H., Torkamani, A., Schork, N. J., Brodeur, G. M., Tonini, G. P., Rappaport, E., Devoto, M., & Maris, J. M. (2008). Identification of ALK as a major familial neuroblastoma predisposition gene. *Nature, 455*(7215), 930-935. doi: 10.1038/nature07261

Mosse, Y. P., Lim, M. S., Voss, S. D., Wilner, K., Ruffner, K., Laliberte, J., Rolland, D., Balis, F. M., Maris, J. M., Weigel, B. J., Ingle, A. M., Ahern, C., Adamson, P. C., & Blaney, S. M. (2013). Safety and activity of crizotinib for paediatric patients with refractory solid tumours or anaplastic large-cell lymphoma: a Children's Oncology Group phase 1 consortium study. *Lancet Oncol, 14*(6), 472-480. doi: 10.1016/S1470-2045(13)70095-0

Pearson, A. D., Pinkerton, C. R., Lewis, I. J., Imeson, J., Ellershaw, C., Machin, D., European Neuroblastoma Study, G., Children's, C., & Leukaemia, G. (2008). High-dose rapid and standard induction chemotherapy for patients aged over 1 year with stage 4 neuroblastoma: a randomised trial. *Lancet Oncol, 9*(3), 247-256. doi: 10.1016/S1470-2045(08)70069-X

Schleiermacher, G., Javanmardi, N., Bernard, V., Leroy, Q., Cappo, J., Rio Frio, T., Pierron, G., Lapouble, E., Combaret, V., Speleman, F., de Wilde, B., Djos, A., Ora, I., Hedborg, F., Trager, C., Holmqvist, B. M., Abrahamsson, J., Peuchmaur, M., Michon, J., Janoueix-Lerosey, I., Kogner, P., Delattre, O., & Martinsson, T. (2014). Emergence of new ALK mutations at relapse of neuroblastoma. *J Clin Oncol, 32*(25), 2727-2734. doi: 10.1200/JCO.2013.54.0674

Smith, M. A., Seibel, N. L., Altekruse, S. F., Ries, L. A., Melbert, D. L., O'Leary, M., Smith, F. O., & Reaman, G. H. (2010). Outcomes for children and adolescents with cancer: challenges for the twenty-first century. *J Clin Oncol, 28*(15), 2625-2634. doi: 10.1200/JCO.2009.27.0421

Solomon, B., Wilner, K. D., & Shaw, A. T. (2014). Current status of targeted therapy for anaplastic lymphoma kinase-rearranged non-small cell lung cancer. *Clin Pharmacol Ther, 95*(1), 15-23. doi: 10.1038/clpt.2013.200

Tucker, E. R., Danielson, L. S., Innocenti, P., & Chesler, L. (2015). Tackling Crizotinib Resistance: The Pathway from Drug Discovery to the Pediatric Clinic. *Cancer Res, 75*(14), 2770-2774. doi: 10.1158/0008-5472.CAN-14-3817

Yu, A. L., Gilman, A. L., Ozkaynak, M. F., London, W. B., Kreissman, S. G., Chen, H. X., Smith, M., Anderson, B., Villablanca, J. G., Matthay, K. K., Shimada, H., Grupp, S. A., Seeger, R., Reynolds, C. P., Buxton, A., Reisfeld, R. A., Gillies, S. D., Cohn, S. L., Maris, J. M., Sondel, P. M., & Children's Oncology, G. (2010). Anti-GD2 antibody with GM-CSF, interleukin-2, and isotretinoin for neuroblastoma. *N Engl J Med, 363*(14), 1324-1334. doi: 10.1056/NEJMoa0911123

Zhang, Z. Y., Clemens, J. C., Schubert, H. L., Stuckey, J. A., Fischer, M. W., Hume, D. M., Saper, M. A., & Dixon, J. E. (1992). Expression, purification, and physicochemical characterization of a recombinant Yersinia protein tyrosine phosphatase. *J Biol Chem, 267*(33), 23759-23766.

Zou, H. Y., Friboulet, L., Kodack, D. P., Engstrom, L. D., Li, Q., West, M., Tang, R. W., Wang, H., Tsaparikos, K., Wang, J., Timofeevski, S., Katayama, R., Dinh, D. M., Lam, H., Lam, J. L., Yamazaki, S., Hu, W., Patel, B., Bezwada, D., Frias, R. L., Lifshits, E., Mahmood, S., Gainor, J. F., Affolter, T., Lappin, P. B., Gukasyan, H., Lee, N., Deng, S., Jain, R. K., Johnson, T. W., Shaw, A. T., Fantin, V. R., & Smeal, T. (2015). PF-06463922, an ALK/ROS1 Inhibitor, Overcomes Resistance to First and Second Generation ALK Inhibitors in Preclinical Models. *Cancer Cell, 28*(1), 70-81. doi: 10.1016/j.ccell.2015.05.010

CHAPTER 4:

Conclusions and Future directions

Over the past quarter century, receptor tyrosine kinases (RTK) signaling has been extensively investigated. Integrative investigations of their genetics, cell biology, biochemistry and structural biology have guided the establishment of a general mechanism of RTK regulation and activation; and these findings have impacted to the discovery and application of numerous important therapeutics for diseases arising from aberrant regulation of RTKs. However, as discussed in Chapter 1, the mechanisms of activation for individual RTKs have distinctive differences in detail – even though they do share key common features. Understanding this mechanistic diversity is crucial for guiding precise therapeutic intervention. Further analysis of the uncharacterized human RTKs that comprise almost half of this family is also needed to complete our view of how RTKs function.

In Chapter 2, I described investigations of the conformational selectivity of EGFR/ErbB family targeted tyrosine kinase inhibitors (TKI). The influence of the kinase's conformational state on inhibitor sensitivity is an important but poorly understood concept in drug discovery. Despite the general assumption that the Type I EGFR inhibitor erlotinib binds selectively to the active configuration of the EGFR tyrosine kinase domain, computational studies of inhibitor-stabilized EGFR conformations suggested that this inhibitor can bind equally well to either the active or inactive configurations. This led to my crystallographic investigations of whether erlotinib can bind to either 'state' – which revealed that erlotinib can indeed bind to the inactive as well as the active state. Using EGFR kinase variants that adopt either the active or inactive configurations in crystals, we also determined that the novel ErbB2 inhibitor 55A – identified and optimized by our collaborator in cell-based screens targeting the relevant conformation of kinase in its endogenous environment – selectively binds the active state of the kinase. This observation could have important clinical utility. These findings argue that the relative abilities of different inhibitors to bind to different kinase conformations and to mutationally activated EGFR variants is likely to be more complicated than previously thought. This dichotomy seems unlikely to simply reflect stabilization of different conformational states of EGFR-TKD, but is rather likely to reflect more

complicated conformational and dynamic characteristics of the kinase and its variants such as differences in inhibitor dissociation or cycling rates. These new considerations for inhibitor binding have important clinical implications, illuminating new avenues for extending the relative success of EGFR-targeted TKIs in NSCLC to other cancers. Other activating (and resistance) mutations may show an even wider range of specificities. More extensive analysis is required to identify the differences between these groups of inhibitors, which will be beneficial for determining which inhibitors to apply in the clinic based on the way in which EGFR has been aberrantly activated. Monitoring differences in inhibitor binding kinetics for a series of reversible inhibitors utilizing a fluorescent affinity probe for the ATP-binding site – as has been done to compare binding to different EGFR mutants in lung cancer and glioblastoma (Barkovich et al., 2012) – would be one approach for gaining insight into the likely effects of different inhibitors on newly discovered oncogenic alleles – for EGFR and other RTKs.

In Chapter 3, my thesis examines the biochemical and cellular analysis of ALK activation and inhibition, as numerous activating mutations in the *ALK* gene have been implicated in neuroblastoma. Since the discovery of the *ALK* oncogene as a tractable molecular target in neuroblastoma, considerable progress has been made in understanding how different mutations activate the ALK kinase domain, and how they alter inhibitor sensitivity. After establishing the pre-clinical rationale for therapeutic stratification of neuroblastoma patients based on ALK genomic status, we have analyzed biochemical consequences of the full spectrum of ALK variants in parallel with functional cellular studies and computational studies of their structural effects. These findings have provided a basis for distinguishing oncogenic mutations from non-oncogenic mutations, which is important for the use of ALK inhibitors in the clinic, and for providing a mechanistic basis to understand/validate how clinically observed ALK mutations activate the kinase when accompanied by proper structural understanding of how ALK TKD is regulated. In order to decipher how ALK kinase becomes activated in normal signaling and how other activating mutations mimic this, structural studies of ALK TKD in its active states – phosphorylated form and mutationally activated form – are crucial to advance our understanding

of regulations of ALK at the molecular-level in path for drug discovery and for guiding for treatment, as individual ALK mutations exhibit different sensitivities to inhibitors. In addition, identification of a novel ligand and potential co-receptors for ALK likely offers important insights into human ALK signaling and further therapeutic intervention. We also present our ongoing work on developing a complementary computational tool to facilitate prediction of the effects of new clinically emerging ALK mutations on its transforming ability and drug sensitivity by iteration between computational prediction and experimentation. Our computational model with successive improvement will serve as a valuable tool toward personalized cancer therapy by enabling rapid and accurate prediction of the functional status of newly identified mutations.

Among the 3 hot spot *ALK* mutations found in neuroblastoma, the F1174L and F1245C mutations confer intrinsic resistance to the currently available FDA-approved drug crizotinib, presenting a serious clinical obstacle. Therefore, our goal was to identify a potent inhibitor that is effective in treating preclinical models of primary resistance, as well as, in crizotinib-sensitive ALK mutants. Biochemical studies of currently available second-generation ALK inhibitors revealed the high inhibitory potency of PF-06463922 on phosphorylation (activation) of recombinant ALK-TKD variants harboring the three most frequently observed mutations. Furthermore, we demonstrated that PF-06463922 is remarkably active in inhibiting oncogenic transformation in NIH3T3 cells, xenografts and PDXs harboring both crizotinib-sensitive and insensitive *ALK* point mutations. Our data argue for the expedited translation of these findings to the clinic for pediatric neuroblastoma – and clinical trials are now being initiated. As is typically the case with single-agent therapies against oncogene-addicted cancers, acquired resistance to PF-06463922 is likely to arise. Given its potent anti-tumor activity at low concentrations *in vitro* and *in vivo*, PF-06463922 is an excellent candidate for use in combinatorial therapies with traditional chemotherapeutics.